# REVERSE-SELECTIVE ZEOLITE/POLYMER NANOCOMPOSITE HOLLOW FIBER MEMBRANES FOR PERVAPORATIVE BIOFUEL/WATER SEPARATION

A Thesis
Presented to
The Academic Faculty

by

Kathrine D. McFadden

In Partial Fulfillment
of the Requirements for the Degree
Master of Science in
Chemical Engineering

School of Chemical & Biomolecular Engineering
Georgia Institute of Technology
May 2010

# REVERSE-SELECTIVE ZEOLITE/POLYMER NANOCOMPOSITE HOLLOW FIBER MEMBRANES FOR PERVAPORATIVE BIOFUEL/WATER SEPARATION

Approved by:

Dr. Sankar Nair, Advisor
School of Chemical & Biomolecular Engineering
*Georgia Institute of Technology*

Dr. Pradeep K. Agrawal
School of Chemical & Biomolecular Engineering
*Georgia Institute of Technology*

Dr. William J. Koros
School of Chemical & Biomolecular Engineering
*Georgia Institute of Technology*

Date Approved: March 18, 2010

*In memory of Chris McFadden, Denise Purdue, Chris Russell, and Richard Parriott.*

*"Those whom we have loved never really leave us. They live on forever in our hearts, and cast their radiant light onto our every shadow."*

*Sylvana Rossetti*

# ACKNOWLEDGEMENTS

There are many people that have helped me tremendously during the past couple years. First and foremost, I am deeply appreciative of the advice and guidance of my advisor, Dr. Sankar Nair. His insight, patience, and support have helped me to develop as a researcher. I am also grateful for the invaluable feedback and suggestions of my committee members, Dr. William Koros and Dr. Pradeep Agrawal.

I have received very helpful advice and instruction from the members of Dr. Nair's and Dr. Koros' research groups. Most notably, I would like to thank Jae Kyu Cho for his improvements to the pervaporation system design and for providing ample amounts of MFI. My special thanks also go to Mohamad Kassaee for providing functionalized MFI and teaching me to synthesize and functionalize MFI; to JR Johnson, Madhava Kosuri, and Shabbir Husain for providing me with non-selective hollow fibers; to Dr. Wulin Qiu for showing me how to prepare pervaporation modules and how to run pervaporation tests on the preexisting system; and to Mariefel Valenzuela Olarte for help and guidance while constructing and testing the vacuum system. I also appreciate the helpful advice of my officemates: Yeny, Chris, and Andres. When times were tough, there was always a smile to be had. Our informal brainstorming sessions were very constructive and beneficial for this work.

I have my family and close friends to thank for keeping me from getting too stressed out over the course of this work. I am grateful for my parents, David and Joan Parriott, my brother, Jon, and my father- and mother-in-law, Chris and Donna McFadden, for their constant love and support of my goals. I am also indebted to Josh, Josephine, Ryan, and Bernadette for helping me relax and have fun away from work.

Finally, I would like to thank my husband, Mike, who has been incredibly supportive, patient, and encouraging throughout this work. His love and friendship have made my life extremely rewarding and enjoyable. May there be peanut butter sandwiches for many years to come.

I gratefully acknowledge financial support of my thesis research by the Institute of Paper Science and Technology All Member Research Consortium (IPST AMRC).

# TABLE OF CONTENTS

ACKNOWLEDGEMENTS . . . . . iv

LIST OF TABLES . . . . . ix

LIST OF FIGURES . . . . . x

SUMMARY . . . . . xiv

I INTRODUCTION . . . . . 1

1.1 Background and Motivation . . . . . 1

1.1.1 Biofuel Production Processes . . . . . 2

1.1.2 Potential Separation Technologies for Dilute Biofuel/Water Streams . . . . . 4

1.2 Membranes for Pervaporation . . . . . 9

1.2.1 Polymeric Membranes . . . . . 10

1.2.2 Zeolitic Membranes . . . . . 11

1.2.3 Composite Flat-Film Membranes . . . . . 11

1.2.4 Proposed Composite Hollow-Fiber Membranes . . . . . 11

1.3 Research Objectives and Strategies . . . . . 13

1.4 Organization of Dissertation . . . . . 14

II MEMBRANE FUNDAMENTALS . . . . . 15

2.1 Mechanism of Liquid Transport in Polymeric and Mixed-Matrix Membranes . . . . . 15

2.1.1 Transport in a Dense Film . . . . . 15

2.1.2 Transport in a Composite Film . . . . . 21

2.2 Membrane Material Selection . . . . . 22

2.2.1 Polymer Selection . . . . . 22

2.2.2 Zeolite Selection . . . . . 23

2.2.3 Hollow Fiber Support . . . . . 24

2.2.4 Organic Solvent Choice . . . . . 24

2.3 Processing Variables . . . . . 25
2.3.1 Composition of Dope Solution . . . . . 25
2.3.2 Zeolite Particle Size . . . . . 27
2.3.3 Zeolite Surface Treatment . . . . . 28
2.3.4 Aging (Prepolymerization) of Polymer . . . . . 28
2.3.5 Membrane Thickness . . . . . 29
2.4 Pervaporation Parameters . . . . . 29
2.4.1 Feed Temperature . . . . . 30
2.4.2 Downstream Pressure . . . . . 30
2.4.3 Feed Concentration . . . . . 30
2.4.4 Feed Circulation Rate . . . . . 32
2.5 Fouling . . . . . 33
III EXPERIMENTAL METHODS . . . . . 35
3.1 Zeolite Synthesis . . . . . 36
3.1.1 Synthesis in Berghof Reactor (Method A) . . . . . 36
3.1.2 Synthesis in Pyrex® Container (Method B) . . . . . 37
3.2 Functionalization . . . . . 39
3.3 Polymers . . . . . 39
3.4 Hollow Fiber Supports . . . . . 40
3.5 Composite Flat Film Preparation . . . . . 40
3.6 MFI/PDMS Coatings on Hollow Fibers . . . . . 41
3.6.1 Dope Preparation . . . . . 42
3.6.2 Fiber Pretreatment . . . . . 42
3.6.3 Coating Method . . . . . 42
3.6.4 Sonication . . . . . 44
3.6.5 Multiple Coatings . . . . . 44
3.6.6 Low- and High-Temperature Vacuum Treatments . . . . . 45
3.7 Zeolite and Membrane Characterization . . . . . 45

3.8 Pervaporation Measurements . . . . . 46
3.8.1 Assembling Pervaporation Modules . . . . . 46
3.8.2 Pervaporation Procedure . . . . . 51
IV RESULTS AND DISCUSSION . . . . . 56
4.1 Verification of Pervaporation Apparatus Results . . . . . 56
4.2 MFI Characterization . . . . . 57
4.3 Characterization of Flat Films . . . . . 57
4.3.1 Effect of Polymer . . . . . 58
4.3.2 Effect of Zeolite Functionalization . . . . . 63
4.3.3 Effect of Vacuum Treatment . . . . . 67
4.4 Characterization of Hollow Fibers . . . . . 68
4.4.1 Characteristics of Bare Hollow-Fiber Supports . . . . . 68
4.4.2 Effect of Increasing Number of Coats . . . . . 70
4.4.3 Effect of Presoaking . . . . . 73
4.4.4 Effect of Zeolite Functionalization . . . . . 75
4.4.5 Effect of Coating Method . . . . . 77
4.4.6 Effect of Increasing Zeolite Loading . . . . . 79
V CONCLUSIONS . . . . . 82
5.1 Recommendations . . . . . 83
REFERENCES . . . . . 85

# LIST OF TABLES


1.1 Historical and projected global energy, petroleum, and natural gas demands and carbon dioxide emissions [1]. . . . . 2

4.1 Film thicknesses and pervaporation results for flat films prepared using RTV615 polymer with butanol-functionalized MFI. . . . . 61

4.2 Film thicknesses and pervaporation results for flat films prepared with DMS-V41/HMS-064 polymer using butanol-functionalized MFI. . . . 61

4.3 Film thicknesses and pervaporation results for flat films prepared using RTV615 polymer with unfunctionalized MFI. . . . . 65

4.4 Film thicknesses and pervaporation results for flat films prepared using RTV615 polymer with butanol-functionalized MFI and treated with a low-temperature (70°C) or high-temperature (110°C) vacuum treatment. 68

4.5 Coating thicknesses and pervaporation results for increasing number of pure PDMS coatings. . . . . 71

4.6 Coating thicknesses and average pervaporation results for membranes prepared with and without presoaking. . . . . 76

4.7 Coating thicknesses and pervaporation results for presoaked, 1-coat pure PDMS membranes prepared by different methods. . . . . 79

# LIST OF FIGURES


1.1 Flow diagram of a typical biomass-to-ethanol process. . . . . 4

1.2 (a) Vapor-liquid equilibrium curves for ethanol-water and $n$-butanol-water mixtures at 101.3 kPa. (b) Effect of alcohol concentration on the relative volatility of ethanol or $n$-butanol over water, $\beta_{AW}$. VLE data from [35]. . . . . 5

1.3 Separation process alternatives. In all processes, the concentrated ethanol must be further dehydrated to fuel-grade purity using molecular sieves, hydrophilic pervaporation, or another dehydration process. 6

1.4 Reported pervaporation performances for polymeric and zeolitic membranes [42–58]. . . . . 10

1.5 Schematic diagram of a mixed-matrix membrane showing the preferential transport of ethanol. . . . . 12

1.6 (a) Cross-section of a polymer/zeolite nanocomposite coating on a porous polymeric hollow-fiber support. (b) Hollow-fiber membrane module with shell-side feed, composed of many hollow fibers bundled together and encapsulated in resin. . . . . 12

2.1 The preferential transport of ethanol through the zeolite/polymer coating. . . . . 21

2.2 Structure of (a) poly(dimethyl siloxane) and (b) vinyl-terminated poly(dimethyl siloxane). . . . . 22

2.3 Structure of zeolite MFI as viewed down crystallographic a, b, and c directions [78]. . . . . 24

2.4 Ethanol flux and separation factor as a function of zeolite loading for MFI-PDMS flat-film membranes reported in the literature. . . . . 26

2.5 Ethanol flux and separation factor as a function of feed temperature for MFI-PDMS flat-film membranes reported in the literature. . . . . 31

2.6 Ethanol flux and separation factor as a function of feed concentration for MFI-PDMS flat-film membranes reported in the literature. . . . . 32

3.1 Schematic cross-section of MFI/PDMS composite . . . . . 35

3.2 Presoaking a hollow fiber in deionized water. . . . . 43

3.3 Hollow fibers suspended horizontally in oven. . . . . 43

3.4 Illustration of the dip-coat method of coating hollow fibers. . . . . 43

3.5 Illustration of the U-tube method of coating hollow fibers. . . . . 44

3.6 Glass U-tube suspended in sonication bath. . . . . 45

3.7 Calibration curve for ethanol-water solutions measured with a Leica ARIAS 500 refractometer. . . . . 46

3.8 Original pervaporation apparatus (System A) shown with a single hollow-fiber membrane. . . . . 47

3.9 Modified pervaporation apparatus (System B) shown with a flat-film membrane. . . . . 48

3.10 Pervaporation module for flat-film membranes. . . . . 49

3.11 Pervaporation module for a single hollow-fiber membrane. . . . . 51

4.1 Comparison of separation factor and water flux for new and original pervaporation apparatuses. An asymmetrically spun Matrimid® hollow fiber was tested with feed conditions alternating between 20 and 0 wt% acetic acid in water. . . . . 56

4.2 XRD patterns for MFI particles synthesized using Method A (Berghof reactor) and Method B (Pyrex® container). A reference ZSM-5 pattern is reproduced for comparison [99]. XRD patterns were provided by Dr. Jae Kyu Cho (Nair group, Georgia Tech). . . . . 57

4.3 SEM images of MFI particles synthesized using Method A (Berghof reactor) and Method B (Pyrex® container). SEM images were taken by Dr. Jae Kyu Cho (Nair group, Georgia Tech). . . . . 58

4.4 SEM cross-sections of flat-film membranes created with butanol-functionalized MFI in RTV615 polymer. Zeolite loadings range from 0 to 60 wt% MFI on a solvent-free basis. SEM images were taken by Dr. Jae Kyu Cho (Nair group, Georgia Tech). . . . . 59

4.5 SEM cross-sections of flat-film membranes created with butanol-functionalized MFI in DMS-V41/HMS-064 polymer. Zeolite loadings range from 0 to 60 wt% MFI on a solvent-free basis. SEM images were taken by Dr. Jae Kyu Cho (Nair group, Georgia Tech). . . . . 60

4.6 Fluxes and separation factors for flat films formed with the two-part RTV615 system and the three part DMS-V41/HMS-064 system. Butanol functionalized MFI particles were used for all membranes. Samples were tested with a 5 wt% ethanol feed at 65°C. Literature data for similar feed conditions are reproduced for comparison [44, 57, 67]. All fluxes have been normalized to a thickness of 100 $\mu$m. . . . . 62

4.7 Small "clumps" of crosslinked, rubbery polymer formed within DMS-V41/HMS-064 membranes during sonication. . . . . 63

4.8 SEM cross-sections of flat-film membranes created with unfunctionalized MFI in RTV615 polymer. Zeolite loadings range from 0 to 60 wt% MFI on a solvent-free basis. SEM images were taken by Dr. Jae Kyu Cho (Nair group, Georgia Tech). . . . . 64

4.9 Fluxes and separation factors for RTV615 flat films with unfunctionalized and butanol-functionalized MFI particles. Samples were tested with a 5 wt% ethanol feed at 65°C. Literature data for similar feed conditions are reproduced for comparison [44, 57, 67]. All fluxes have been normalized to a thickness of 100 $\mu$m. . . . . 66

4.10 Unfunctionalized (Vial A) and butanol-functionalized (Vial B) MFI in iso-octane after being sonicated for 15 min. Pictures were taken 30 sec, 2 min, 5 min, and 10 min after removal from the sonication bath. At 10 min, the vials were turned over to show the gel formed with the unfunctionalized MFI. . . . . 67

4.11 Fluxes and separation factors for RTV615 flat films with butanol-functionalized MFI particles. The low-temperature vacuum treatment involved placing the samples in a vacuum oven at 70°C for more than 18 hr. The high-temperature vacuum treatment was run in a vacuum oven at 110°C for more than 18 hr. Samples were tested with a 5 wt% ethanol feed at 65°C. Literature data for similar feed conditions are reproduced for comparison [44, 57, 67]. All fluxes have been normalized to a thickness of 100 $\mu$m. . . . . 69

4.12 SEM images of bare Torlon® hollow fibers. SEM images were taken by Dr. Madhava Kosuri (Koros group, Georgia Tech). . . . . 70

4.13 SEM images of Torlon® hollow fibers coated with one, two, and three coats of pure PDMS (RTV615, 0 wt% MFI). . . . . 71

4.14 Ethanol flux versus separation factor for 1-, 2-, and 3-coat pure PDMS samples tested with a 5 wt% ethanol feed at 65°C. . . . . 72

4.15 SEM images of Torlon® hollow fibers coated with one coat of pure PDMS (RTV615, 0 wt% MFI) using the dip-coat with and without presoaking. . . . . 74

4.16 SEM images of untreated and presoaked Torlon® hollow fibers coated with one coat 20 wt% unfunctionalized or butanol-functionalized MFI in PDMS using the U-tube method. . . . . 75

4.17 Ethanol flux versus separation factor for hollow fibers coated with one coat of pure PDMS (RTV615, 0 wt% MFI) using the dip-coat method with and without presoaking and the U-tube method with presoaking. Samples were tested with a 5 wt% ethanol feed at 65°C. . . . . 76

4.18 Ethanol flux versus separation factor for untreated or presoaked hollow fibers coated with one coat of 20 wt% MFI (unfunctionalized or butanol-functionalized) in PDMS using the U-tube method. Samples were tested with a 5 wt% ethanol feed at 65°C. . . . . 77

4.19 SEM images of presoaked Torlon® hollow fibers coated with one coat of pure PDMS (0 wt% MFI) using the dip-coat and U-tube methods. 78

4.20 SEM images of presoaked Torlon® hollow fibers coated with one coat of 0 wt% and 20 wt% MFI using the U-tube method. . . . . 80

4.21 Ethanol flux versus separation factor for presoaked hollow fibers coated with one coat of 0 or 20 wt% MFI (unfunctionalized or butanol-functionalized) in PDMS using the U-tube method. Samples were tested with a 5 wt% ethanol feed at 65°C. . . . . 81

# SUMMARY

Pervaporation with a "reverse-selective" (hydrophobic) membrane is a promising technology for the energy-efficient separation of alcohols from dilute alcohol-water streams, such as those formed in the production of biofuels. Pervaporation depends on the selectivity and throughput of the membrane, which in turn is highly dependent on the membrane material. A nanocomposite approach to membrane design is desirable in order to combine the advantages and eliminate the individual limitations of previously-reported polymeric and zeolitic membranes. In this work, a hollow-fiber membrane composed of a thin layer of polymer/zeolite nanocomposite material on a porous polymeric hollow fiber support is developed. The hollow fiber geometry offers considerable advantages in membrane surface area per unit volume, allowing for easier scaling and higher throughput than flat-film membranes.

Poly(dimethyl siloxane) (PDMS) and pure-silica MFI zeolite (silicalite-1) were investigated for these membranes. Iso-octane was used to dilute the dope solution to provide thinner coatings. Previously-spun non-selective Torlon® hollow fibers were used as the support layer for the nanocomposite coatings. To determine an acceptable method for coating fibers with uniform, defect-free coatings, flat-film membranes (0 to 60 wt% MFI on a solvent-free basis) and hollow-fiber membranes (0 and 20 wt% MFI) were fabricated using different procedures. Pervaporation experiments were run for all membranes at 65°C with a 5 wt% ethanol feed. The effects of membrane thickness, fiber pretreatment, coating method, zeolite loading, and zeolite surface treatment on membrane pervaporation performance were investigated.

For flat-film membranes, it was seen that increasing the molecular weight of the

pre-polymer slightly improved pervaporation performance, however, the membranes were more difficult to fabricate due to the lower work-life of the polymer, which resulted in the formation of clumps of crosslinked polymer embedded within the membrane. Similarly, better pervaporation performance was seen with unfunctionalized MFI zeolite particles than with butanol-functionalized MFI, but the unfunctionalized particles formed a gel-like substance in the organic solvent, which made membrane fabrication more difficult and less reproducible than when functionalized particles were used. Neither low- nor high-temperature vacuum treatments affected membrane performance.

Nanocomposite coatings on Torlon® hollow fibers were also created using various fabrication methods. The best flux through pure PDMS-coated fibers (0.526 kg/m$^2$hr) was very large compared to pure PDMS flat films in the literature (0.003-0.060 kg/m$^2$hr) while similar selectivities were achieved. This indicated that the very thin ($\sim$1-10 $\mu$m) coatings were defect-free. The thickness of the coatings was decreased by soaking the fibers in deionized water before coating with the dope solution. This presoaking step improved the membrane performance for pure PDMS samples. However, for 20 wt% MFI coatings, the presoaked coating thicknesses were extremely small and aggregates of MFI particles formed pinhole defects in the membranes, leading to a decrease in the pervaporation performance below the pure PDMS values. Several challenges have been identified for further development of our coated nanocomposite hollow-fiber membrane prototype into a highly selective nanocomposite membrane device.

# CHAPTER I

# INTRODUCTION

## *1.1 Background and Motivation*

As the world population grows and countries become more industrially developed, global energy demands and carbon dioxide emissions are expected to increase dramatically, as shown in Table 1.1. These rapidly increasing global energy demands, as well as the adverse environmental impacts of "carbon-positive" fossil fuel production and utilization, will require petroleum and natural gas supplies to be supplemented with as many alternative/renewable energy sources as possible. Production of renewable biofuels, such as ethanol and butanol, is expected to make up approximately 25%, or 20 million barrels per day, of total liquid fuel production by the year 2030 [1]. To become a viable alternative to fossil fuels, a prime requirement is that the biofuel production process must consume as little energy as possible relative to the biofuel energy content and relative to fossil fuel production. Current bioethanol production methods (using crops, lignocellulosic matter, or algae) all deliver a dilute aqueous alcohol stream (0.5-10 wt% ethanol) that must be purified to >99 wt% ethanol to meet transportation fuel standards [2]. As improvements are made to other stages in the biofuel production process, this purification step is quickly becoming the most energy-intensive part of the process.

For most mixtures, thermally-driven separation processes, such as distillation, provide an easy, well-established method for the purification of one or more components with distinct boiling points. However, for constant-boiling azeotropic mixtures, such as a mixture of ethanol and water, distillation can become capital- and energy-intensive, as additional steps must be used to purify the azeotrope to the desired

**Table 1.1:** Historical and projected global energy, petroleum, and natural gas demands and carbon dioxide emissions [1].

| Global Demand | Year 2000 | Year 2030 | % Increase |
|---|---|---|---|
| Total Energy (quadrillion BTU) | 400 | 600-850 | 50-110 |
| Petroleum (million barrels/day) | 76 | 98-138 | 29-82 |
| Natural Gas (billion $ft^3$/day) | 243 | 356-581 | 47-139 |
| $CO_2$ Emissions (billion metric tons) | 24 | 34-51 | 42-113 |

purity. There are several non-thermally-driven separation processes that may be able to offer inexpensive, energy-efficient alternatives to azeotropic distillation. Of these, one of the most promising processes is pervaporation, in which liquid feed components permeate through a membrane barrier at different rates and evaporate on the downstream side, after which they are condensed and collected. Pervaporation depends critically on the permselectivity and throughput of the membrane, which is influenced by the fundamental sorption and diffusion properties of the feed components in the membrane material.

In this work, a method of coating a hollow fiber with a polymer/zeolite nanocomposite was developed and studied for the pervaporation of ethanol from dilute aqueous solutions. Once optimized, this membrane could permeate alcohol directly from dilute aqueous streams leaving the fermentation process, completely eliminating the need for energy-intensive distillation processes.

### 1.1.1 Biofuel Production Processes

Although the majority of biofuels are currently produced from agricultural crops, such as corn and sugar cane, many other sources of biomass may also be used, ranging from intentionally grown materials, such as algae, to agricultural and industrial waste materials, such as plant trimmings, pulp and paper sludge, and wood chips [3, 4]. As discussed in the literature, there are several environmental and economic issues surrounding the use of corn or other food products for biofuel production [3–9]. Many

of these concerns, such as soil erosion, excess water usage, increased greenhouse gas emissions, fertilization demands, and rising food prices, may be resolved with the use of alternative, non-food biomass [4]. Early in the development of bioethanol production processes, some studies found that biomass-to-ethanol processes had a net-negative energy balance [10–14]. However, process improvements over the past few decades have increased the conversion efficiency. With few exceptions [15–18], recent reports find that corn ethanol production is a net-positive energy process, meaning the ethanol produced contains more energy than the energy required to produce it [19–32].

A common bio-based conversion to ethanol is shown in Figure 1.1. For lignocellulosic starting materials, an enzymatic process is usually employed to produce ethanol. The starting biomass is first pretreated to make the cellulose fibers more accessible to the enzymes, which increases the speed of conversion of cellulose to glucose and increases the yield. The resulting hemicellulose and cellulose are then hydrolyzed to release sugars. The sugars are fermented, producing a dilute ethanol stream that is typically 0.5-10 wt% ethanol. This product stream is usually filtered to remove yeast and crop particles and then purified to the final fuel-grade purity using one of the methods described in Section 1.1.2. Once separated from the ethanol, "stillage" (residual water containing yeast cells, soluble nutrients, and crop particles) can be used directly as a fertilizer for crops, or evaporated to produce animal feeds (distillers' dried grains or distillers' dried solubles), or used to produce methane biogas. Lignin residues may be processed to generate steam for electricity generation. [33]

Over the past few decades, many advances have been made in the conversion efficiency of biomass to ethanol in the biofuel production process. Although there have also been many advancements in separation technologies for purifying biofuels, purification remains the most energy-intensive step in biofuel production.

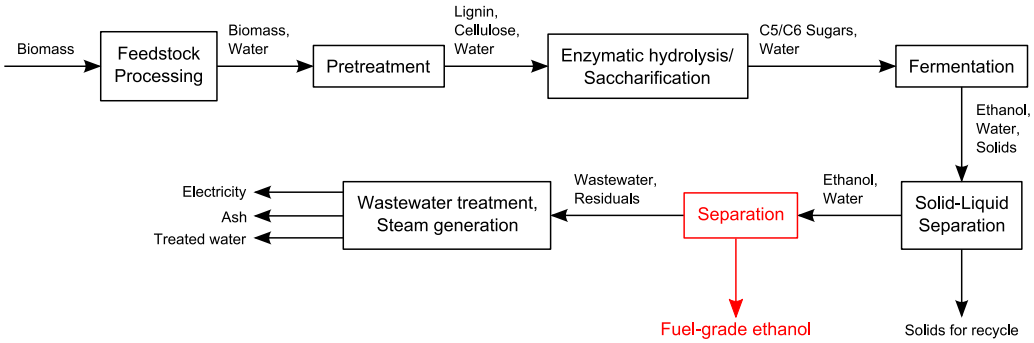


**Figure 1.1:** Flow diagram of a typical biomass-to-ethanol process.

### 1.1.2 Potential Separation Technologies for Dilute Biofuel/Water Streams

Purification of ethanol or butanol from dilute aqueous streams is commonly performed in two stages. First, alcohol is recovered from the dilute aqueous stream leaving the fermenter, resulting in a concentrated alcohol stream (~80-95 wt% alcohol). Second, the concentrated alcohol stream is dehydrated (for example, using molecular sieves or hydrophilic pervaporation) to give fuel-grade alcohol. Common alcohol recovery methods will be discussed briefly below. A more detailed description of each separation method may be found in Vane's review of separation technologies for fermentation broths [34] and references within.

**Distillation** The most commonly employed alcohol recovery technology in biofuel plants is distillation, which separates alcohol from water using the different volatilities of the components in a boiling liquid mixture. For *dilute* streams, the vapor-liquid equilibrium (VLE) behavior for mixtures of ethanol or $n$-butanol with water (see Figure 1.2(a)) is ideal for distillation. This is illustrated by the relative volatility, which is defined as the ratio of vapor concentrations divided by the ratio of liquid concentrations ($\beta_{AW} = (y_A/y_W)/(x_A/x_W)$). A large $\beta_{AW}$ value indicates a large degree of separation between the two components is possible using thermal methods. As shown in Figure 1.2(b), the relative volatility is favorable for both systems at low alcohol concentrations. However, $\beta_{AW}$ quickly decreases for both systems

as the alcohol concentration increases, making distillation unfavorable as the alcohol streams are purified.

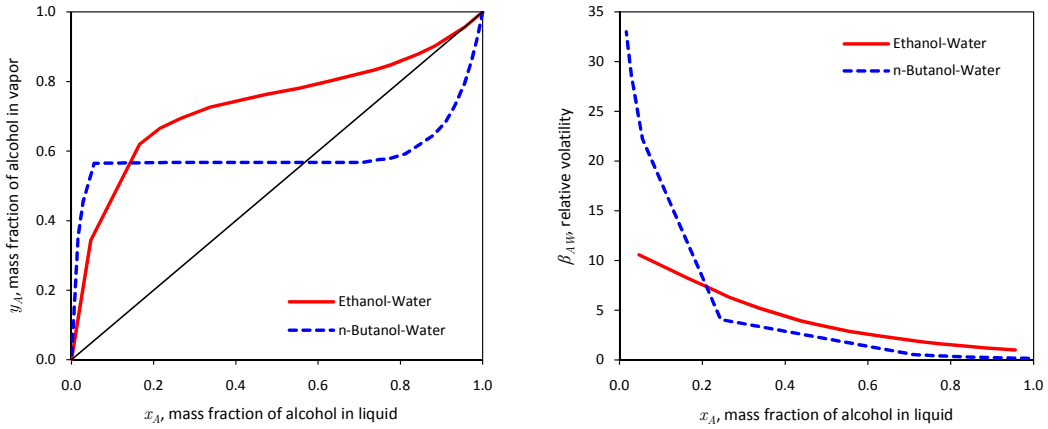


(a) (b)

**Figure 1.2:** (a) Vapor-liquid equilibrium curves for ethanol-water and $n$-butanol-water mixtures at 101.3 kPa. (b) Effect of alcohol concentration on the relative volatility of ethanol or $n$-butanol over water, $\beta_{AW}$. VLE data from [35].

Azeotropes present another difficulty that must be dealt with in distillation. At atmospheric pressure, the ethanol-water and $n$-butanol-water mixtures form minimum-boiling azeotropes at 95.6 wt% ethanol (78.15°C) and 57.8 wt% $n$-butanol (92.25°C), respectively [35]. For ethanol separations, the azeotrope can be overcome by introducing an entrainer, such as benzene, to change the VLE behavior. This azeotropic (or ternary) distillation, shown schematically in Figure 1.3(a), requires additional distillation columns for the introduction and recovery of the entrainer.

The $n$-butanol-water system behaves differently than the ethanol-water system since butanol is soluble in water up to only ∼7.7 wt%. Above this limit, two liquid phases are formed. At the azeotrope, the upper and lower phases consist of 79.9 and 7.7 wt% $n$-butanol, respectively. Since the VLE behaviors at these compositions are favorable, the two phases can be decanted into separate distillation columns for further separation. However, since water is more volatile than $n$-butanol, large amounts of

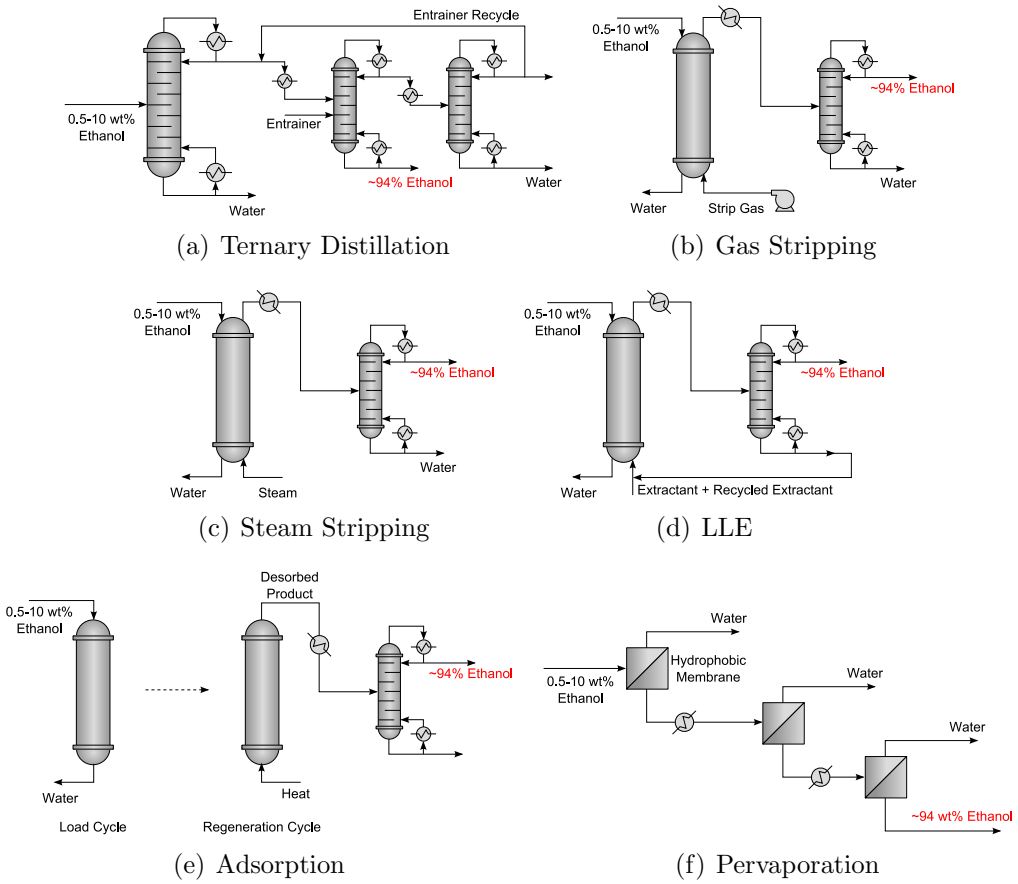


(a) Ternary Distillation (b) Gas Stripping

(c) Steam Stripping (d) LLE

(e) Adsorption (f) Pervaporation

**Figure 1.3:** Separation process alternatives. In all processes, the concentrated ethanol must be further dehydrated to fuel-grade purity using molecular sieves, hydrophilic pervaporation, or another dehydration process.

water must be evaporated to reach a pure *n*-butanol bottoms stream, making the separation process energy-intensive.

Distillation energy requirements include reboilers, condensers, and pumps. For a typical distillation setup, a 5 wt% ethanol feed requires ∼5.2-6.9 MJ of fuel equivalents to produce 1 kg of ethanol [34]. For comparison, 29.7 MJ is stored in 1 kg of ethanol.

**Gas Stripping** Separation by gas stripping is performed by passing the alcohol-water stream and an inert gas (such as carbon dioxide) through a gas-liquid contactor, as shown in Figure 1.3(b). Alcohol and water equilibrate in the gas phase and are later recovered by condensation, membrane separation, or adsorption.

The degree of ethanol recovery depends on the strip gas and the condensation temperature, among other things. A simulated gas stripping process using carbon dioxide as the strip gas and a condensation temperature of -10°C recovered ∼80% of the ethanol from a 5 wt% feed [34]. This separation method is capable of purifying ethanol to ∼60 wt%, after which an additional distillation step is used to reach the azeotrope and a dehydration step is used to reach the fuel-grade purity.

The energy requirements for gas stripping include heating the column to counteract evaporative cooling, powering a blower to move the inert gas through the column, condensing the ethanol and water from the inert gas, and an additional distillation step to reach the azeotrope from ∼60 wt% ethanol. For a simulated 5 wt% ethanol feed using carbon dioxide as the strip gas in a 35°C column with a -10°C fractional chiller and an additional distillation column to reach 94 wt% ethanol, ∼9.0 MJ of fuel equivalents are required to produce 1 kg of ethanol [34].

**Steam Stripping** Separation by steam stripping, shown in Figure 1.3(c), is similar to gas stripping. The alcohol-water stream is contacted with steam, which eliminates the need for a blower and allows for complete condensation of the concentrated alcohol stream. Steam stripping can achieve ethanol recoveries greater than 95% and does not require such low temperatures for condensing the alcohol and water. As with gas stripping, this separation method is capable of purifying ethanol to ∼60 wt% and an additional distillation step must be used to reach the azeotrope [34].

For a simulated 5 wt% ethanol feed in a 35°C column with a 20°C fractional chiller and an additional distillation column to reach 94 wt% ethanol, ∼6.1 MJ of fuel equivalents are required to produced 1 kg of ethanol using steam stripping [34].

**Liquid-Liquid Extraction** In liquid-liquid extraction (LLE), shown in Figure 1.3(d), the alcohol-water stream is contacted with an extractant liquid. Components

absorb into the extractant and are removed in a regeneration unit. Selecting an appropriate extractant depends on several factors. The separation factor of alcohol over water, $\beta_{AW}$, and the equilibrium distribution coefficient, $K_D$ ($\beta_{AW} = K_{D,A}/K_{D,W}$), affect the purity of the concentrated alcohol stream and the amount of extractant that will be necessary for the separation. There is a tradeoff between the selectivity and the amount of the extractant required. Extractant regeneration can be accomplished by vacuum flash vaporization, distillation, gas stripping, or membrane-based pervaporation. Depending on the method used, the mutual solubility, ability to separate the extractant and aqueous phases, interfacial tension, extractant viscosity, and extractant volatility may be important. Finally, the toxicity, safety, reactivity, and cost should be taken into account.

Extractant regeneration energies for a 5 wt% ethanol feed were estimated by Vane to be 5.7, 3.3, and 2.1 MJ of fuel equivalents per kg of ethanol for extractant separation factors of 10, 20, and 40, respectively [34]. Feldman estimated the total energy demands for a 4.5 wt% ethanol feed to be 6.1 MJ of fuel equivalents to produce 1 kg of ethanol using 5,6,7,8-tetrahydroquinoline as the extractant and an additional distillation column to reach the azeotrope [36].

**Adsorption** Another way to recover alcohols is by passing them over solid adsorbent materials. The adsorbent typically remains stationary in a packed-column contactor and the process is run in a series of loading and regeneration cycles, as shown in Figure 1.3(e). Similar to LLE extractants, adsorbents are chosen based on their $\beta_{AW}$ and $K_D$ properties. Hydrophobic zeolites, polymeric resins, and activated carbon have been studied as adsorbents for alcohol-water streams. Holtzapple and Brown calculated the energy required to produce 95 wt% ethanol from a 5 wt% feed [37]. Silicalite-1 was used as the adsorbent and distillation was required to reach the azeotrope. With these conditions, the process required 10.7 MJ of fuel equivalents to

produce 1 kg of ethanol.

**Reverse-Selective Pervaporation** Another promising alcohol recovery technique is pervaporation, in which the dilute alcohol-water stream is passed through a selective membrane and concentrated alcohol is condensed downstream. Pervaporation is illustrated in Figure 1.3(f). Hydrophilic, water-selective pervaporation is already commonly used for dehydrating alcohol enriched streams (∼90 wt% ethanol) to meet the final fuel-grade purity. Hydrophobic membranes for alcohol recovery must have a high separation factor for alcohol over water and must have a high alcohol throughput. Research into membrane design for alcohol recovery is discussed in the next section.

Energy requirements for pervaporation include heat addition to counteract evaporative cooling, condensation of the permeated ethanol and water, and energy required to operate a vacuum pump. For a 5 wt% ethanol feed and using membranes with $\beta$=8, 15, 30, or 60, Vane estimated the energy required for pervaporation to be approximately 15.7, 9.0, 5.0, or 3.0 MJ of fuel equivalents to produce 1 kg of ethanol, respectively [34]. For these separation factors, the permeated ethanol concentration after a single pass would be approximately 30, 44, 61, and 76 wt%. By passing the alcohol-water stream through several membranes in series, the dilute alcohol stream could be concentrated to near-azeotrope without needing a final distillation step.

## *1.2 Membranes for Pervaporation*

A wide range of materials, including polymers, ceramics, glass, metals, liquids, and gases, have been used to form membranes for various applications [38]. This thesis focuses heavily on polymeric and zeolitic membranes, but overviews of other membrane materials can be found in the works of Baker [39] and Mulder [40] on membrane technologies.

### 1.2.1 Polymeric Membranes

Polymers have long dominated membrane technology because of their versatility and relative ease of processing. However, polymeric membranes suffer from certain fundamental shortcomings for demanding applications such as the separation of ethanol or butanol from a dilute aqueous stream. Pure polymeric membranes are constrained by relatively slow ethanol transport, shown in Figure 1.4, as well as a deteriorated performance due to swelling when exposed to highly aqueous feed streams [41].

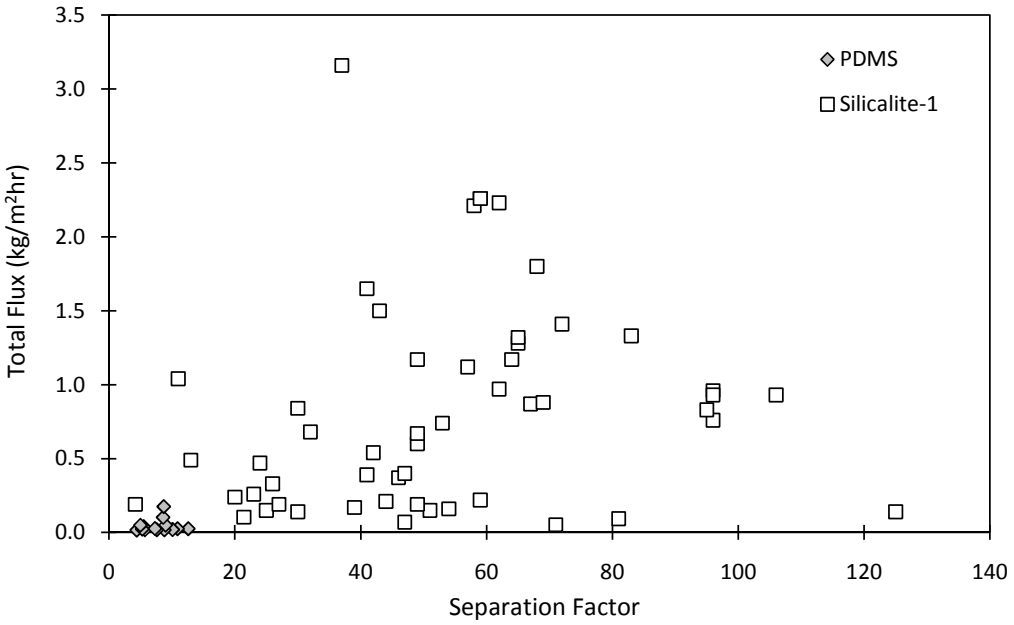


**Figure 1.4:** Reported pervaporation performances for polymeric and zeolitic membranes [42–58].

Although polymeric membranes are not ideal for dilute alcohol streams, conventional hydrophilic polymeric membranes are effective for dehydrating alcohol-enriched streams (∼90 wt% alcohol) to meet the final fuel-grade purity. Commercial ethanol dehydration membranes are available from Mitsui & Co., Membrane Technology and Research (MTR), Vaperma, and Sulzer Chemtech.

### 1.2.2 Zeolitic Membranes

High-performance, low-cost nanostructured materials, such as zeolites, have been investigated to overcome the difficulties encountered with pure polymeric membranes. Zeolites are nanoporous aluminosilicate crystalline materials that have pores of extremely precise dimensions and tunable hydrophilicity/hydrophobicity [45, 59–61]. Additionally, zeolitic membranes do not swell and are more chemically and thermally stable than polymeric membranes [60]. These properties allow them to exhibit high preferential selectivity for molecules based on shape, size, and polarity. However, zeolitic membranes are much more expensive to manufacture and are more brittle than polymeric membranes [60]. Data reported in the literature for ethanol-water separations using zeolitic membranes are reproduced in Figure 1.4.

### 1.2.3 Composite Flat-Film Membranes

To combine the positive aspects and eliminate the individual limitations of polymeric and zeolitic membranes, a nanocomposite approach is desirable, such as that shown in Figure 1.5. Composite films of this nature have been demonstrated over the last decade, but all reported membranes are thick (50-500 $\mu$m), laboratory-scale, flat-films [44–47, 52, 57, 62–67]. A thorough review of MMM flat film performance was conducted by Vane [3]. These composite flat-films show the highly selective separation characteristics expected from the incorporation of zeolite nanoparticles into polymers, but they are limited by a low throughput and are difficult to scale up for industrial applications.

### 1.2.4 Proposed Composite Hollow-Fiber Membranes

In this thesis, a hollow-fiber membrane composed of a thin ($\sim$5 $\mu$m) layer of polymer/zeolite nanocomposite material on a porous polymeric hollow-fiber support is developed. A cross-section of the proposed fiber is shown in Figure 1.6(a). Large numbers of these hollow fibers can be bundled together in compact modules (Figure

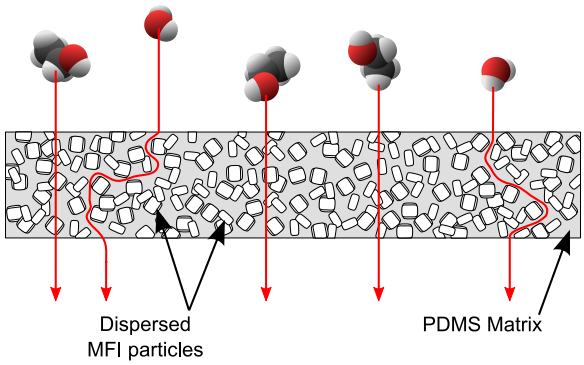


**Figure 1.5:** Schematic diagram of a mixed-matrix membrane showing the preferential transport of ethanol.

1.6(b)) that can be used in series or in parallel for industrial use. To form a module, the ends of the fiber bundle are encapsulated in resin. A vacuum is applied to the inner bores ("tube-side") of the fibers, thereby drawing alcohol from the "shell-side" through to be collected downstream while water is hindered by the hydrophobicity of the membrane.

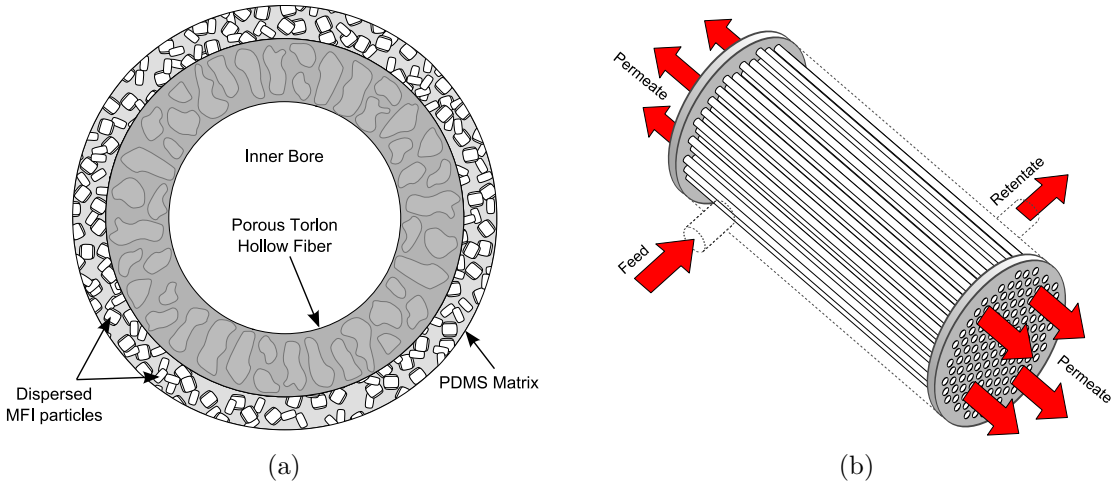


**Figure 1.6:** (a) Cross-section of a polymer/zeolite nanocomposite coating on a porous polymeric hollow-fiber support. (b) Hollow-fiber membrane module with shell-side feed, composed of many hollow fibers bundled together and encapsulated in resin.

Unlike the flat-film geometry, hollow fibers offer considerable advantages in membrane surface area per unit volume. In general, the production rate and scalability of a membrane module can be improved by increasing its area density, which is the

ratio of the membrane surface area to the volume of the module. A single hollow-fiber module can reach area densities of $\sim 5,000 - 10,000$ $m^2/m^3$, depending on the outer diameter of the fibers and the number of fibers in the bundle. For comparison, flat-film membranes can be packaged in plate-and-frame or spiral-wound modules, which have area densities of $\sim 350 - 700$ $m^2/m^3$ and $\sim 3,500$ $m^2/m^3$, respectively [68]. The large area density of hollow-fiber modules provides a high throughput and makes them easily scalable to industrial needs.

## *1.3 Research Objectives and Strategies*

The main objective of this thesis is to develop a method for forming a uniform, defect-free polymer/zeolite nanocomposite layer on a porous hollow-fiber support. Once developed, this method may be used to fabricate and optimize a reverse-selective polymer/zeolite nanocomposite hollow-fiber membrane that can selectively remove ethanol or butanol from a dilute aqueous stream.

To achieve this objective, the following goals are proposed:

- Build a pervaporation system capable of characterizing the flux and selectivity of hollow-fiber or flat-film membranes.
- Study the effect of dope compositions and coating methods in order to determine an acceptable method for coating fibers with uniform, defect-free coatings.
- Perform pervaporation experiments with coated hollow fibers to determine membrane performance for ethanol-water mixtures.
- Identify the main scientific or technological challenges for optimizing the performance of these membranes for practical applications in ethanol-water separations.

## *1.4 Organization of Dissertation*

A brief introduction to biofuel production and membrane separations has been given in this chapter. In Chapter 2, transport phenomena through polymeric and mixed-matrix membranes will be described. Membrane formation and performance will also be reviewed. The materials and procedures used for this thesis will be presented in Chapter 3. Chapter 4 will discuss the results of various dope concentrations and coating methods. Our conclusions and recommendations for further studies will be presented in Chapter 5.

# CHAPTER II

# MEMBRANE FUNDAMENTALS

Many variables affect the development of membranes for economical biofuel separation processes. Membrane material selection, membrane geometry, module design, and numerous processing parameters and operating variables may affect separation performance. In this chapter, the theory of transport through polymeric and mixed-matrix membranes (MMM) will first be given. Then a brief review of the known effects of significant parameters on membrane performance will be discussed.

## *2.1 Mechanism of Liquid Transport in Polymeric and Mixed-Matrix Membranes*

### 2.1.1 Transport in a Dense Film

The solution-diffusion model is commonly used to predict transport properties in polymeric membranes. A detailed review of the solution-diffusion model is provided by Wijmans and Baker [69].

The flux of a component through a membrane barrier is proportional to its chemical potential gradient,

$$J_i = -L_i \frac{d\mu_i}{dz}, \tag{2.1}$$

where $L_i$ is a proportionality coefficient and $d\mu_i/dz$ is the chemical potential gradient of component $i$. In pervaporation, pressure and concentration gradients exist across the membrane, in which case the chemical potential may be written as

$$d\mu_i = RTd\ln(\gamma_i x_i) + v_i dp, \tag{2.2}$$

where $R$ is the gas law constant, $T$ is the temperature, $\gamma_i$ is the activity coefficient of component $i$, $x_i$ is the mole fraction of component $i$, $v_i$ is the molar volume of

component $i$, and $p$ is the pressure.

The solution-diffusion model assumes equilibrium at both membrane interfaces: between the feed liquid and the membrane material at the upstream interface, and between the vapor permeate and the membrane material at the downstream interface. This assumption provides a continuous chemical potential gradient across the membrane and implies adsorption and desorption rates in the membrane are much greater than diffusion rates through the membrane. The model also assumes that the pressure within the membrane remains constant at the upstream value and the concentration profile within the membrane is linear. With these assumptions, $d\mu_i/dz$ can be found using Equation 2.2 with constant pressure:

$$\begin{aligned} \frac{d\mu_i}{dz} &= RT\frac{d\ln(\gamma_i x_i)}{dz} + v_i\frac{dp}{dz} \\ &= \frac{RT}{\gamma_i x_i}\frac{d(\gamma_i x_i)}{dz} + 0 \\ &= \frac{RT}{x_i}\frac{dx_i}{dz} \\ &= \frac{RT}{c_i}\frac{dc_i}{dz}, \end{aligned} \tag{2.3}$$

where $c_i = x_i c$ is the concentration of component $i$. Substituting this expression into Equation 2.1 gives

$$J_i = -\frac{RTL_i}{c_i}\frac{dc_i}{dz}, \tag{2.4}$$

which is analogous to Fick's law and can be rewritten using the diffusion coefficient, $D_i = RTL_i/c_i$:

$$J_i = -D_i\frac{dc_i}{dz} \tag{2.5}$$

Using the assumption that the concentration profile is linear, this expression can be integrated over the thickness of the selective layer of the membrane, from $z = 0$ to $z = l$, to yield

$$J_i = -\frac{D_i}{l}(c_{i_{m_l}} - c_{i_{m_0}}), \tag{2.6}$$

where $c_{i_{m_0}}$ and $c_{i_{m_l}}$ are the concentration of $i$ in the membrane at $z = 0$ and $z = l$, respectively.

The flux through the membrane can also be expressed in terms of the solubility of the components in the membrane. As mentioned above, the solution-diffusion model assumes the liquid feed and the vapor permeate are in equilibrium with the membrane. Using this assumption, the chemical potentials of the two phases can be equated to find expressions for $c_{i_{m_0}}$ and $c_{i_{m_l}}$ in terms of the component sorption coefficients. For an incompressible fluid, where $v_i$ is independent of pressure, Equation 2.2 can be integrated to yield

$$\mu_i = \mu_i^o + RT \ln \left( \frac{\gamma_i x_i}{\gamma_i^o x_i^o} \right) + v_i (p - p^o). \tag{2.7}$$

Taking the reference chemical potential, $\mu_i^o$, to be the chemical potential of pure $i$ ($\gamma_i^o x_i^o = 1$) at the saturation vapor pressure, $p^o = p_{i_{\text{sat}}}$, Equation 2.7 can be written as

$$\mu_i = \mu_i^o + RT \ln (\gamma_i x_i) + v_i (p - p_{i_{\text{sat}}}). \tag{2.8}$$

For a compressible gas, assuming ideal behavior, $v_i = RT/p$, Equation 2.2 can be integrated to yield

$$\mu_i = \mu_i^o + RT \ln \left( \frac{\gamma_i x_i}{\gamma_i^o x_i^o} \right) + RT \ln \left( \frac{p}{p^o} \right). \tag{2.9}$$

Again, taking the reference chemical potential to be the chemical potential of pure $i$ at the saturation vapor pressure, Equation 2.9 can be written as

$$\mu_i = \mu_i^o + RT \ln (\gamma_i x_i) + RT \ln (p/p_{i_{\text{sat}}}). \tag{2.10}$$

Using the assumption of equilibrium at the upstream interface, Equation 2.8 can be written for both the liquid feed solution (subscript $F$) and the membrane at $z = 0$

(subscript $m_0$):

$$\begin{aligned}
\mu_{i_F} &= \mu_{i_{m_0}}, \\
\mu_i^o + RT\ln\left(\gamma_{i_F}x_{i_F}\right) + v_i(p_F - p_{i_{\text{sat}}}) &= \mu_i^o + RT\ln\left(\gamma_{i_{m_0}}x_{i_{m_0}}\right) + v_i(p_F - p_{i_{\text{sat}}}), \\
RT\ln\left(\gamma_{i_F}x_{i_F}\right) &= RT\ln\left(\gamma_{i_{m_0}}x_{i_{m_0}}\right), \\
\gamma_{i_F}x_{i_F} &= \gamma_{i_{m_0}}x_{i_{m_0}}, \\
\gamma_{i_F}c_{i_F} &= \gamma_{i_{m_0}}c_{i_{m_0}}.
\end{aligned} \tag{2.11}$$

Rearranging Equation 2.11, the concentration of $i$ in the membrane at $z = 0$ can be written as

$$c_{i_{m_0}} = \frac{\gamma_{i_F}}{\gamma_{i_{m_0}}}c_{i_F} = S_i^L c_{i_F}, \tag{2.12}$$

where $S_i^L$ is the liquid-phase sorption coefficient, defined as $S_i^L = \gamma_{i_F}/\gamma_{i_{m_0}}$.

Similarly, using the assumption of equilibrium at the downstream interface, Equation 2.8 is written for the membrane at $z = l$ (subscript $m_l$) and Equation 2.10 is written for the vapor permeate (subscript $P$):

$$\begin{aligned}
\mu_{i_{m_l}} &= \mu_{i_P}, \\
\mu_i^o + RT\ln\left(\gamma_{i_{m_l}}x_{i_{m_l}}\right) + v_i(p_F - p_{i_{\text{sat}}}) &= \mu_i^o + RT\ln\left(\gamma_{i_P}x_{i_P}\right) + RT\ln\left(p_P/p_{i_{\text{sat}}}\right), \\
\ln\left(\gamma_{i_{m_l}}x_{i_{m_l}}\right) + v_i(p_F - p_{i_{\text{sat}}})/RT &= \ln\left(\gamma_{i_P}x_{i_P}\right) + \ln\left(p_P/p_{i_{\text{sat}}}\right), \\
\ln\left(\gamma_{i_{m_l}}x_{i_{m_l}}\exp\left[\frac{v_i}{RT}(p_F - p_{i_{\text{sat}}})\right]\right) &= \ln\left(\gamma_{i_P}x_{i_P}\frac{p_P}{p_{i_{\text{sat}}}}\right), \\
\gamma_{i_{m_l}}x_{i_{m_l}}\exp\left[\frac{v_i}{RT}(p_F - p_{i_{\text{sat}}})\right] &= \gamma_{i_P}x_{i_P}\frac{p_P}{p_{i_{\text{sat}}}}, \\
\gamma_{i_{m_l}}c_{i_{m_l}}\exp\left[\frac{v_i}{RT}(p_F - p_{i_{\text{sat}}})\right] &= \gamma_{i_P}c_{i_P}\frac{p_P}{p_{i_{\text{sat}}}}.
\end{aligned} \tag{2.13}$$

Rearranging for $c_{i_{m_l}}$ gives

$$c_{i_{m_l}} = \frac{\gamma_{i_P}c_{i_P}p_P}{\gamma_{i_{m_l}}p_{i_{\text{sat}}}}\exp\left[-\frac{v_i}{RT}(p_F - p_{i_{\text{sat}}})\right]. \tag{2.14}$$

The quantity $v_i(p_F - p_{i_{\text{sat}}})/RT$ is small, yielding an exponential term close to unity. Using this simplification, the concentration of $i$ in the membrane at $z = l$ can be

written as

$$c_{i_{m_l}} = \frac{\gamma_{i_P}}{\gamma_{i_{m_l}} p_{i_{\text{sat}}}} c_{i_P} p_P = \frac{\gamma_{i_P}}{\gamma_{i_{m_l}} p_{i_{\text{sat}}}} p_{i_P} = S_i^G p_{i_P}, \tag{2.15}$$

where $p_{i_P}$ is the partial pressure of $i$ in the permeate and $S_i^G$ is the gas-phase sorption coefficient, defined as $S_i^G = \gamma_{i_P}/\gamma_{i_{m_l}} p_{i_{\text{sat}}}$.

Before substituting Equations 2.12 and 2.15 into Fick's law, it is desirable to express $c_{i_{m_0}}$ in terms of $S_i^G$ instead of $S_i^L$. To do this, a hypothetical vapor phase is assumed to be in equilibrium with the liquid feed at the membrane interface. Using this assumption, the chemical potential of the liquid phase (superscript $L$) can be equated with the hypothetical gas phase (superscript $G$):

$$\begin{aligned}
\mu_{i_F}^L &= \mu_{i_F}^G, \\
\mu_i^o + RT \ln\left(\gamma_{i_F}^L x_{i_F}^L\right) + v_i(p_F - p_{i_{\text{sat}}}) &= \mu_i^o + RT \ln\left(\gamma_{i_F}^G x_{i_F}^G\right) + RT \ln\left(p_F/p_{i_{\text{sat}}}\right), \\
\ln\left(\gamma_{i_F}^L x_{i_F}^L\right) + v_i(p_F - p_{i_{\text{sat}}})/RT &= \ln\left(\gamma_{i_F}^G x_{i_F}^G\right) + \ln\left(p_F/p_{i_{\text{sat}}}\right), \\
\ln\left(\gamma_{i_F}^L x_{i_F}^L \exp\left[\frac{v_i}{RT}(p_F - p_{i_{\text{sat}}})\right]\right) &= \ln\left(\gamma_{i_F}^G x_{i_F}^G \frac{p_F}{p_{i_{\text{sat}}}}\right), \\
\gamma_{i_F}^L x_{i_F}^L \exp\left[\frac{v_i}{RT}(p_F - p_{i_{\text{sat}}})\right] &= \gamma_{i_F}^G x_{i_F}^G \frac{p_F}{p_{i_{\text{sat}}}}, \\
\gamma_{i_F}^L c_{i_F}^L \exp\left[\frac{v_i}{RT}(p_F - p_{i_{\text{sat}}})\right] &= \gamma_{i_F}^G c_{i_F}^G \frac{p_F}{p_{i_{\text{sat}}}}.
\end{aligned} \tag{2.16}$$

Using the assumption that $v_i(p_F - p_{i_{\text{sat}}})/RT$ is small, this can be rearranged for $c_{i_F}$ ($c_{i_F} = c_{i_F}^L, \gamma_{i_F} = \gamma_{i_F}^L$) to give

$$c_{i_F} = \frac{\gamma_{i_F}^G}{\gamma_{i_F} p_{i_{\text{sat}}}} c_{i_F}^G p_F = \frac{\gamma_{i_F}^G}{\gamma_{i_F} p_{i_{\text{sat}}}} p_{i_F}, \tag{2.17}$$

where $p_{i_F}$ is the partial pressure of the hypothetical gas in equilibrium with the feed liquid. The quantity $(\gamma_{i_F} p_{i_{\text{sat}}})/\gamma_{i_F}^G$ is the Henry's law coefficient. Substituting Equation 2.17 into Equation 2.12 gives

$$c_{i_{m_0}} = \frac{\gamma_{i_F}}{\gamma_{i_{m_0}}} \left(\frac{\gamma_{i_F}^G p_{i_F}}{\gamma_{i_F} p_{i_{\text{sat}}}}\right) = \frac{\gamma_{i_F}^G}{\gamma_{i_{m_0}} p_{i_{\text{sat}}}} p_{i_F} = S_i^G p_{i_F}. \tag{2.18}$$

Now the expressions for $c_{i_{m_0}}$ in Equation 2.18 and $c_{i_{m_l}}$ in Equation 2.15 can be substituted into Equation 2.6:

$$J_i = -\frac{D_i S_i^G}{l}(p_{i_P} - p_{i_F}). \tag{2.19}$$

The product $D_i S_i^G$ is the permeability of $i$ in the membrane, $P_i$. When the thickness of the selective layer is difficult to determine, the membrane permeance, $\mathcal{P}_i$, defined as the ratio of the permeability to the thickness of the selective layer, is often measured instead:

$$J_i = -\frac{P_i}{l}(p_{i_P} - p_{i_F}) = -\mathcal{P}_i(p_{i_P} - p_{i_F}). \tag{2.20}$$

The degree of separation is usually gauged by the separation factor or selectivity of the membrane. The separation factor is given by

$$\alpha_{a/b} = \frac{y_a/y_b}{x_a/x_b} = \frac{J_a/J_b}{x_a/x_b}, \tag{2.21}$$

where $y_i$ is the mass fraction of component $i$ in the permeate and $x_i$ is the mass fraction of component $i$ in the feed. The selectivity of the membrane is given by

$$\beta_{a/b} = \frac{P_a}{P_b} = \frac{\mathcal{P}_a}{\mathcal{P}_b}. \tag{2.22}$$

For the pervaporation of a binary mixture of alcohol (A) and water (W), the component fluxes through a membrane can be calculated from the amount of permeate collected per unit membrane area and unit time:

$$J_A = \frac{y_A w}{At} \tag{2.23}$$

$$J_W = \frac{(1 - y_A)w}{At} \tag{2.24}$$

$$J_{Total} = J_A + J_W = \frac{w}{At}, \tag{2.25}$$

where $y_A$ is the mass fraction of alcohol in the permeate, $w$ is the total weight of the collected permeate, $A$ is the membrane surface area available for separation, and $t$ is the total collection time. The separation factor can be determined using

$$\alpha_{A/W} = \frac{y_A/(1 - y_A)}{x_A/(1 - x_A)}, \tag{2.26}$$

where $x_A$ is the mass fraction of alcohol in the feed.

### 2.1.2 Transport in a Composite Film

Figure 2.1 shows the transport of ethanol and water through a composite zeolite-polymer membrane. The theory for permeation through dense films may be used with composite films if an effective permeability, $P_{eff}$, is used. Many models have been developed to predict $P_{eff}$ for zeolite-polymer membranes. For instance, the Maxwell model has been applied to estimate $P_{eff}$ for mixed-matrix membranes [70–75]. For a dilute concentration of spherical particles dispersed in a homogeneous matrix, $P_{eff}$ is found using

$$\frac{P_{eff}}{P_p} = 1 + 3\phi_z \left( \frac{\frac{P_z}{P_p} + 2}{\frac{P_z}{P_p} - 1} - \phi_z \right)^{-1} = \frac{P_z + 2P_p - 2\phi_z(P_p - P_z)}{P_z + 2P_p + \phi_z(P_p - P_z)}, \tag{2.27}$$

where $P_p$ and $P_z$ are the permeability of the polymer and zeolite, respectively, and $\phi_z$ is the volume fraction of zeolite particles in the membrane. Although developed for dilute concentrations, the Maxwell model has also been shown to work for higher volume fractions [70].

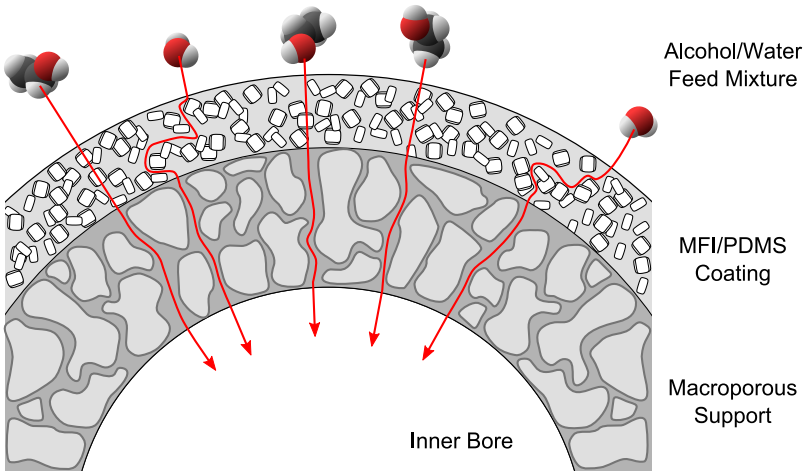


**Figure 2.1:** The preferential transport of ethanol through the zeolite/polymer coating.

If voids are formed between the zeolite and the polymer, a three-phase Maxwell model can be employed [76]. To use the three-phase model, $P_z$ in Equation 2.27 is

replaced with $P_{z,eff}$:

$$\frac{P_{z,eff}}{P_i} = \frac{P_z + 2P_i - 2\phi_s(P_i - P_z)}{P_z + 2P_i + \phi_s(P_i - P_z)}, \tag{2.28}$$

where $P_i$ is the permeability of the interfacial voids and $\phi_s = \phi_z/(\phi_z + \phi_s)$ is the volume fraction of zeolite contained in the zeolite + interfacial region.

## *2.2 Membrane Material Selection*

There are several aspects that characterize a desirable membrane. First and foremost, the membrane must have a high permeability and selectivity for the desired component. The permeability and selectivity of the membrane are directly related to the sorption and diffusion properties of the feed components in the membrane materials. The membrane materials must also be chemically, mechanically, and thermally stable in the separation environment, and little or no fouling of the membrane should occur during operation. With these criteria in mind, the materials commonly chosen for mixed matrix membranes for ethanol-water separation will be discussed below.

### 2.2.1 Polymer Selection

Of the several polymers have been investigated for ethanol-water separations, poly(dimethyl siloxane) (PDMS), shown in Figure 2.2, has been studied most frequently [3]. PDMS is an elastomeric (rubbery) polymer with mechanical properties that have been shown to improve with the addition of zeolite particles [47, 62, 77]. PDMS is also highly hydrophobic and preferentially sorbs ethanol over water [47], making it a good matrix polymer for composite membranes targeted at ethanol-water separations.

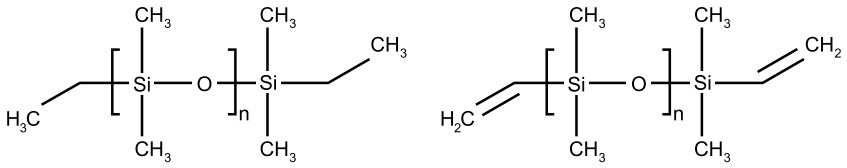


**Figure 2.2:** Structure of (a) poly(dimethyl siloxane) and (b) vinyl-terminated poly(dimethyl siloxane).

The source or "type" of poly(dimethyl siloxane) has a small effect on the pervaporation characteristics of a membrane. The most commonly used source in the literature is a room-temperature vulcanizing PDMS, RTV615. RTV615 is a two-part polymer consisting of (1) a prepolymer with terminal vinyl groups (RTV615A) and (2) a crosslinking agent mixed with a platinum catalyst (RTV615B). Other RTV agents, such as RTV103, RTV107, and RTV108, have also been studied and show similar flux and separation properties as RTV615 [57]. A three-part system, consisting of (1) vinyl-terminated PDMS prepolymer (DMS-V41), (2) trimethylsiloxane-terminated poly(methylhydrosiloxane-dimethylsiloxane) copolymer (HMS-064), and (3) platinum divinyltetramethyldisiloxane complex in xylene (SIP6831.2), has also been studied and shows similar pervaporation performance as RTV615 [67].

In this latter study, it was found that increasing the molecular weight of the vinyl-terminated prepolymer led to an increase in the ethanol-water selectivity. Above a certain molecular weight, though, membrane performance became inconsistent as the high-molecular weight membranes tended to incur damage upon removal from the support.

### 2.2.2 Zeolite Selection

Zeolite MFI, shown in Figure 2.3, is particularly well-suited for use in membranes for ethanol-water separation. MFI has elliptical pores 0.51-0.56 nm in diameter, large enough to allow either water or ethanol through. However, the pores are highly hydrophobic due to the high silica content of MFI, causing the material to preferentially sorb ethanol [47, 57]. This hydrophobicity makes it an ideal candidate for selectively removing ethanol from ethanol-water streams.

The MFI class of zeolites includes both silicalite-1, a pure-silica form, and ZSM-5, in which Al replaces some of the Si atoms in the lattice. It has been shown that ethanol-water separation improves as the ratio of Si to Al is increased in ZSM-5 [57].

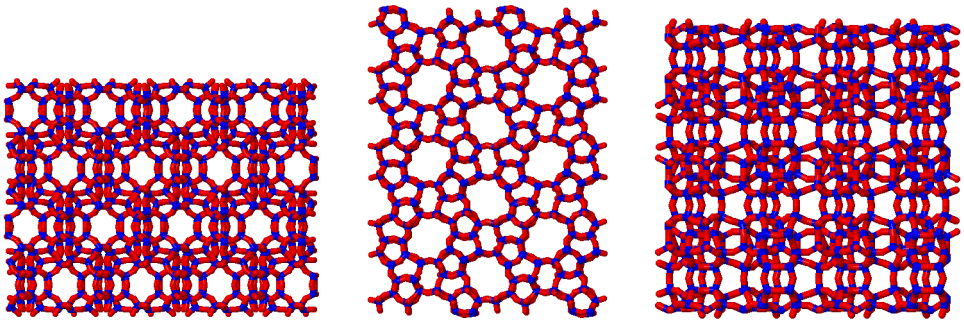

(a) (b) (c)

**Figure 2.3:** Structure of zeolite MFI as viewed down crystallographic a, b, and c directions [78].

Furthermore, the pure-silica silicalite-1 form has been shown to outperform high Si/Al ZSM-5 [47].

Other zeolites and porous fillers have also been studied for ethanol-water separations. Some examples include Zeolite Y [47, 62], ultrastable zeolite Y [63], ALPO-5 [63], and carbon black [64]. Of these, only ultrastable zeolite Y demonstrated slightly better flux and separation factor than silicalite-1 [63].

### 2.2.3 Hollow Fiber Support

Torlon® has recently been explored for hollow fibers for gas separations [79–83] and ethanol-water dehydration [84, 85]. Torlon® is a polyamide-imide polymer developed by Solvay Advanced Polymers to be mechanically durable and chemically and thermally stable. Large-pore, Torlon® hollow fibers without a dense skin layer have been fabricated by members of Dr. W. J. Koros' research group at Georgia Tech. These fibers are ideal for a durable, stable, non-selective hollow fiber support structure.

### 2.2.4 Organic Solvent Choice

The earliest successful attempts to prepare MFI-PDMS flat films were done without the addition of solvent, which resulted in a gum-like polymer mixture that was

mechanically cast onto a plate [45]. Adding an organic solvent improves zeolite dispersion within the polymer matrix and allows for the formation of thinner membranes. Different solvents, including iso-octane [46, 67], toluene [44, 63, 67], methyl isobutyl ketone [47, 62], and heptane [57, 86] have been used for MFI-PDMS film preparation. Membranes prepared using different solvents showed similar pervaporation characteristics. However, Vane et al. determined that the solvent choice may interact with the membrane support undesirably, causing difficulty when removing the membrane from the support [67]. The group also found that MFI particles remained dispersed in toluene longer than in iso-octane, which could improve the quality of the membrane and ease of preparation.

## *2.3 Processing Variables*

The quality of the zeolite-polymer film and the pervaporation characteristics can be drastically altered by changing the processing conditions. The composition of the dope solution, the size and treatment of the zeolite particles, and the procedure for curing the membrane may all affect the membrane performance.

### 2.3.1 Composition of Dope Solution

**Concentration of Zeolite Particles** The most commonly studied parameter has been the amount of zeolite incorporated into the membrane. With few exceptions, it has been found that both flux and separation factor increase as the membrane zeolite loading is increased [44, 45, 47, 62, 63, 67]. Literature data are reproduced in Figure 2.4. The increase in flux is expected due to the increasing number of pores that are available for transport as MFI is added. The rise in selectivity occurs because the zeolite preferentially sorbs ethanol [47, 57], allowing ethanol through but increasing the tortuosity of the transport path for water (see Figure 2.1) [45]. Contrary to other reports, Chen et al. found a maximum in ethanol flux at ∼10 wt% [57]. This discrepancy may be due to blockages of zeolite pores following several treatments that

were tested.

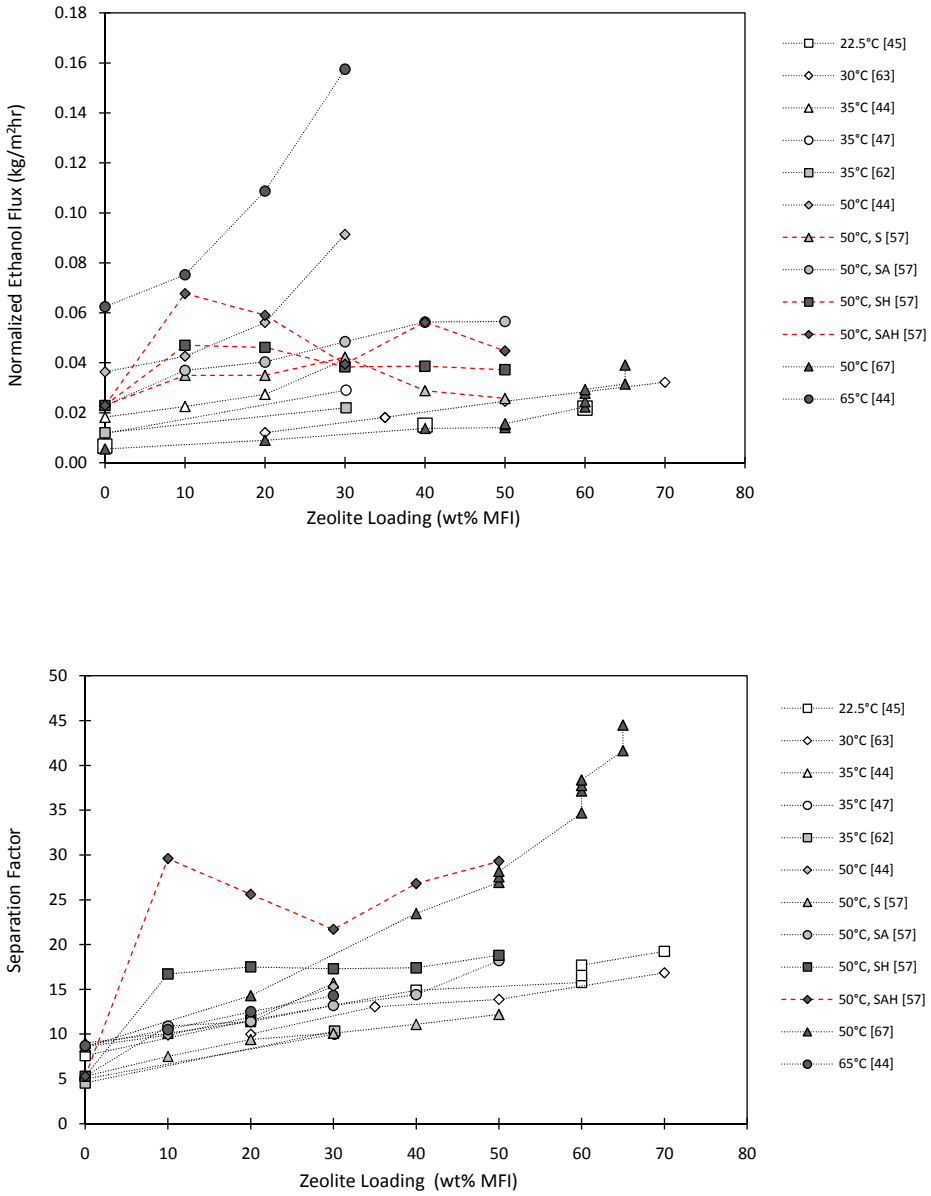


**Figure 2.4:** Ethanol fluxes and separation factors as a function of zeolite loading for MFI-PDMS flat-film membranes reported in the literature [44, 45, 47, 57, 62, 63, 67]. Feed temperatures are noted in the legend. Feed concentrations ranged from 4.4-6.0 wt% ethanol. Membrane thicknesses ranged from 50-500 $\mu$m, but all data are normalized to a thickness of 100 $\mu$m. RTV615 PDMS was used for all membranes except for the DMS-V41/HMS-064 system used in [67] and the RTV107 system used in [57]. Chen et al. investigated several membrane treatments, denoted S, SA, SH, and SAH in the legend [57]. Abnormal trends are marked with a dashed red line.

**Concentration of Organic Solvent** The amount of solvent used in membrane preparation has varied widely (0-98 wt%) in the literature [44–46, 63, 67]. Very few studies have been performed that quantify the effects of varying the solvent concentration in the dope solution. Jia et al. investigated the effect of varying the solvent concentration between 95 and 98 wt% on a zeolite-free basis [46]. As the solvent fraction was increased, the flux more than tripled and the separation factor was halved. However, the thickness of each membrane was not reported, so it is unclear whether the trend that appears is identical to the inverse proportionality expected with film thickness or if the solvent concentration may have some other effect. Vane et al. noted that increasing the solvent concentration slowed the rate of polymerization of high molecular weight PDMS sources, but no relationship between solvent fraction and membrane performance was noted [67].

### 2.3.2 Zeolite Particle Size

Zeolite particle sizes reported in the literature range from 70 nm to 40 $\mu$m. Although Jia et al. found that particles less than 0.5 $\mu$m dispersed well in PDMS [46], other groups have found that smaller particles lead to dispersion problems. Vankelecom et al. compared membrane properties for membranes prepared with 0.2 $\mu$m and 2.0 $\mu$m MFI, and found that the smaller particles were not as well dispersed as larger particles, leading to a decrease in membrane tensile strength [62]. Moermans et al. also had difficulty with dispersion of smaller particles. The group measured the performance of composite membranes created with 70 nm and 0.4-0.8 $\mu$m silicalite-1 particles [44]. Both flux and separation factor improved when smaller particles were used, however, they found that decreasing the particle size led to dispersion problems, which limited the maximum zeolite loading. Vane et al. encountered dispersion and agglomeration problems for submicron (0.35 $\mu$m and 0.70 $\mu$m) silicalite-1 particles [67]. These membranes underperformed large-particle (2.4 $\mu$m) membranes due

to pinhole defects attributed to particle aggregates. By coating the small-particle membranes with a pure-PDMS overcoat, the membrane performance was improved.

### 2.3.3 Zeolite Surface Treatment

Although MFI pores are highly hydrophobic, the outer surfaces of MFI particles are hydrophilic, which leads to dispersion problems when mixed with hydrophobic PDMS and solvent. To overcome this difficulty, Moermans et al. treated 70 nm silicalite-1 particles with a silane coupling agent (*N*-methyl-*N*-(trimethylsilyl)trifluoroacetamide) to coat the surfaces with hydrophobic trimethylsilyl groups [44]. Although they saw a decrease in the flux and separation factor for any particular zeolite loading, they were able to achieve higher zeolite loadings with the silylated particles. The decrease in membrane performance after silylation may be due to partial blockage of the zeolite pores by the coupling agent.

As an alternative to silane coupling agents, aliphatic alcohols might also increase particle surface hydrophobicity, and thus improve dispersion and pervaporation performance. In an early study, silica particles were reacted with alcohols to successfully convert their hydrophilic external surfaces to hydrophobic surfaces [87]. After treatment with alcohols, the hydrophobic characteristics of mesoporous materials were shown to increase significantly [87–91]. These treated materials also showed an improved dispersion in organic solvents [92]. The degree of hydrophobicity can be increased by increasing the length of the alkyl group or the number of alkyl groups per area [89]. Pervaporation performance for composite films consisting of alcohol-functionalized MFI particles has not been reported in the literature and merits investigation.

### 2.3.4 Aging (Prepolymerization) of Polymer

Jia et al. reported that partially polymerizing the MFI-PDMS solution prior to curing the membrane improved the dispersion of the zeolite by preventing particles from

precipitating [46]. This "prepolymerization" step was performed at 70°C for 2 hr, after which the more viscous solution was poured onto a Teflon® plate and cured at 80°C overnight. Both Vankelecom et al. [47, 62] and Moermans et al. [44] prepolymerized their membranes prior to casting (for 1 hr at room temperature with stirring and for 45 min at 70°C without stirring, respectively), but neither group compared the prepolymerized samples with samples prepared without the prepolymerization step.

Vane et al. compared the performance of membranes prepared with and without prepolymerization [67]. They determined that the prepolymerization step did not affect the pervaporation performance of the membranes. Furthermore, they found that prepolymerization made sample preparation more difficult because of the much shorter working life of the polymer.

### 2.3.5 Membrane Thickness

As membrane thickness was increased from 50 to 200 $\mu$m, Adnadjević et al. saw a slight decrease in flux and increase in separation factor [63]. For polymeric dense films, the flux is expected to increase proportionately as the membrane thickness decreases, but the separation factor is expected to remain constant. For composite films though, the permeability of the membrane depends on the volume fraction of zeolite particles in the film. Since the separation factor and flux depend on the permeability of the membrane, they are more complicated functions of film thickness. Most reported fluxes are normalized to a thickness of 100 $\mu$m, assuming an inverse proportionality of flux and membrane thickness.

## *2.4 Pervaporation Parameters*

The pervaporation parameters also affect the pervaporation performance of membranes. The feed temperature, composition, and circulation rate, as well as the downstream pressure all affect the pervaporation results.

### 2.4.1 Feed Temperature

Many studies have been done on the effect of temperature on pervaporation performance. Although the flux has clearly been shown to rise as feed temperature rises [44, 45, 47, 57, 63], the effect on the separation factor is less clear. Several groups have seen a rise in separation factor as temperature increases [44, 47, 57], while others have seen a fall with increasing temperature [44, 45, 63]. Pervaporation data from the literature are shown in Figure 2.5.

### 2.4.2 Downstream Pressure

Li and Wang investigated the effect of downstream pressure on pervaporation characteristics [86]. They found that as the downstream pressure was lowered from 50 torr to 10 torr, the flux increased and the separation factor decreased. Li and Wang attribute these results to a decrease in saturation in the downstream chamber as the pressure is decreased. At the lower pressure and saturation, the desorption rate increases, resulting in an increase in flux.

### 2.4.3 Feed Concentration

The effect of ethanol feed concentration on the flux and separation factor for composite membranes was studied by te Hennepe et al. [45] and Chen et al. [57]. The results of these studies are reproduced in Figure 2.6. Both groups found that the ethanol flux increased as the feed concentration was increased. However, the results for separation factor were less clear. For high zeolite loadings, te Hennepe et al. saw an increase in separation factor as the ethanol in the feed was raised from 3.5 to 7.5 wt%. However, at lower loadings, the separation factor remained nearly constant over the range tested. Contrary to these findings, Chen et al. found that the separation factor decreased drastically when the feed concentration was raised from 5 to 7 wt% and then continued to decrease steadily as the feed concentration was raised from 7 to 90 wt% ethanol.

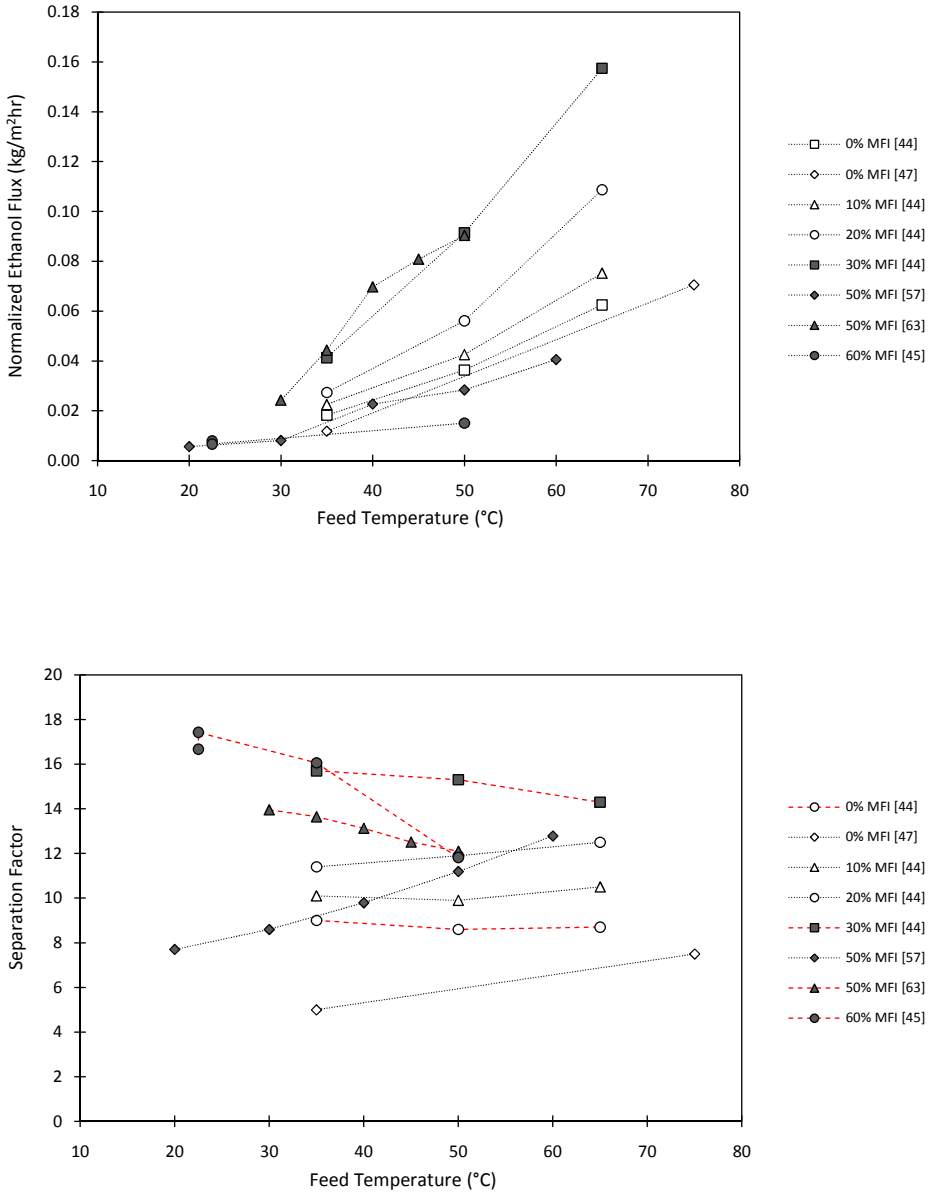


**Figure 2.5:** Ethanol flux and separation factor as a function of feed temperature for MFI-PDMS flat-film membranes reported in the literature [44, 45, 47, 57, 63, 67, 86]. Zeolite loadings are noted in the legend. Feed concentrations ranged from 4.4-6.0 wt% ethanol. Membrane thicknesses ranged from 50-500 $\mu$m, but all data are normalized to a thickness of 100 $\mu$m. RTV615 PDMS was used for all membranes except for the DMS-V41/HMS-064 system used in [67] and the RTV107 system used in [57]. Decreasing trends are marked with a dashed red line.

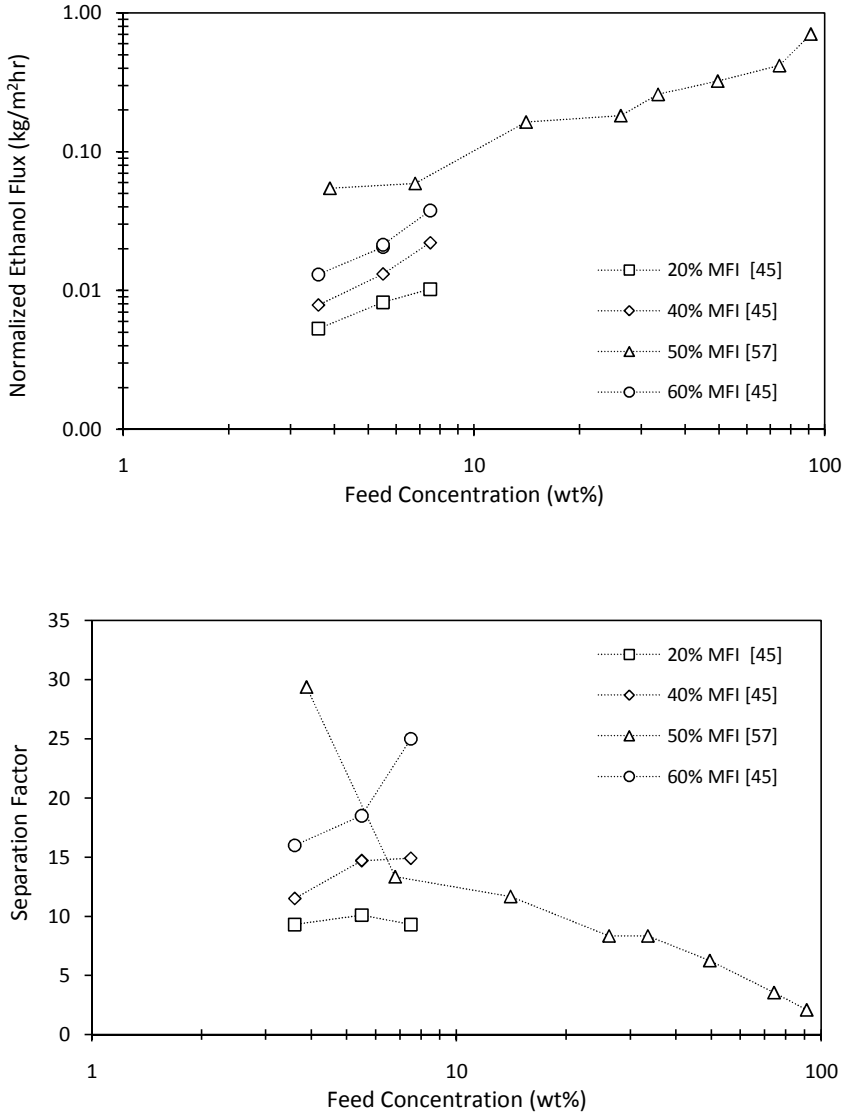


**Figure 2.6:** Ethanol flux and separation factor as a function of feed concentration for MFI-PDMS flat-film membranes reported in the literature [45, 57]. Feed temperatures ranged from 22.5 to 50°C. Membrane zeolite loadings are noted in the legend. All data are normalized to a thickness of 100 $\mu$m. RTV615 PDMS was used in [45] and RTV107 was used in [57].

### 2.4.4 Feed Circulation Rate

The rate of circulation of the feed solution was studied by Li and Wang [86]. They varied the flow rate of the feed solution from 70 to 110 L/hr and found that both the flux and the separation factor increased with increasing circulation rate. A higher

circulation rate is expected to lessen concentration polarization, which is where the feed near the membrane surface becomes depleted in the more permeable species causing a local decrease in the feed concentration. As discussed in the previous subsection, this lower feed concentration will result in a decreased flux.

## *2.5 Fouling*

Under realistic conditions in a biofuel production plant, membranes may be exposed to many contaminants that could potentially cause a decrease in flux or selectivity by blocking pores or interacting unfavorably with the chemicals to be separated. Such contaminants can be grouped into four categories [3]:

1. Particulates - live or dead whole cells and cell components, such as proteins and cell walls
2. Organic/fatty acids - such as acetic, succinic, and stearic acid
3. Dissolved solids - such as sodium chloride and sodium lactate
4. Sugars - such as glucose, lactose, glycerol, and xylose

Most fermentation broths are passed through an ultra-, micro-, or nanofiltration unit to remove particulates (type 1) before entering a membrane system, although some studies suggest that this solid-liquid separation may be unnecessary if the broth is passed over the shell-side of the membrane system, rather than the tube-side [3]. On the other hand, organic or fatty acids (type 2), dissolved solids (type 3), and sugars (type 4) may have a dramatic effect on the membrane performance.

For example, Ikegami et al. studied a feed solution containing glucose, ethanol, succinic acid, and glycerol [65]. Membrane performance showed a drastic decrease in flux and separation factor through a pure MFI zeolite membrane, due to adsorption of succinic acid in the zeolite. However, when the membrane was coated with a silicone rubber film, the effect was reduced significantly, keeping the selectivity constant at

the expected value. A model feed solution with 0.8 wt% glycerol in an ethanol-water mixture was also tested. Although glycerol was not adsorbed by MFI or silicone rubber, it decreased the vapor pressures of ethanol and water and resulted in a slight decrease in throughput. Interestingly, washing the membranes with distilled water restored their original pervaporation performance and allowed for repeated use [51].

The effect of pH, which determines the degree of protonation of organic acids, was also investigated by Ikegami et al. [66]. Below pH 5, where organic acids are protonated and volatile, both MFI membranes and silicone-coated MFI membranes showed greatly decreased separation factor and flux. Increasing the pH from 5 to 8.5 induced acid deprotonation and created a much smaller likelihood of the negatively charged carboxylate ions entering the hydrophobic MFI pores, resulting in negligible effects on the performance. The deteriorated performance of coated membranes could also be restored by washing with neutral buffer solutions.

Acetone-butanol-ethanol (ABE) fermentation broths were found to create no significant fouling effect for either short term [93] or longer term ($\sim$870 hours) operation [94]. For a fermentation broth containing 1-propanol, glucose, sodium chloride, and magnesium chloride, it was shown that the addition of salts to the fermentation broth increased the activity coefficient of alcohol resulting in enhanced performance [95]. However, the presence of glucose, fructose, and citric acid somewhat reduced the activity coefficient of alcohol and hence the flux.

These previous studies seem to indicate that molecular contaminants represent, at worst, a manageable concern for the continuous operation of a membrane system. For the work in this thesis, only binary mixtures of ethanol and water were investigated. However, long-term fouling studies should be performed to determine the effect of the four types of contaminants on the proposed composite hollow-fiber membranes.

# CHAPTER III

# EXPERIMENTAL METHODS

This chapter describes the methods and materials used to form and characterize our hollow fiber coatings. As shown in Figure 3.1, the composite hollow-fiber membrane consists of a non-selective polymer hollow-fiber support layer and a thin selective layer of dispersed MFI nanoparticles in a polymer matrix. Such a composite hollow fiber could potentially be formed using one of two methods: (1) by direct spinning of a two-layer fiber or (2) by coating a pre-formed fiber with a composite coating. The first approach works well for glassy polymers, such as Torlon®, but these polymers have low alcohol permeabilities. Elastomeric polymers, such as PDMS, have much better alcohol permeation properties, but they tend to adhere to processing surfaces during extrusion, making it difficult to directly spin a composite fiber. For this reason, the second approach will be used in this work.

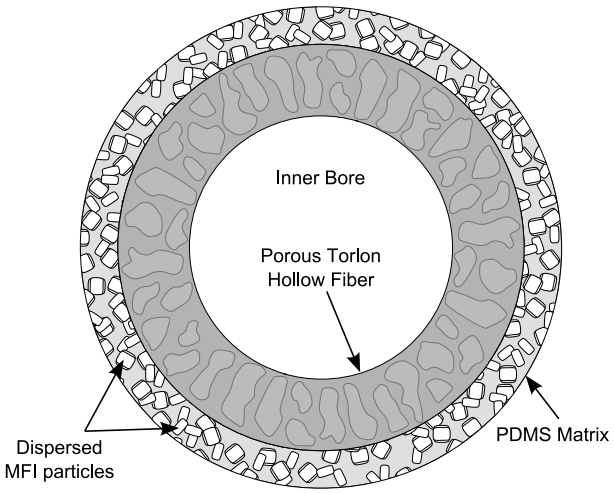


**Figure 3.1:** Schematic cross-section of MFI/PDMS composite

## *3.1 Zeolite Synthesis*

Silicalite-1 was prepared in house using one of two methods. In both procedures, tetraethylorthosilicate (TEOS, 98%, ACROS), tetrapropylammonium hydroxide (TPAOH, 40% w/w aqueous solution, Alfa Aesar), and deionized (DI) water were used.

### 3.1.1 Synthesis in Berghof Reactor (Method A)

Using the first method, the reaction mixture was prepared in a glass beaker, then transferred to a Teflon® vessel. The reaction took place in a Berghof reactor at 150°C with stirring for 48 hours. The resulting crystals were washed with DI water until the pH was below 8. The powder was then dried and calcined. The detailed procedure is outlined below.

1. Mix 25 g TEOS and 368.12 g DI water together.
2. Add 21.53 g TPAOH solution dropwise while stirring vigorously with a PTFE-coated stir bar. The composition of the precursor solution will be 1 TEOS : 0.36 TPAOH : 180 DI water. Continue stirring at room temperature for 18 hr.
3. Transfer the zeolite precursor solution into a Teflon® sleeve. Place a stirrer shaft into the Teflon® sleeve and close the reaction vessel.
4. Set the synthesis temperature to 150°C and the stirring speed between 150-200 RPM. Let the reaction run for 48 hr.
5. Turn off the heater, but continue stirring. Allow the reactor to cool completely (∼6 hr).
6. After the reactor cools to room temperature, decant the resulting milky solution into centrifuge tubes.
7. Centrifuge the solution at 6000 RPM for 10 min.

8. Decant the supernatant.

9. Add DI water into the centrifuge tubes and sonicate for 20 min or until the particles re-suspend in the water homogeneously.

10. Repeat steps 7 to 9 four times or until the pH of supernatant is below 8.

11. Re-disperse the particles in DI water, decant the solution into a Petri dish, and dry at 70°C overnight.

12. Grind the resulting granular powder and place in a calcination oven to decompose and remove TPA template molecules from the pores. Calcination conditions: Increase the oven temperature from room temperature to 120°C at 5 K/min. Soak at 120°C for 1 hr. Then increase the temperature from 120°C to 550°C at 5 K/min. Soak at 550°C for 8 hr. Then cool down the material from 550°C to room temperature at 0.5 K/min.

13. Grind the powder again and place in a vacuum oven at 120°C overnight.

14. Place the resulting crystals in a vial sealed with Parafilm® and store in a desiccator.

### 3.1.2 Synthesis in Pyrex® Container (Method B)

The second method, developed by Dr. Jae Kyu Cho (Nair group, Georgia Tech), is similar to the first method with several variations. The reaction took place in a vented Pyrex® container at 95°C without stirring for 4 days. The resulting crystals were washed with DI water until the pH was below 8. The powder was then dried and calcined. The detailed procedure is outlined below.

1. Mix 112 g TEOS and 130 g DI water together.

2. Add 46 g TPAOH solution dropwise while stirring vigorously with a PTFE-coated stir bar. The composition of the precursor solution will be 1 TEOS :

0.411 TPAOH : 1.161 DI water. Continue stirring at room temperature for 18 hr.

3. Transfer the zeolite precursor into a Pyrex® container with a vented Teflon® lid.

4. Place the container in a 95°C oven. Let the reaction run for 4 days.

5. Remove from the oven and allow the container to cool completely.

6. After the container cools to room temperature, decant the resulting milky solution into centrifuge tubes.

7. Centrifuge the solution at 6000 RPM for 10 min.

8. Decant the supernatant.

9. Add DI water into the centrifuge tubes and sonicate for 20 min or until the particles re-suspend in the water homogeneously.

10. Repeat steps 7 to 9 four times or until the pH of supernatant is below 8.

11. Re-disperse the particles in DI water, decant the solution into a Petri dish, and dry at 70°C overnight.

12. Grind the resulting granular powder and place in a calcination oven to decompose and remove TPA template molecules from the pores. Calcination conditions: Increase the oven temperature from room temperature to 120°C at 5 K/min. Soak at 120°C for 1 hr. Then increase the temperature from 120°C to 550°C at 5 K/min. Soak at 550°C for 8 hr. Then cool down the material from 550°C to room temperature at 0.5 K/min.

13. Grind the powder again and place in a vacuum oven at 120°C overnight.

14. Place the resulting crystals in a vial sealed with Parafilm® and store in a desiccator.

## *3.2 Functionalization*

MFI particles were functionalized using a procedure similar to that described by Cheng et al. [91]. 60 g 1-Butanol (ACS grade, >99.4%, J.T. Baker) was added to 3 g MFI particles in a 100 mL round-bottom flask. The flask was connected to a distillation head (ChemGlass Inc. CG-1237-01) and was immersed in a silicone oil bath (110°C) with stirring (500 RPM) for 48 hr. The solution was then centrifuged at 6000 RPM for 10 min. After decanting the supernatant, the particles were redispersed in hexane (ACS grade, EMD) using sonication. The centrifugation and redispersion steps were repeated three times. Then the particles were dried under vacuum at room temperature for at least 18 hr, after which they were placed in a vial sealed with Parafilm® and stored in a desiccator.

## *3.3 Polymers*

Two PDMS sources were used in this work. The first was RTV615, a two-part polymer consisting of (1) a prepolymer with terminal vinyl groups (RTV615A, General Electric) and (2) a crosslinking agent mixed with a platinum catalyst (RTV615B, General Electric). Once the two components were mixed, the polymer had a working life of ∼20 min at room temperature. This working life could be extended to ∼1 hr by dilution with iso-octane (2,2,4-trimethylpentane, anhydrous, 99.8%, Sigma-Aldrich). The second PDMS source used in this work was the three-part polymer investigated by Vane et al. [67]. This polymer consisted of (1) a vinyl-terminated PDMS prepolymer (DMS-V41, Gelest, Inc.), (2) a trimethylsiloxane-terminated poly(methylhydrosiloxane-dimethylsiloxane) copolymer (HMS-064, Gelest, Inc.), and (3) a platinum divinyltetramethyldisiloxane complex in xylene (SIP6831.2, Gelest, Inc.). Once the catalyst was added, the work-life of the solution was ∼5 min.

Extending the working life by further dilution with iso-octane was not explored in this work, but is mentioned as a possibility by Vane et al. [67].

## *3.4 Hollow Fiber Supports*

Torlon® (4000T, Solvay Advanced Polymers) hollow fibers were fabricated for this work by Dr. Shabbir Hussain and Justin Johnson in Dr. W.J. Koros' research group at Georgia Tech. The fibers were designed to have large pores and no skin layer to minimize the transfer resistance of the support.

## *3.5 Composite Flat Film Preparation*

**RTV615** MFI particles (unfunctionalized or *n*-butanol functionalized) were dispersed in iso-octane (2,2,4-trimethylpentane, anhydrous, 99.8%, Sigma-Aldrich) and sonicated for 15 min. RTV615A was then added to the vial and the solution was sonicated for another 15 min. To this, RTV615B was added, and the solution was sonicated for 10 min. The MFI-PDMS solution was then slowly poured into an acrylic Petri dish. Bubbles were avoided by minimizing the distance between the vial and the dish while pouring. The Petri dish was covered and left at room temperature for 1 hr. The dish was then placed in a 70°C oven at atmospheric pressure for at least 8 hr. Cured membranes were cut into circles with a diameter of 4.89 cm for pervaporation experiments.

The fraction of iso-octane was kept constant as 70% of the total weight (wt iso-octane = 0.7×[wt MFI + wt RTV615A + wt RTV615B]/0.3). The weight of MFI was varied depending on the desired zeolite loading (wt% MFI = wt MFI / [wt MFI + wt RTV615A + wt RTV615B]). The weight ratio of polymer components was held constant at 10 RTV615A : 1 RTV615B. For example, for a 50 wt% MFI/PDMS film, 0.500 g MFI, 0.455 g RTV615A, 0.045 g RTV615B, and 2.333 g iso-octane would be mixed.

**DMS-V41/HMS-064** MFI particles (unfunctionalized or *n*-butanol functionalized) were dispersed in iso-octane and sonicated for 15 min. DMS-V41 was added and the mixture was shaken vigorously by hand until it appeared to have a homogeneous consistency (∼30 sec). The vial was then sonicated for 1 min. HMS-064 was then added, shaken by hand for ∼30 sec, and sonicated for 2 min. Finally, SIP6831.2 was added. The solution was sonicated for 1 min and immediately poured into a Petri dish in the same manner as the RTV615 procedure. The Petri dish was covered and left at room temperature for 1 hr before being moved to a 70°C oven at atmospheric pressure for at least 8 hr. Cured membranes were cut into circles with a diameter of 4.89 cm for pervaporation experiments.

As with RTV615, the fraction of iso-octane was kept constant as 70% of the total weight (wt iso-octane = 0.7×[wt MFI + wt DMS-V41 + wt HMS-064 + wt SIP6831.2]/0.3) and the weight of MFI was varied depending on the desired zeolite loading (wt% MFI = wt MFI/[wt MFI + wt DMS-V41 + wt HMS-064 + wt SIP6831.2]). The weight ratio of polymer components was held constant at 10 DMS-V-41 : 0.623 HMS-064 : 0.024 SIP6381.2. For example, for a 50 wt% MFI/PDMS film, 0.500 g MFI, 0.471 g DMS-V41, 0.029 g HMS-064, 0.0011 g SIP6831.2, and 2.335 g iso-octane would be mixed. The required amount of catalyst for each solution was very small and was difficult to control. As a result, the ratio of catalyst to DMS and HMS had a large variability.

## *3.6 MFI/PDMS Coatings on Hollow Fibers*

Hollow fiber coating procedures were varied to determine an acceptable method for forming uniform, defect-free coatings.

### 3.6.1 Dope Preparation

Only RTV615 PDMS was used for hollow fiber coatings in this work. First, MFI (unfunctionalized or *n*-butanol functionalized) and half of the final amount of iso-octane were sonicated for 10 min. In a second vial, RTV615A was added to the remaining half of iso-octane and the solution was sonicated for 4 min. RTV615B was added and the resulting solution was sonicated for an additional 2 min. Finally, the PDMS solution was poured into the MFI solution and the vial was sonicated for 4 min.

The fraction of iso-octane was held at 80% of the total weight. The weight of MFI was varied depending on the desired zeolite loading. The weight ratio of the polymer components was kept constant at 10 RTV615A : 1 RTV615B.

### 3.6.2 Fiber Pretreatment

For some preparations, the hollow fiber support was soaked in DI water prior to coating with MFI/PDMS. This treatment will be referred to as "presoaking" in this thesis. Presoaking was investigated to prevent possible polymer intrusion into the pores of the hollow fiber. To presoak, the fiber was coiled loosely around the bottom of a milled Teflon® dish and covered with DI water for 15 min, as shown in Figure 3.2. The fiber was removed from the water immediately before coating with polymer. Water droplets on the surface of the fiber were gently and quickly removed with a Kimwipe®.

### 3.6.3 Coating Method

Two coating methods were investigated in this work. The first method was performed by pouring the dope solution into a shallow milled Teflon® dish in a manner similar to that described for the Petri dish in Section 3.5. The hollow fiber was then held by both ends, allowing it to form a U-shape. The bottom of the U was carefully placed into the dope solution. One end of the fiber was then raised while the other end was

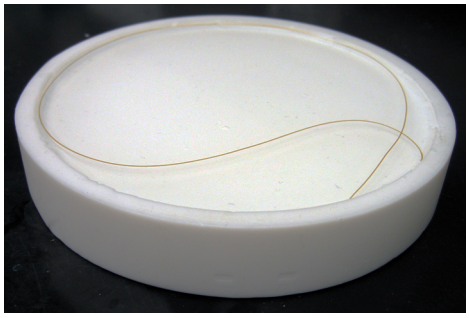

**Figure 3.2:** Presoaking a hollow fiber in deionized water.

lowered, allowing the entire length of the fiber to be dipped in the solution. The entire fiber was pulled through the solution at least three times at a rate of ∼5 cm/s. The coated fiber was then suspended horizontally (see Figure 3.3) in a 60-80°C oven for at least 8 hr. This method, which is illustrated in Figure 3.4, will be referred to as the "dip-coat" method in this thesis.

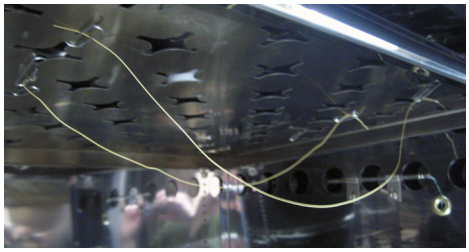

**Figure 3.3:** Hollow fibers suspended horizontally in oven.

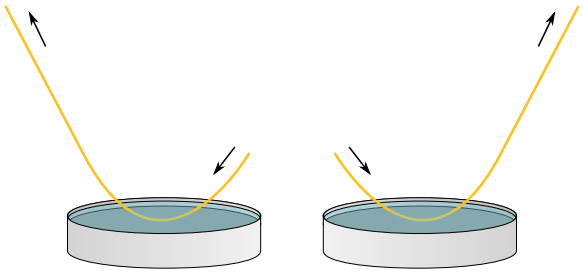

**Figure 3.4:** Illustration of the dip-coat method of coating hollow fibers.

The second method was developed to allow for sonication during coating. A U-shaped glass tube was fabricated by the glass shop. The inner diameter of the tube was 1 cm, with a radius of curvature of ∼10 cm, and a total arc length of ∼30 cm.

The tube was suspended in a sonication bath and the dope solution was poured into it. A hollow fiber was then fed through the solution from one end of the tube until it could be pulled out the other end. One end of the fiber was then raised while the other end was lowered, allowing the entire length of the fiber to be immersed in the dope solution. After the entire fiber was pulled through the solution at least three times at a rate of ∼5 cm/s, the coated fiber was carefully pulled out of the glass U-tube from one side so as not to make contact between the fiber coating and the tube. The coated fiber was then suspended horizontally (Figure 3.3) in a 60-80°C oven for at least 8 hr. This method, which is illustrated in Figure 3.5, will be referred to as the "U-tube" method in this thesis.

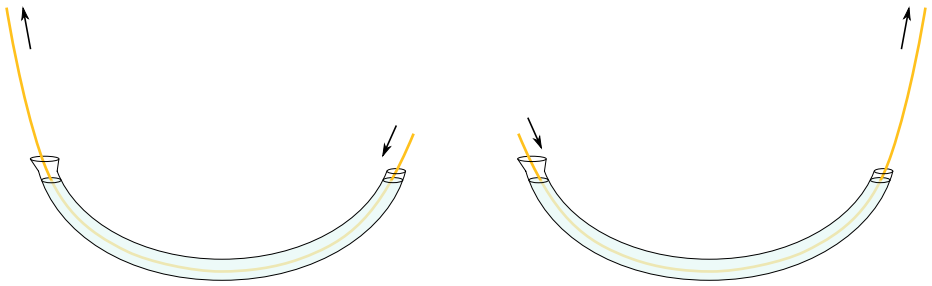

**Figure 3.5:** Illustration of the U-tube method of coating hollow fibers.

### 3.6.4 Sonication

Unfunctionalized particles tended to rapidly precipitate from solution after sonication was stopped. For this reason, sonication during coating was explored using the U-tube method described above. The U-tube was held in place in a sonication bath by clamping each end, as shown in Figure 3.6.

### 3.6.5 Multiple Coatings

For some fibers, multiple coatings were applied to the hollow fiber. Each coating was applied following one of the procedures in Section 3.6.3. Following each coating, the fiber was placed in a 60-80°C oven for at least 20 min before applying the next coat. After the final coat was applied, the fiber was cured for at least 8 hr at 60-80°C.

**Figure 3.6:** Glass U-tube suspended in sonication bath.

### 3.6.6 Low- and High-Temperature Vacuum Treatments

Two vacuum treatments were tested to determine if iso-octane or water were trapped in the pores of the zeolite. To perform the vacuum treatment, the membranes were first created and tested like normal. Following the pervaporation tests, the membranes were placed in a vacuum oven at either 70°C (low-temperature vacuum treatment) or 110°C (high-temperature vacuum treatment) for more than 18 hr.

## *3.7 Zeolite and Membrane Characterization*

MFI particle size and shape were observed using scanning electron microscopy (SEM, Hitachi S-800 or LEO 1350) images and the crystallographic structure was investigated using X-ray diffraction (XRD). Particle dispersions and hollow-fiber coating thickness were observed using SEM images. Flat-film membrane thicknesses were determined using an electronic thickness gauge.

The separation properties of the synthesized membranes were characterized using pervaporation measurements described in the following section. Feed and permeate samples were analyzed using one of two methods: (1) by gas chromotography (GC, SRI 310C) with a flame ionization detector using an MXT-WAX column (30 m, 0.53 mm ID) and n-propanol as an internal standard, or (2) by refractive index values measured on a benchtop refractometer (Leica ARIAS 500). The refractometer was calibrated with known concentrations of ethanol (200 proof, EMD) in DI water. The calibration curve is given in Figure 3.7.

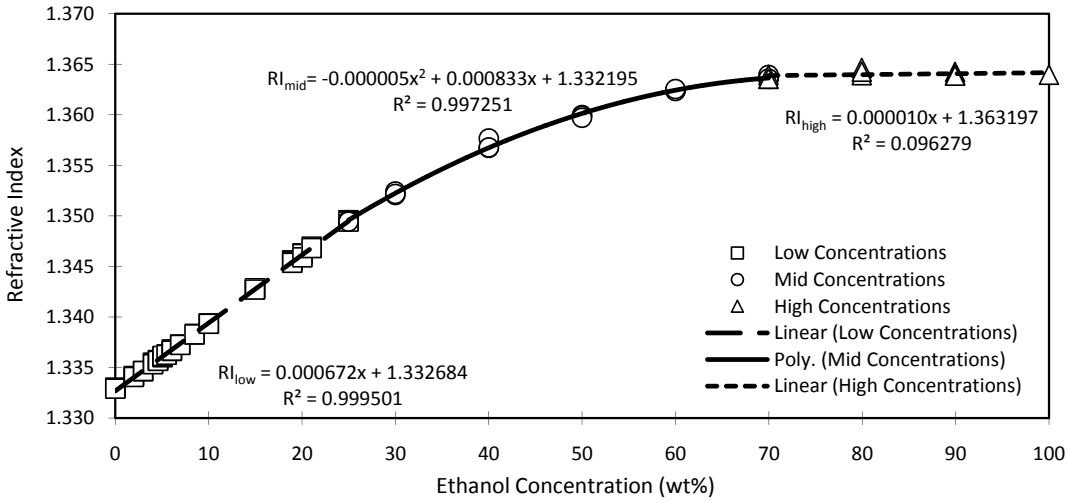


**Figure 3.7:** Calibration curve for ethanol-water solutions measured with a Leica ARIAS 500 refractometer.

## *3.8 Pervaporation Measurements*

Two pervaporation apparatuses were used during the course of this work. The first system (System A), shown in Figure 3.8, was replicated from Zhou's work [96]. Improvements to this design were made by Dr. Jae Kyu Cho, allowing for longer collection times and consistent pressure driving forces. The modified system (System B) is shown in Figure 3.9. Although both systems are capable of measuring pervaporation performance for either hollow-fiber or flat-film membranes, all flat-film membranes in this work were tested on System B and all hollow-fiber membranes were tested using System A.

### 3.8.1 Assembling Pervaporation Modules

To run pervaporation experiments in either system, the membrane to be tested was first secured in a membrane module.

**Flat-Film Modules** The flat-film module shown in Figure 3.10 was designed by Dr. Jae Kyu Cho based on designs by Chafin [97] and Boudreau [98]. The glass

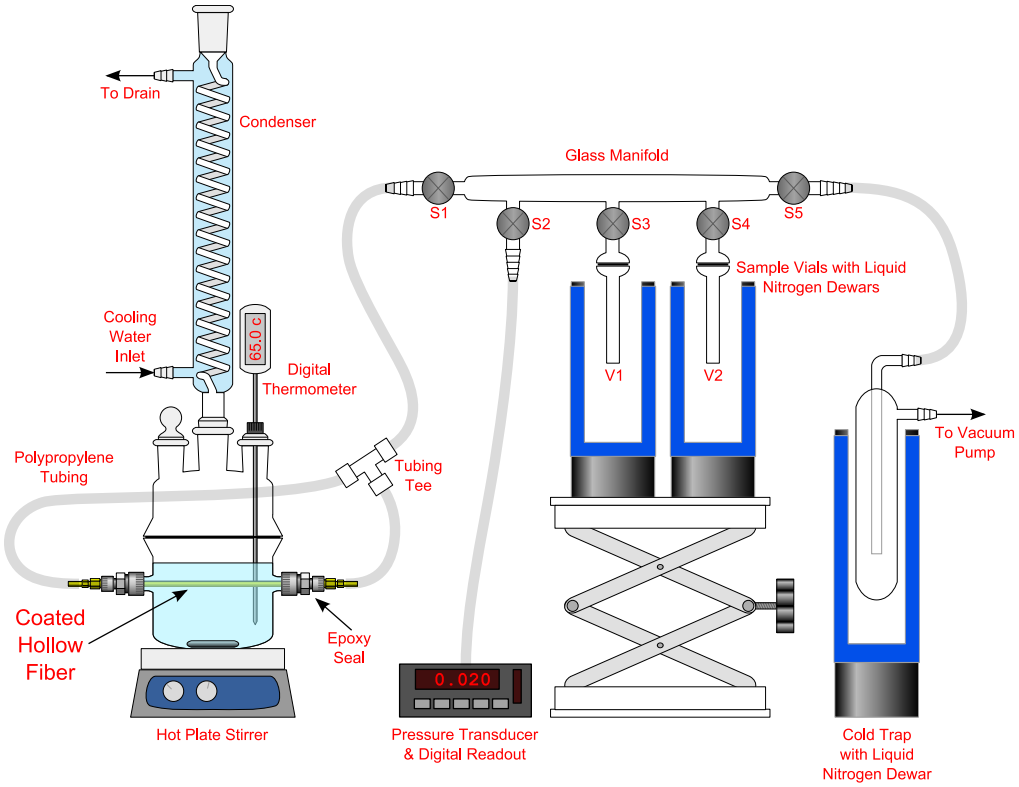


(a) Diagram of System A.

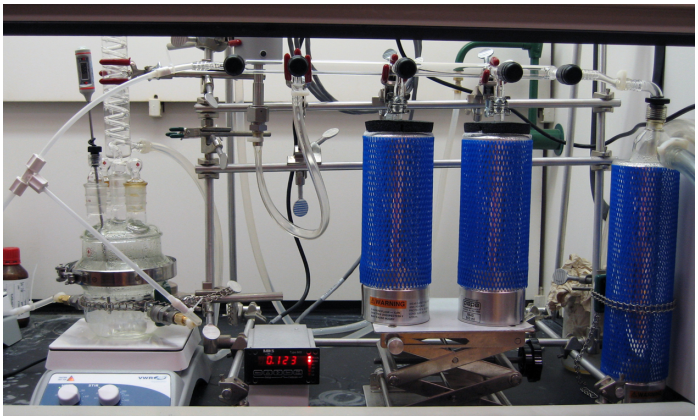

(b) Photograph of System A.

**Figure 3.8:** The original pervaporation apparatus (System A) for characterizing hollow-fiber and flat-film membranes. A single hollow-fiber membrane is shown in place. The feed components permeate through the hollow-fiber or flat-film membrane at different rates, evaporate on the downstream side, and are condensed in the two sample vials, V1 and V2. The feed temperature and downstream pressure are monitored. A water-cooled condenser minimizes feed loss during the experiment. Valves S1-S5 are used to control and test the system.

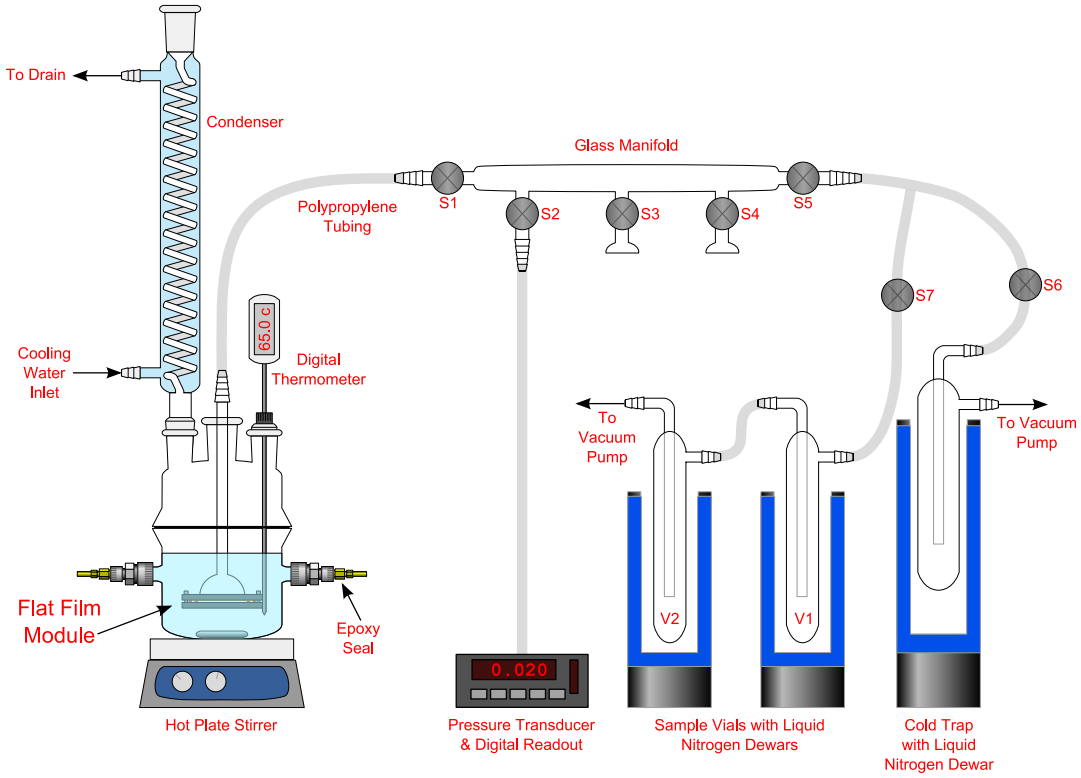


(a) Diagram of System B.

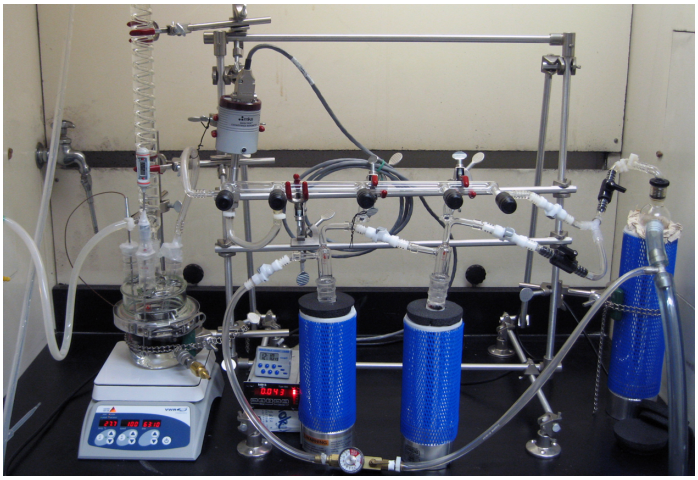

(b) Photograph of System B.

**Figure 3.9:** The modified pervaporation apparatus (System B) for characterizing hollow-fiber and flat-film membranes. A flat-film membrane is shown in place. The feed components permeate through the hollow-fiber or flat-film membrane at different rates, evaporate on the downstream side, and are condensed in the two sample traps, V1 and V2. The feed temperature and downstream pressure are monitored. A water-cooled condenser minimizes feed loss during the experiment. Valves S1, S2, and S5-S7 are used to control and test the system.

piece was fabricated by the glass shop. The top and bottom plates were milled from a Delrin® cylinder by the machine shop. Silicone rubber was used to connect the glass to the Delrin®. The sintered stainless steel disk was provided by Mott Corporation (Farmington, CT).

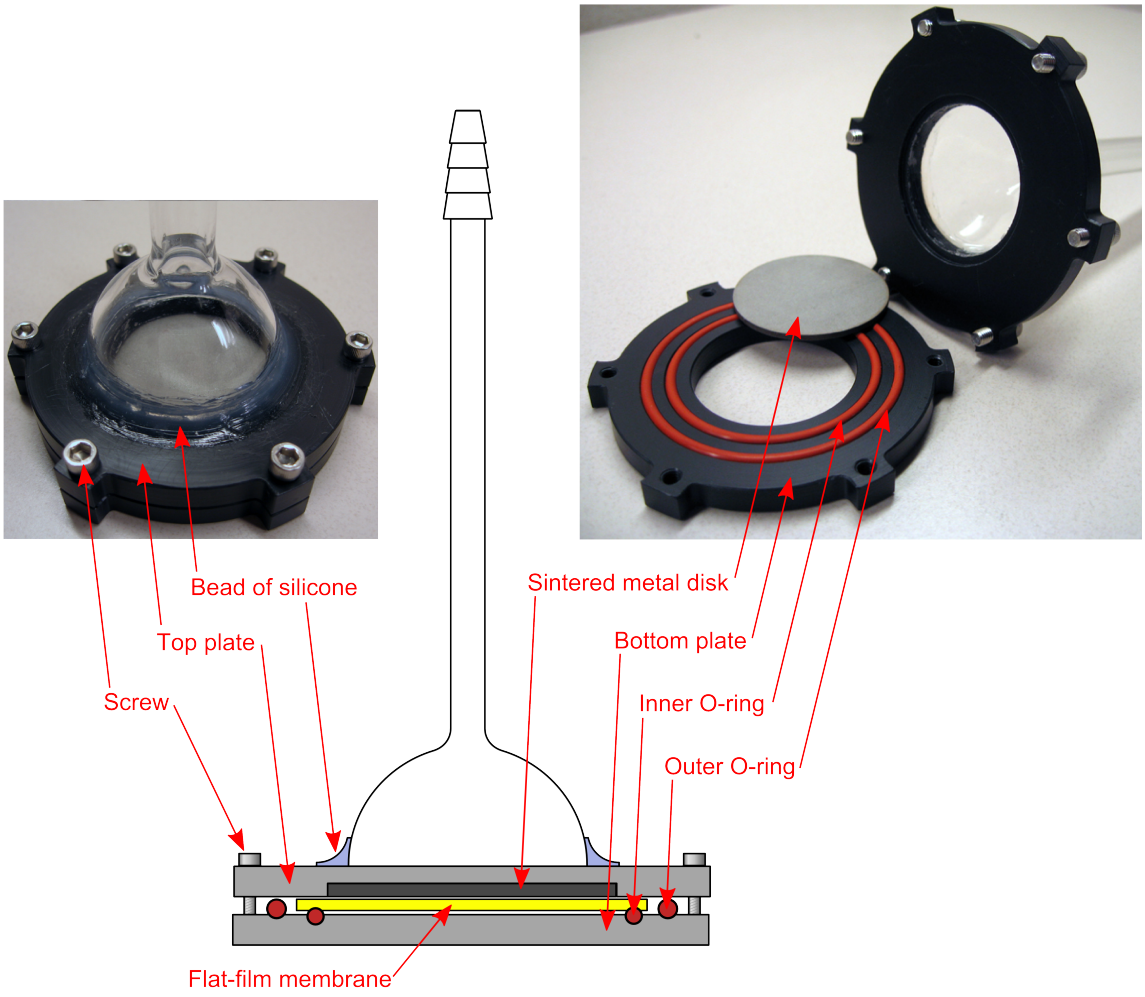


**Figure 3.10:** Pervaporation module for flat-film membranes.

To prepare the flat-film module, the cured membrane was first cut into a circular disk (4.89 cm diameter) and placed on the bottom plate of the module, centered between the inner and outer O-rings. The sintered metal disk was then fitted into the groove in the top plate. The two plates were brought together carefully, assuring that the holes were aligned and that the membrane did not slip from between the

two O-rings. Screws were then used to clamp the two plates together tightly. Once assembled, the module was connected to the pervaporation system with a short piece of tubing fed through one of the ports of the feed container lid, as shown in Figure 3.9.

**Hollow-Fiber Modules** The hollow-fiber module shown in Figure 3.11 was designed by Zhou [96]. A glass reaction vessel from Ace Glass was modified to have two 1/2" OD arms on either side. Swagelok fittings were assembled on each arm as shown in Figure 3.11 using the following procedure: First, Ultra-torr unions were tightened onto the glass joints. Then, female NPT adapters were secured in the Ultra-torr connectors. The cured hollow-fiber membrane was then fed through the connectors. A small length of Teflon® tape was carefully wrapped around the fiber at the base of each female connector, making sure the fiber was not crushed. At this point, the entire module was turned on its side, such that one of the arms was facing the ceiling. Next, epoxy resin (3M DP-100) was used to fill the cavity of the female connector. A male NPT connector, fitted with a short length of Tygon® tubing, was then screwed into the epoxy-filled female connector. The male was filled with epoxy to the top of the tubing. The epoxy was allowed to set for 10 min, then the module was turned so that the other arm faced the ceiling and the epoxy procedure was repeated. After both arms were filled with epoxy, the module was allowed to cure at room temperature for at least 8 hr. Once the epoxy had cured, the filled Tygon® tubing was very brittle and could be snapped at the edge of the male connector. This resulted in a clean epoxy face with the hollow fiber completely surrounded by resin, as shown in Figure 3.11.

Once cured, the module was connected to the pervaporation system with two lengths of tubing connected with a tubing tee, as shown in Figure 3.8. The extra port in the feed container lid was stoppered to prevent evaporation of the feed solution.

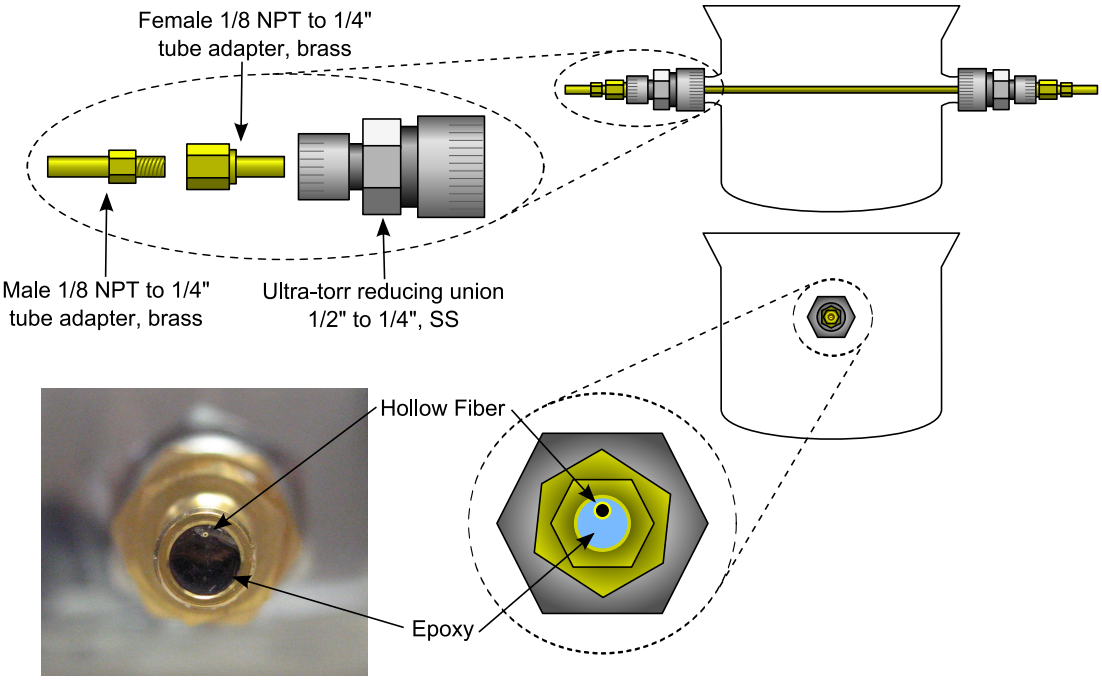


**Figure 3.11:** Pervaporation module for a single hollow-fiber membrane.

### 3.8.2 Pervaporation Procedure

For a binary feed solution, both systems allow for the measurement of component fluxes (Equations 2.23 and 2.24) and separation factor (Equation 2.26) for a single hollow fiber or a flat film. To run a pervaporation test, 20 g ethanol (200 proof, EMD) and 380 g DI water were placed in the modified 500 mL flask described in the previous section. For flat-film membranes, the same modified flask was used, but the two arms were fitted with epoxy-filled connectors to prevent leaks or evaporation of the feed. The detailed procedures followed for the two pervaporation systems are described below.

#### Pervaporation with System A

1. Connect the Swagelok connectors to the system using lengths of tubing connected with a tubing tee. Clamp the container lid and bottom together, with an O-ring in between.

2. Add 20 g ethanol and 380 g DI water to the feed container.

3. Place feed container on hot plate, begin stirring at 100 RPM.

4. Weigh Vials 1 and 2 and two squares of Parafilm®. Record the weight as $w_0$.

5. Collect a sample of the feed solution and set aside.

6. Insert temperature probe and condenser.

7. Set the hot plate to 65°C and turn on the condenser water.

8. Connect Vials 1 and 2.

9. Check that the pump oil is between the min and max marks. If not, unplug the pump and add oil.

10. Make sure all valves are closed. Add liquid nitrogen to the pump cold trap dewar and start the pump.

11. Open valves S5, S4, S3, and S2 sequentially, waiting ∼10 sec between each. The pressure should decrease to ∼0.2 torr.

12. Open S1 very slowly (try to keep the pressure under 5 torr while opening).

13. Monitor the pressure and temperature and add liquid nitrogen to the pump cold trap dewar when necessary.

14. When the pressure stabilizes (usually ∼0.4 torr) and the temperature reaches the set point, fill the Vial 1 and 2 dewars with liquid nitrogen.

15. Close S5 and note the time as $t_0$. Turn off the pump.

16. Continue monitoring the pressure and temperature and add liquid nitrogen to the dewars as needed.

17. After ∼2-4 hours, close S1. Note the time as $t_f$.

18. When the pressure stabilizes again, close S3 and S4 and allow the vials to warm to room temperature.

19. Turn off the pressure transducer and hot plate.

20. Once the traps have reached room temperature, remove them from the manifold and quickly cover them with the two squares of Parafilm® that were measured earlier. Record their weight as $w_f$.

21. Take a sample of the final feed solution and a sample of the permeate.

22. Measure the concentrations of the three collected samples to find $x_E$ and $y_E$.

**Pervaporation with System B**

1. Connect the pervaporation module to the system through the feed container lid. Clamp the container lid and bottom together, with an O-ring in between.

2. Add 20 g ethanol and 380 g DI water to the feed container.

3. Place feed container on hot plate, begin stirring at 100 RPM.

4. Weigh Traps 1 and 2 and record weight as $w_0$.

5. Collect a sample of the feed solution and set aside.

6. Insert temperature probe and condenser.

7. Set the hot plate to 65°C and turn on the condenser water.

8. Connect Traps 1 and 2.

9. Check that the pump oil is between the min and max marks. If not, unplug the pump and add oil.

10. Make sure all valves are closed. Add liquid nitrogen to the pump cold trap dewar and start the pump.

11. Open valves S6, S5, and S2 sequentially, waiting ∼10 sec between each. The pressure should decrease to ∼0.2 torr.

12. Open S1 very slowly (try to keep the pressure under 5 torr while opening).

13. Monitor the pressure and temperature and add liquid nitrogen to the pump cold trap dewar when necessary.

14. When the pressure stabilizes (usually ∼0.4 torr) and the temperature reaches the set point, fill the Trap 1 and 2 dewars with liquid nitrogen.

15. As quickly as possible, open S7 and close S6. Note the time as $t_0$.

16. Continue monitoring the pressure and temperature and add liquid nitrogen to the dewars as needed.

17. After ∼2-4 hours, close S1. Note the time as $t_f$. Let the pressure stabilize, then close S7.

18. Disconnect Trap 1 and 2 from the system and allow them to warm to room temperature.

19. Turn off the pump, pressure transducer, and hot plate.

20. Once the traps have reached room temperature, dry them, release the vacuum, and record their weight as $w_f$.

21. Take a sample of the final feed solution and a sample of the permeate.

22. Measure the concentration of the three collected samples to find $x_E$ and $y_E$.

**Calculated Results** The ethanol flux and separation factor were calculated using Equations 2.23 and 2.26, respectively. For Equation 2.23, $w = w_f - w_0$ and $t = t_f - t_0$ were used. The area of the hollow fiber was taken to be $A = \pi DL$, where $D$ is the outer diameter of the fiber coating and $L$ is the length of the fiber exposed to the feed solution. The area of the flat-film membranes was taken to be $A = \pi D$, where $D$ is the diameter of the inner O-ring.

# CHAPTER IV

# RESULTS AND DISCUSSION

## *4.1 Verification of Pervaporation Apparatus Results*

Before fabricating new membranes, a pervaporation system was built as described in Section 3.8. After construction was completed, the new system was compared against the original, replicated system using an asymmetrically spun Matrimid® hollow fiber following a test procedure outlined in [96]. To perform the test, a series of pervaporation experiments were run with feed conditions alternating between 20 wt% acetic acid in water and 0 wt% acetic acid in water. Four experiments were run on the new system and four on the original system. The results are shown in Figure 4.1. The separation factors and fluxes were similar on both systems for the duration of the test (∼5% error), which indicated that the new system was working properly.

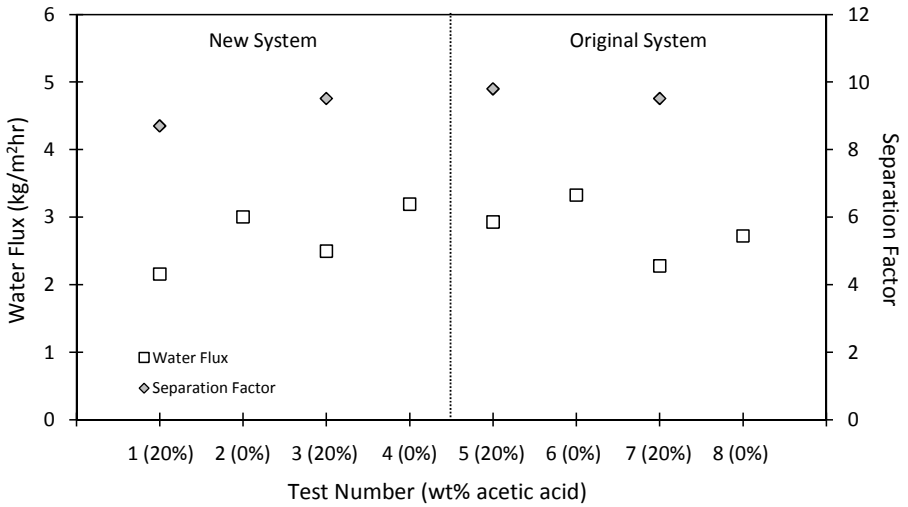


**Figure 4.1:** Comparison of separation factor and water flux for new and original pervaporation apparatuses. An asymmetrically spun Matrimid® hollow fiber was tested with feed conditions alternating between 20 and 0 wt% acetic acid in water.

## 4.2 MFI Characterization

The MFI particles used in this work were synthesized in house in several batches. Representative XRD patterns for particles synthesized using Methods A and B (described in Section 3.1) are shown in Figure 4.2. A reference ZSM-5 XRD pattern is also shown [99]. The crystal structures of the particles synthesized for this work agree well with the known structure, verifying that silicalite-1 crystals were synthesized.

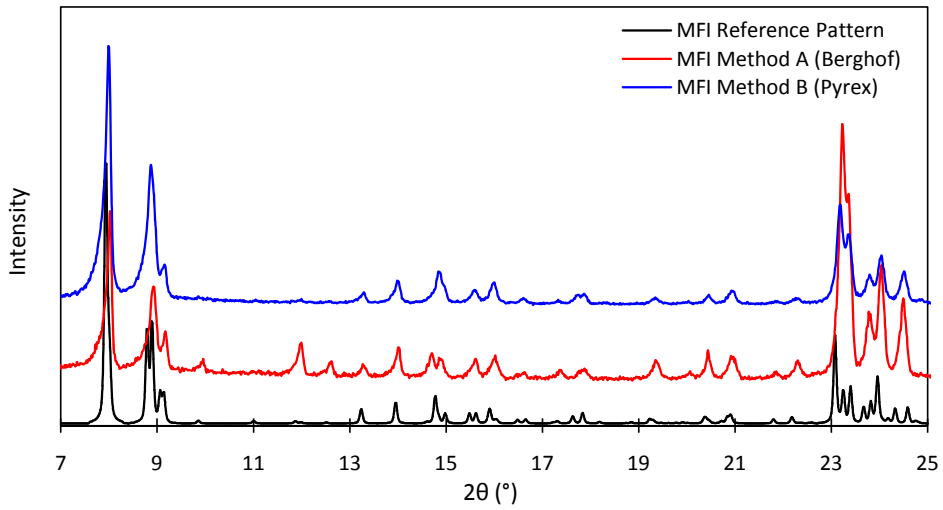


**Figure 4.2:** XRD patterns for MFI particles synthesized using Method A (Berghof reactor) and Method B (Pyrex® container). A reference ZSM-5 pattern is reproduced for comparison [99]. XRD patterns were provided by Dr. Jae Kyu Cho (Nair group, Georgia Tech).

SEM images of MFI particles synthesized using Methods A and B are shown in Figure 4.3. As can be seen in the images, the particles in each batch had a narrow size distribution. Particles in this work ranged from 0.2 to 0.3 $\mu$m.

## 4.3 Characterization of Flat Films

Flat-film membranes were fabricated to test the effects of zeolite functionalization, polymer selection, and vacuum treatment. For each condition tested, membrane loadings were varied between 0 and 60 wt% MFI. The membrane characterization

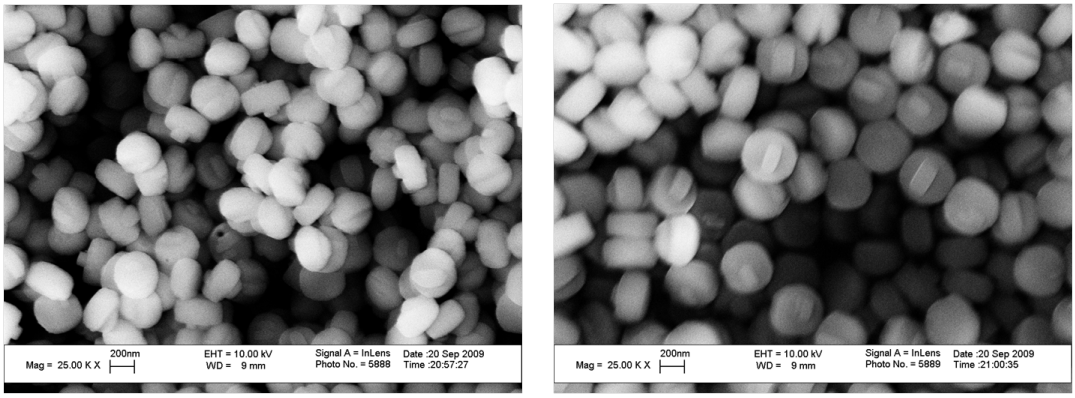


(a) Method A (b) Method B

**Figure 4.3:** SEM images of MFI particles synthesized using Method A (Berghof reactor) and Method B (Pyrex® container). SEM images were taken by Dr. Jae Kyu Cho (Nair group, Georgia Tech).

and pervaporation results for each set of membranes are discussed in the following sections.

### 4.3.1 Effect of Polymer

A series of flat films were made using the two-part RTV615 system and the three-part DMS-V41/HMS-064 system as described in Section 3.5. Butanol-functionalized MFI particles were used, with loadings ranging from 0 to 60 wt% on a solvent-free basis. Representative SEM images of each film are shown in Figures 4.4 and 4.5. The zeolite appears to be well-dispersed within each polymer system. No large agglomerations of zeolite are seen. The zeolite is also well-incorporated into the polymer matrix. No voids are present at the zeolite-polymer interfaces. Small cracks can be seen on the surface of the 40 wt% DMS-V41/HMS-064 sample, however these cracks did not appear to extend throughout the film, as will be discussed below. Average membrane thicknesses are given in Tables 4.1 and 4.2.

Each membrane was tested using a 5 wt% ethanol feed at 65°C. Pervaporation results are given in Tables 4.1 and 4.2 and are shown in Figure 4.6. Ethanol fluxes in

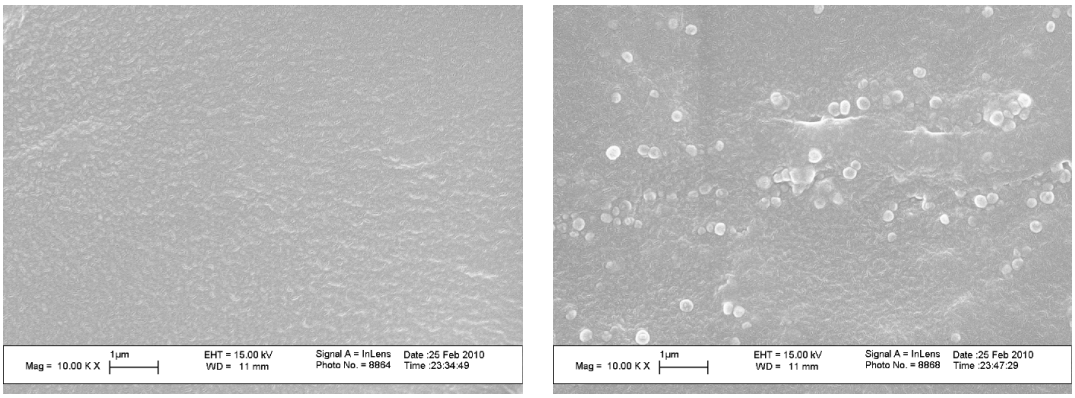


(a) 0 wt%

(b) 20 wt%

(c) 40 wt%

(d) 60 wt%

**Figure 4.4:** SEM cross-sections of flat-film membranes created with butanol-functionalized MFI in RTV615 polymer. Zeolite loadings range from 0 to 60 wt% MFI on a solvent-free basis. SEM images were taken by Dr. Jae Kyu Cho (Nair group, Georgia Tech).

Figure 4.6 have been normalized to a membrane thickness of 100 $\mu$m. The pervaporation results agree favorably with data in the literature for similar feed conditions, which are reproduced in Figure 4.6. For both polymers, as the zeolite loading is increased from 0 to 60 wt%, the ethanol flux increases by a factor of more than 4 and the separation factor nearly triples. The DMS-V41/HMS-064 polymer had a slightly higher separation factor than the RTV615 membranes at each zeolite loading, though both polymers had similar fluxes. This increase in separation factor agrees with the findings of Vane et al. that higher molecular weight prepolymers tend to have higher separation factors [67]. As mentioned above, small cracks were seen on

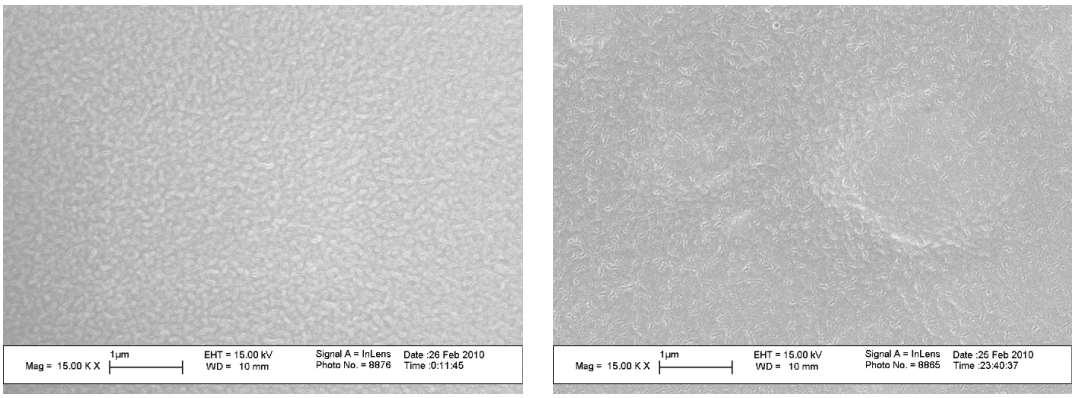


(a) 0 wt%

(b) 20 wt%

(c) 40 wt%

(d) 60 wt%

**Figure 4.5:** SEM cross-sections of flat-film membranes created with butanol-functionalized MFI in DMS-V41/HMS-064 polymer. Zeolite loadings range from 0 to 60 wt% MFI on a solvent-free basis. SEM images were taken by Dr. Jae Kyu Cho (Nair group, Georgia Tech).

the SEM cross-section of the 40 wt% MFI DMS-V41/HMS-064 sample. However, the separation performance agrees well with the reported performance for a defect-free membrane [67], which indicates that the cracks do not extend throughout the entire membrane. It is possible that the cracks were formed due to stresses incurred during SEM sample preparation.

Although the DMS-V41/HMS-064 system performed better than the RTV615 system, problems were encountered during membrane formation using this polymer. To form these membranes, MFI particles were first dispersed in iso-octane. Then the prepolymer was added and the solution was sonicated for a short time. Following this

**Table 4.1:** Film thicknesses and pervaporation results for flat films prepared using RTV615 polymer with butanol-functionalized MFI.

| Zeolite Loading | Film Thickness ($\mu$m) | wt% EtOH in Permeate | $\beta_{E/W}$ | $J_E$ (kg/m$^2$hr) | $J_{Total}$ (kg/m$^2$hr) |
|---|---|---|---|---|---|
| 0 wt% | 137.2 | 31.7 | 8.11 | 0.027 | 0.086 |
| 10 wt% | 117.4 | 30.0 | 9.32 | 0.035 | 0.108 |
| 19 wt% | 106.4 | 29.0 | 8.48 | 0.067 | 0.229 |
| 29 wt% | 103.8 | 38.7 | 12.3 | 0.048 | 0.125 |
| 39 wt% | 132.4 | 42.6 | 14.0 | 0.050 | 0.118 |
| 48 wt% | 124.8 | 45.1 | 15.0 | 0.061 | 0.136 |
| 58 wt% | 143.6 | 52.5 | 21.2 | 0.081 | 0.155 |
| 60 wt% | 131.5 | 55.4 | 23.3 | 0.124 | 0.224 |

**Table 4.2:** Film thicknesses and pervaporation results for flat films prepared with DMS-V41/HMS-064 polymer using butanol-functionalized MFI.

| Zeolite Loading | Film Thickness ($\mu$m) | wt% EtOH in Permeate | $\beta_{E/W}$ | $J_E$ (kg/m$^2$hr) | $J_{Total}$ (kg/m$^2$hr) |
|---|---|---|---|---|---|
| 0 wt% | 150.0 | 32.3 | 9.41 | 0.015 | 0.047 |
| 19 wt% | 142.6 | 39.0 | 12.4 | 0.037 | 0.095 |
| 40 wt% | 102.0 | 50.0 | 19.9 | 0.077 | 0.154 |
| 56 wt% | 146.5 | 53.0 | 21.9 | 0.120 | 0.226 |

step, the copolymer was added and the solution was quickly sonicated again. At this step, the consistency of the solution was checked for homogeneity. Once fully mixed, a very small amount of the crosslinker was added. The solution was then sonicated quickly before being poured into a Petri dish for curing.

As soon as the crosslinking agent was added to the solution, the polymer began to crosslink. With the RTV615 system, the crosslinking reaction was relatively slow, allowing for ∼30 min of working time before a viscosity change was noticeable. By diluting with solvent, the RTV615 work-life was extended to ∼1 hr. For the DMS-V41/HMS-064 system, though, the crosslinking reaction occurred very rapidly. During preliminary tests with this polymer system, several dope solutions formed

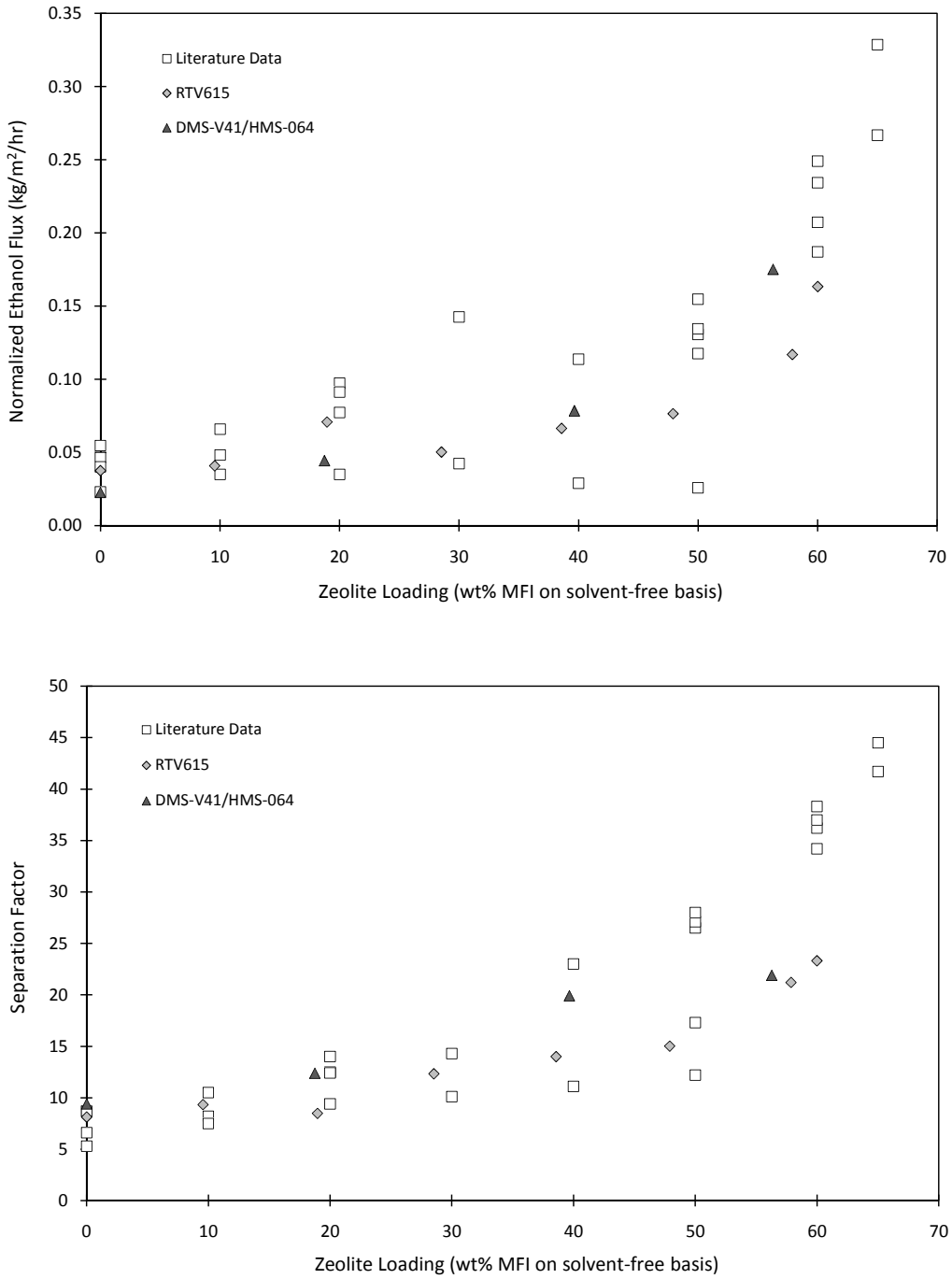


**Figure 4.6:** Fluxes and separation factors for flat films formed with the two-part RTV615 system and the three part DMS-V41/HMS-064 system. Butanol functionalized MFI particles were used for all membranes. Samples were tested with a 5 wt% ethanol feed at 65°C. Literature data for similar feed conditions are reproduced for comparison [44, 57, 67]. All fluxes have been normalized to a thickness of 100 $\mu$m.

clumps of crosslinked, rubbery material before the solution was poured into the Petri dish. Examples of this behavior are shown in Figure 4.7.

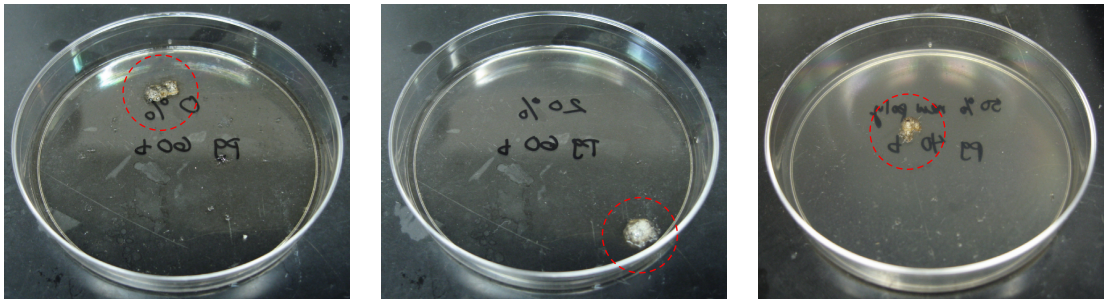

(a) 0 wt% MFI (b) 20 wt% MFI (c) 50 wt% MFI

**Figure 4.7:** Small "clumps" of crosslinked, rubbery polymer formed within DMS-V41/HMS-064 membranes during sonication.

The clumping problem was partially resolved by changing the mixing procedure to the final procedure outlined above and in Section 3.5. Specifically, adding each component separately, sonicating between each addition, and using a very short final sonication step reduced the problem. Still, clumping occurred on occasion using the final procedure if too much crosslinker was added to the mixture. The amount of crosslinker required for the reaction was very small (∼0.005 g) for the total amount of solution formed for the membranes in this work (∼5 g). The issue could most likely be resolved by increasing the total amount of solution to lessen the uncertainty and variability of the amount of crosslinker added. Although this merits further investigation, the DMS-V41/HMS-064 system was not used for further flat films and hollow-fiber coatings in this work.

### 4.3.2 Effect of Zeolite Functionalization

To study the effect of zeolite functionalization, a series of RTV615 flat films were created with unfunctionalized and butanol-functionalized zeolite loadings ranging from 0 to 60 wt% MFI on a solvent-free basis. Representative SEM images of the films are shown in Figures 4.4 and 4.8. The dispersion of zeolite particles is equally good for

both unfunctionalized and butanol-functionalized samples. The zeolite particles are also well-incorporated into the polymer matrix for both samples. Average membrane thicknesses are reported in Tables 4.1 and 4.3 .

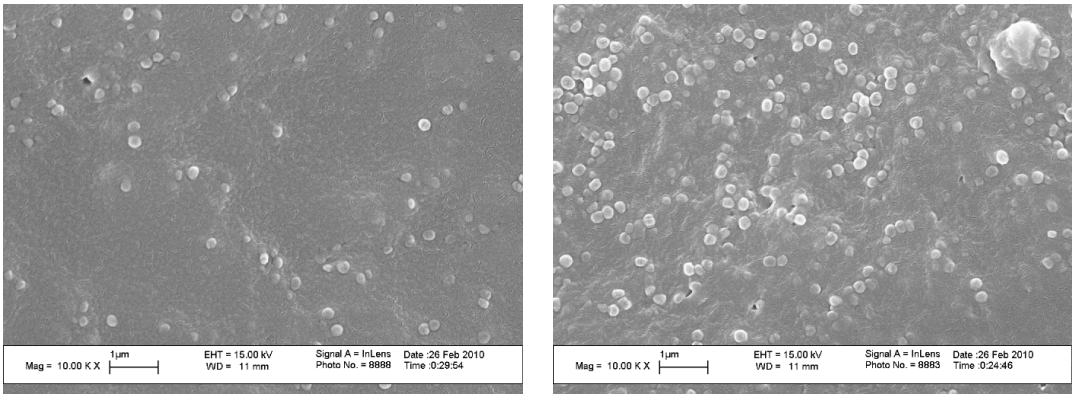


(a) 20 wt% (b) 40 wt%

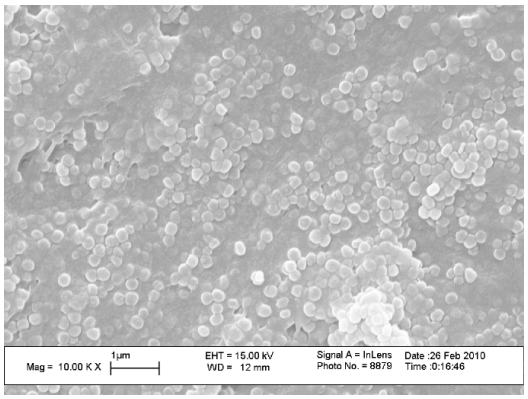


(c) 60 wt%

**Figure 4.8:** SEM cross-sections of flat-film membranes created with unfunctionalized MFI in RTV615 polymer. Zeolite loadings range from 0 to 60 wt% MFI on a solvent-free basis. SEM images were taken by Dr. Jae Kyu Cho (Nair group, Georgia Tech).

Each membrane was tested with a 5 wt% ethanol feed at 65°C. Pervaporation results are given in Tables 4.1 and 4.3 and are shown in Figure 4.9. Ethanol fluxes in Figure 4.9 have been normalized to a membrane thickness of 100 $\mu$m. The pervaporation results for both types of particles agree well with reported membranes for similar feed conditions, which are reproduced in Figure 4.9. The unfunctionalized samples performed slightly better than the functionalized samples over the range tested. The decrease in flux and separation factor for the functionalized samples could be due to

partial blockage of the pores of the zeolite. If the pores were fully blocked, one could expect to see a decrease in flux below the pure polymer value and a separation factor approximately the same as the pure polymer value. Since the functionalized-zeolite membranes in this work still showed an improved flux and separation factor over the pure polymer membranes, the pores must not be fully blocked.

**Table 4.3:** Film thicknesses and pervaporation results for flat films prepared using RTV615 polymer with unfunctionalized MFI.

| Zeolite Loading | Coating Thickness ($\mu$m) | wt% EtOH in Permeate | $\beta_{E/W}$ | $J_E$ (kg/m$^2$hr) | $J_{Total}$ (kg/m$^2$hr) |
|---|---|---|---|---|---|
| 0 wt% | 137.2 | 31.7 | 8.11 | 0.027 | 0.086 |
| 19 wt% | 103.2 | 37.1 | 11.3 | 0.053 | 0.144 |
| 38 wt% | 121.0 | 46.0 | 16.3 | 0.078 | 0.078 |
| 57 wt% | 169.0 | 54.6 | 24.2 | 0.120 | 0.219 |

Although the separation performance decreased slightly for the functionalized samples, membrane preparation was much easier and more repeatable for membranes created with butanol-functionalized MFI. After sonication, the butanol-functionalized samples tended to form homogeneous solutions in iso-octane, whereas the unfunctionalized MFI tended to form a gel-like substance that coated the walls of the vials. For example, solutions of 0.5 g MFI in 10 g iso-octane are shown in Figure 4.10. The solutions were sonicated for 15 min and pictures were taken 30 sec, 2 min, 5 min, and 10 min after removal from the sonication bath. After 10 minutes, the vials were turned over to show the gelling that occurred in the unfunctionalized sample. The effect of functionalization was also studied for hollow fiber coatings, which will be discussed in Section 4.4.4.

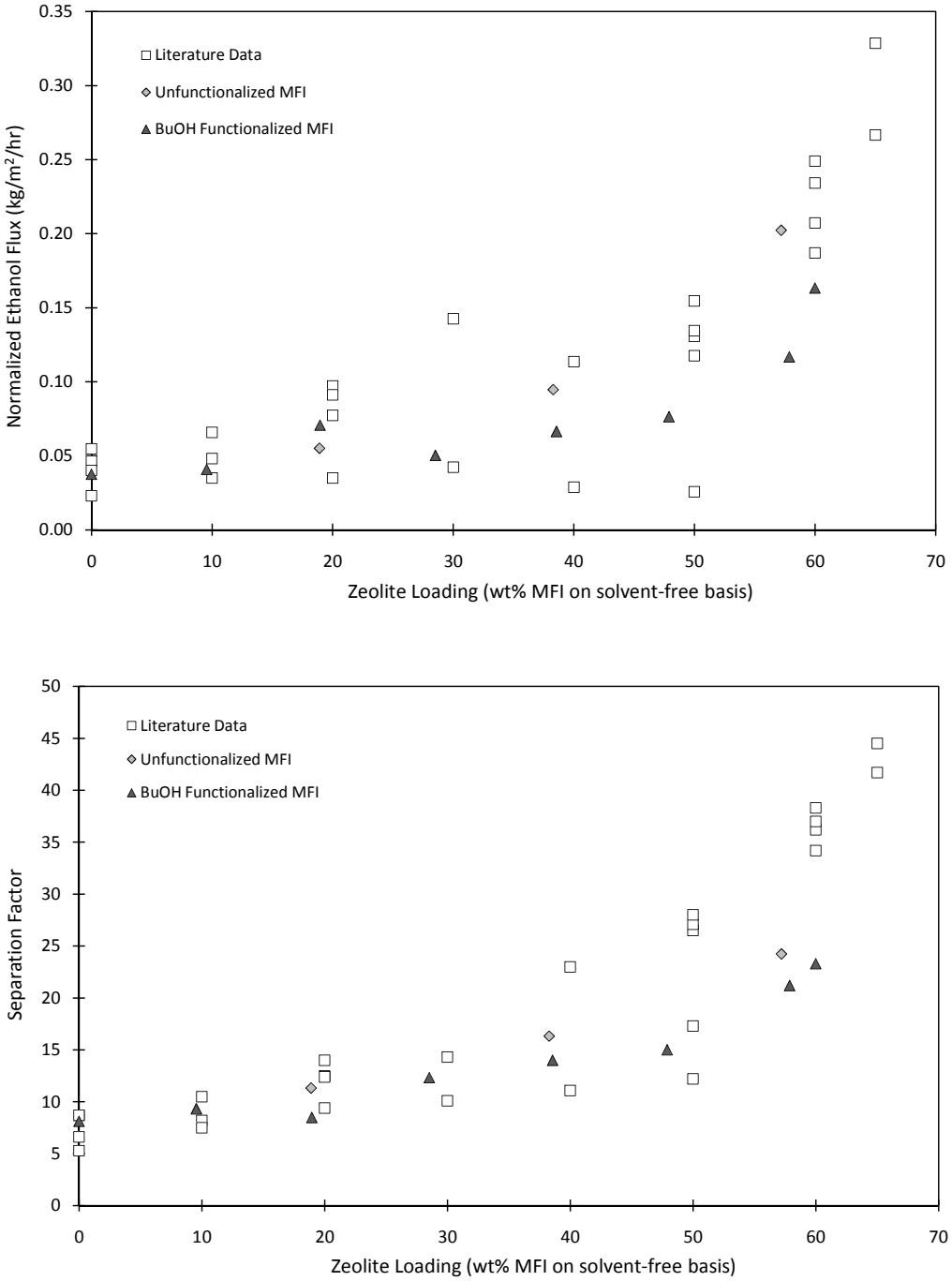


**Figure 4.9:** Fluxes and separation factors for RTV615 flat films with unfunctionalized and butanol-functionalized MFI particles. Samples were tested with a 5 wt% ethanol feed at 65°C. Literature data for similar feed conditions are reproduced for comparison [44, 57, 67]. All fluxes have been normalized to a thickness of 100 $\mu$m.

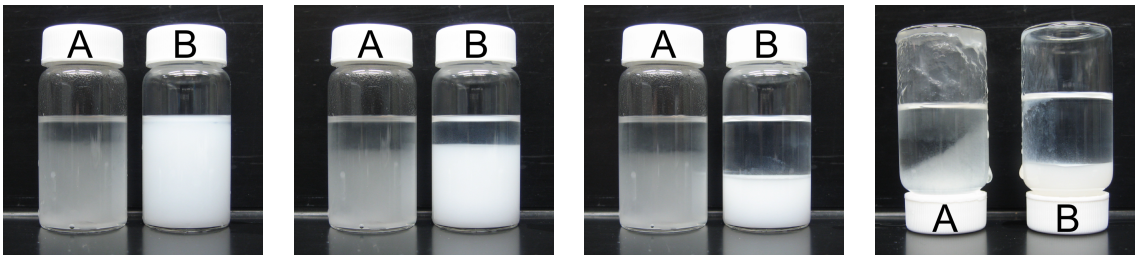


(a) 30 sec (b) 2 min (c) 5 min (d) 10 min

**Figure 4.10:** Unfunctionalized (Vial A) and butanol-functionalized (Vial B) MFI in iso-octane after being sonicated for 15 min. Pictures were taken 30 sec, 2 min, 5 min, and 10 min after removal from the sonication bath. At 10 min, the vials were turned over to show the gel formed with the unfunctionalized MFI.

### 4.3.3 Effect of Vacuum Treatment

Two vacuum treatments were tested to determine if iso-octane or water were trapped in the pores of the zeolite, which would have negatively affected the membrane performance. A series of 0 to 60 wt% butanol-functionalized MFI membranes were made and pervaporation experiments were run with a 5 wt% ethanol feed at 65°C. Following the pervaporation tests, some of the membranes (0, 20, 50, and 60 wt%) were placed in a vacuum oven at 70°C (low-temperature vacuum treatment) for more than 18 hr. The other membranes (10 and 40 wt%) were placed in a vacuum oven at 110°C (high-temperature vacuum treatment) for more than 18 hr. Each membrane was then retested with a 5 wt% ethanol feed at 65°C. Pervaporation results are given in Tables 4.1 and 4.4 and are shown in Figure 4.11. Ethanol fluxes in Figure 4.11 have been normalized to a membrane thickness of 100 $\mu$m. The pervaporation results for both untreated and vacuum-treated samples are in good agreement with data in the literature for similar feed conditions, which are reproduced in Figure 4.11.

Most of the membranes performed identically before and after the vacuum treatment. For samples that did not perform identically, the untreated samples showed a higher flux or separation factor than their vacuum-treated counterpart. The samples that were treated in a low-temperature vacuum performed equally well as the

**Table 4.4:** Film thicknesses and pervaporation results for flat films prepared using RTV615 polymer with butanol-functionalized MFI and treated with a low-temperature (70°C) or high-temperature (110°C) vacuum treatment.

| Zeolite Loading | Coating Thickness ($\mu$m) | wt% EtOH in Permeate | $\beta_{E/W}$ | $J_E$ (kg/m$^2$hr) | $J_{Total}$ (kg/m$^2$hr) |
|---|---|---|---|---|---|
| **Low temp.** | | | | | |
| 0 wt% | 137.2 | 29.7 | 7.99 | 0.025 | 0.084 |
| 19 wt% | 106.4 | 30.7 | 8.71 | 0.036 | 0.116 |
| 48 wt% | 124.8 | 43.4 | 14.7 | 0.060 | 0.137 |
| 58 wt% | 143.6 | 46.6 | 17.1 | 0.072 | 0.154 |
| **High temp.** | | | | | |
| 10 wt% | 117.4 | 32.0 | 9.14 | 0.034 | 0.107 |
| 39 wt% | 132.4 | 35.2 | 10.0 | 0.040 | 0.113 |

high-temperature samples, indicating no benefit for a higher-temperature treatment. Since no improvement in membrane performance was seen following either vacuum treatment, the hollow fiber samples in the next section were left untreated.

## *4.4 Characterization of Hollow Fibers*

Hollow-fiber supports were coated with PDMS and MFI-PDMS composite coatings using various procedures. The effect of each procedure on membrane performance is discussed in the following sections.

### 4.4.1 Characteristics of Bare Hollow-Fiber Supports

The bare Torlon® hollow fiber support is shown in Figure 4.12. The inner and outer diameter as estimated from the SEM image are approximately 200 and 300 $\mu$m, respectively. Large pores can be seen throughout the cross-section of the fiber and no skin layer is present.

The bare fiber was tested with a 5 wt% ethanol feed at 65°C. During the pervaporation measurement, the feed liquid flowed freely through the membrane, flooding the downstream system with liquid. The concentration of the collected sample was

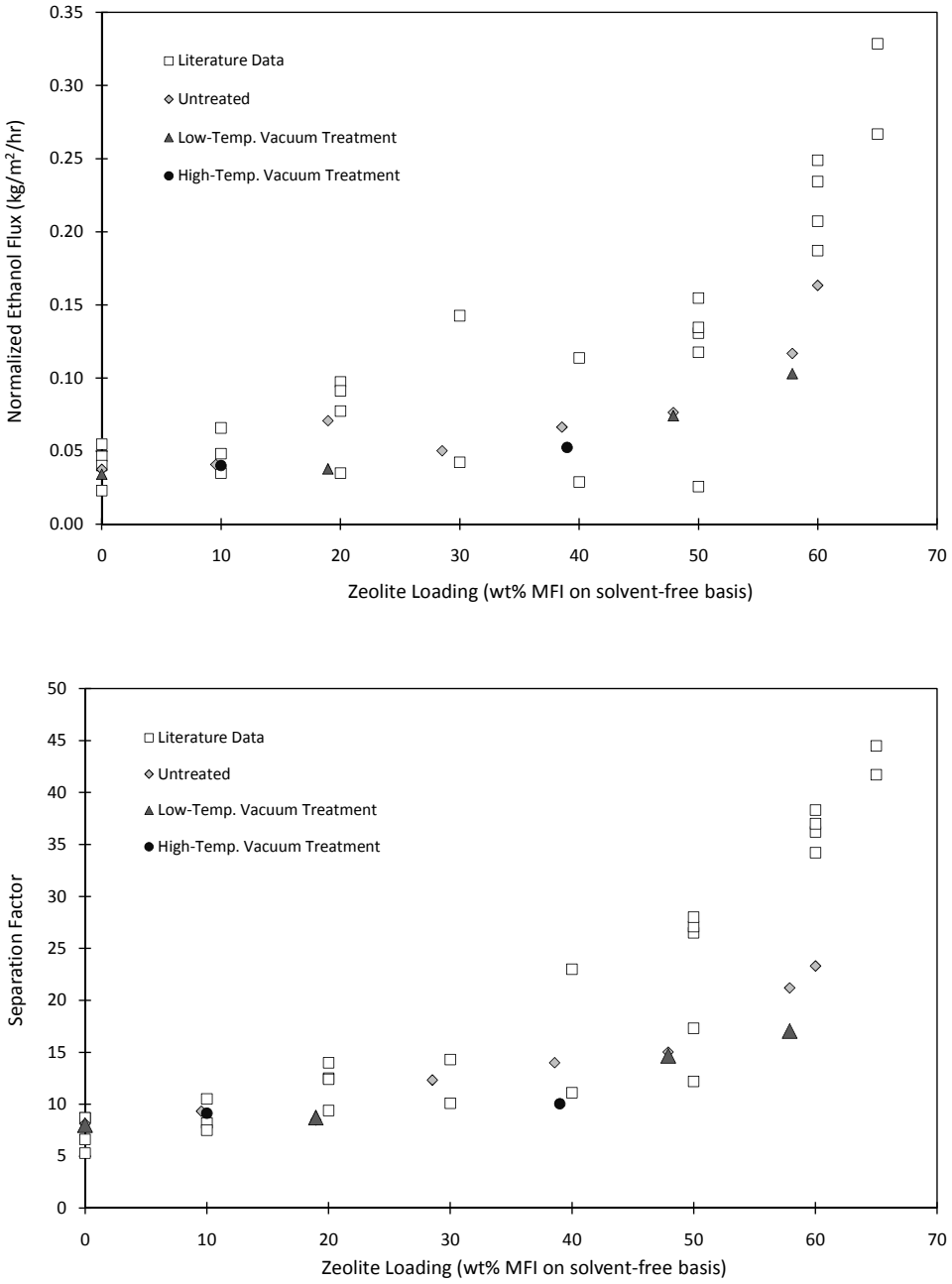


**Figure 4.11:** Fluxes and separation factors for RTV615 flat films with butanol-functionalized MFI particles. The low-temperature vacuum treatment involved placing the samples in a vacuum oven at 70°C for more than 18 hr. The high-temperature vacuum treatment was run in a vacuum oven at 110°C for more than 18 hr. Samples were tested with a 5 wt% ethanol feed at 65°C. Literature data for similar feed conditions are reproduced for comparison [44, 57, 67]. All fluxes have been normalized to a thickness of 100 $\mu$m.

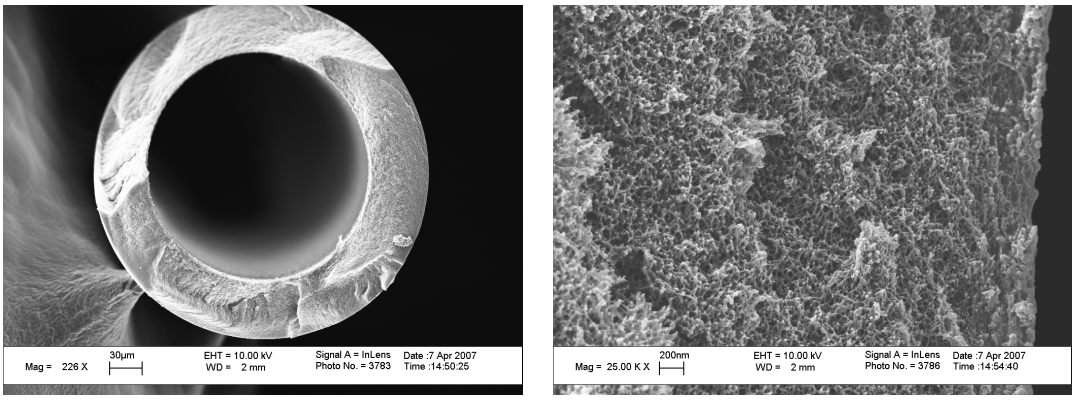


**Figure 4.12:** SEM images of bare Torlon® hollow fibers. SEM images were taken by Dr. Madhava Kosuri (Koros group, Georgia Tech).

7.6 wt% ethanol, which is a separation factor of only 1.6. The flux was 64.8 kg/m$^2$hr, three orders of magnitude higher than typical fluxes through PDMS flat films. These pervaporation results indicate that the hollow fiber shows very little resistance to transport, as desired.

### 4.4.2 Effect of Increasing Number of Coats

To test the effect of increasing the coating thickness, hollow fibers were coated with one, two, and three coats of pure PDMS (RTV615, 0 wt% MFI). SEM images of the samples are shown in Figure 4.13. The average, minimum, and maximum coating thicknesses were estimated from these images and are given in Table 4.5. Pervaporation tests were performed with a 5 wt% ethanol feed at 65°C. Results are given in Table 4.5 and are shown in Figure 4.14. In the figure, ethanol flux has been plotted against separation factor. In this form, the best membrane performance would appear in the top-right corner of the plot. All plots in Section 4.4 use the same axis scales to facilitate comparison.

There were large variations in the coating thicknesses around the circumference of the fiber for each membrane. The coatings tended to sag to one side, resulting in a very thin coating on one side of the fiber and a very thick coating on the other side. This asymmetry was most likely a result of the curing procedure. After coating each

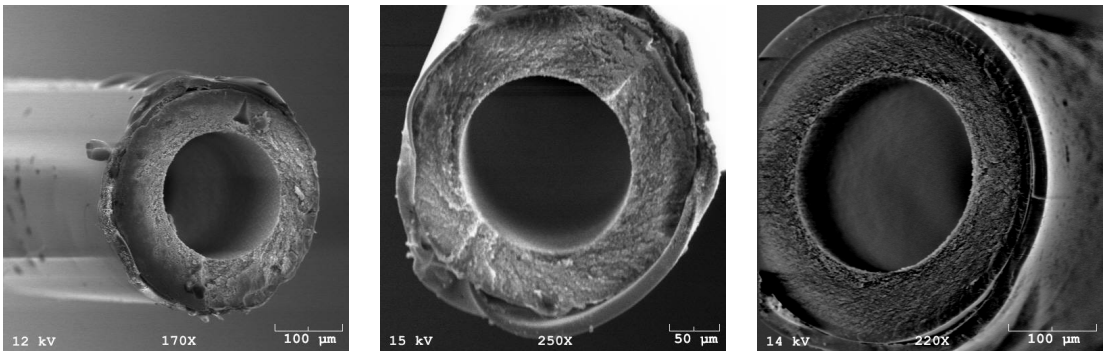


(a) 1-coat (b) 2-coat (c) 3-coat

**Figure 4.13:** SEM images of Torlon® hollow fibers coated with one, two, and three coats of pure PDMS (RTV615, 0 wt% MFI).

**Table 4.5:** Coating thicknesses and pervaporation results for increasing number of pure PDMS coatings.

| | Coating Thickness Avg. (Min-Max) ($\mu$m) | wt% EtOH in Permeate | $\beta_{E/W}$ | $J_E$ (kg/m$^2$hr) | $J_{Total}$ (kg/m$^2$hr) |
|---|---|---|---|---|---|
| 1-coat | 9.3 (4-23) | 27.1 | 7.47 | 0.077 | 0.284 |
| 2-coat | 10.9 (6-16) | 25.0 | 6.61 | 0.127 | 0.506 |
| | | 27.1 | 7.48 | 0.123 | 0.453 |
| 3-coat | 20.7 (16-31) | 27.3 | 7.70 | 0.061 | 0.222 |
| | | 27.0 | 7.48 | 0.058 | 0.214 |

fiber with the dope solution, they were hung horizontally in an oven without rotation. Rotating the samples at room temperature for several minutes before placing in the oven, or rotating the samples inside the oven while curing may improve the uniformity of the coating and should be further investigated.

As shown in Figure 4.14, the 2-coat sample achieved the highest flux of the three samples tested. The ethanol flux through the 2-coat sample was nearly double the best reported pure PDMS fluxes at similar temperatures, whereas the 1- and 3-coat samples showed similar fluxes to the literature results (0.071 kg/m$^2$hr at 75°C [47] and 0.066 kg/m$^2$hr at 50°C [67]). The 2-coat sample may have had a higher flux than the 1-coat sample due to the asymmetry of the coating. It is possible that sections of the 2-coat sample were thinner than the coating seen in the SEM image in Figure

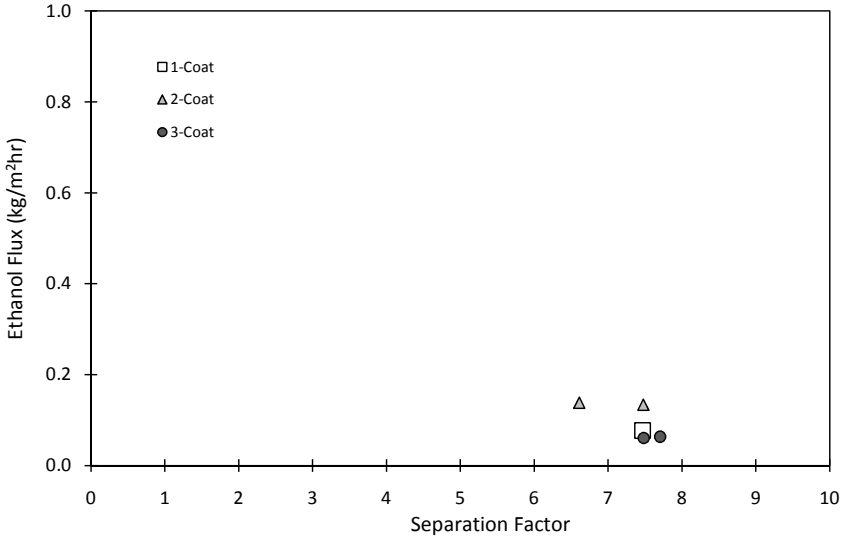


**Figure 4.14:** Ethanol flux versus separation factor for 1-, 2-, and 3-coat pure PDMS samples tested with a 5 wt% ethanol feed at 65°C.

4.13(b). Controlling the coating rate or rotating the fiber during curing may improve the uniformity of the thickness of the composite layer along the length of the fiber.

Each fiber achieved similar separation factors as the membranes reported in the literature (Section 2.3.1). The separation factor did not appear to be affected by the membrane thickness, despite the trend noted in Section 2.3.5. The asymmetry of the coatings also did not appear to affect the separation factor, indicating that a defect-free coating must have been formed along the entire length of the fiber even at the thinnest areas. It is important to note that the fluxes reported in Table 4.5 and Figure 4.14 are *not* normalized to a membrane thickness of 100 $\mu$m. If the fluxes are normalized using the apparent coating thicknesses reported in Table 4.5, which were measured from the SEM images in Figure 4.13, the observed fluxes are much lower than expected. A possible explanation for this is that the dope solution may penetrate into the large pores of the hollow fiber support while coating. This would lead to a coating thickness that is much larger than seen in the SEM images. This theory was investigated and the results are discussed in the following section.

The results above indicate that a defect-free layer is created with a single coat of PDMS. Two coats may be applied without damaging the separation performance, but this additional coat is not necessary to form a defect-free coating and more than two coats may result in deteriorated separation performance.

### 4.4.3 Effect of Presoaking

As discussed in the previous section, the fluxes through pure polymer coatings on hollow fiber supports were lower than expected while the separation factors matched the reported values, indicating the thickness of the coating layer may have been larger than seen in SEM images. If the dope solution entered the pores of the hollow fiber during the coating process, the flux would be lower than expected. The actual thickness of the coat would also be difficult to determine from the SEM images.

To test if the dope solution entered the pores of the fiber, hollow fibers were soaked in deionized water before being coated. It was expected that the water would fill the pores of the fiber, which would repel the hydrophobic dope solution and prevent it from entering the pores, leading to a thinner coat. SEM images of untreated and presoaked pure PDMS membranes are shown in Figure 4.15. Untreated and presoaked 20 wt% MFI membranes are shown in Figure 4.16. Pervaporation tests were run and averaged results are given in Table 4.6 and are shown in Figures 4.17 and 4.18. Observed coating thickness are also listed in the table.

For pure PDMS coatings, the separation factors were similar for both untreated and presoaked membranes, indicating both methods formed defect-free coatings. However, the ethanol flux was an order of magnitude higher for the presoaked sample than for the untreated sample. When normalized to a thickness of 100 $\mu$m, the flux through the presoaked membrane (0.012 kg/m$^2$hr) was much closer to reported pure polymer fluxes at similar temperatures. For comparison, the normalized flux through the untreated sample was only 0.007 kg/m$^2$hr. From these results, there appears to

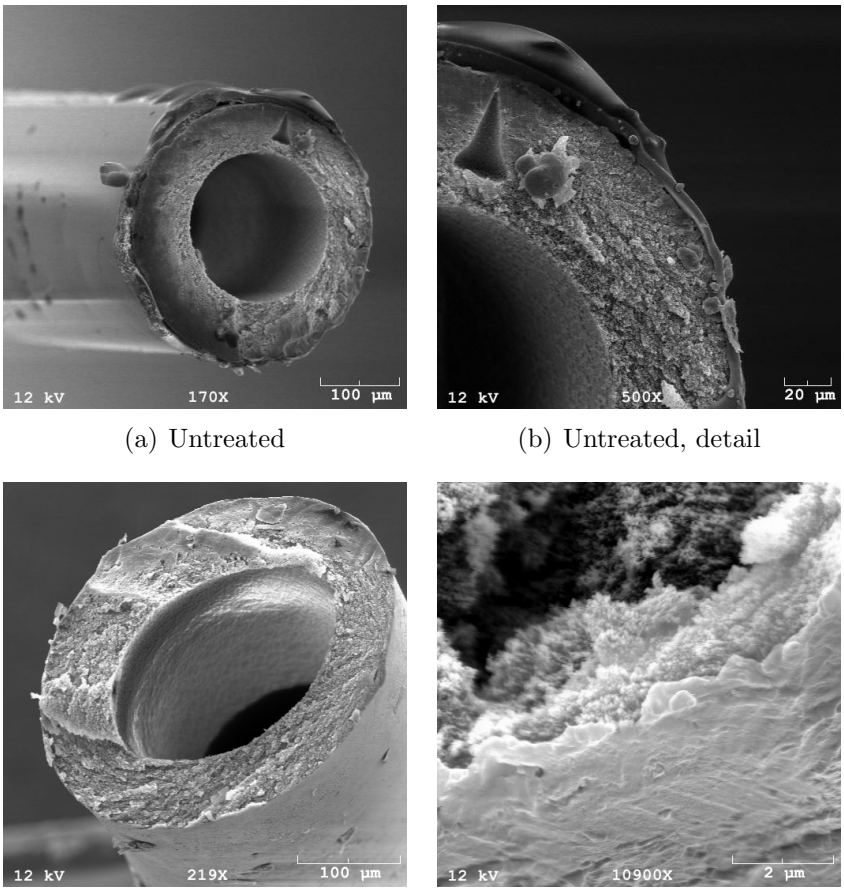


(a) Untreated (b) Untreated, detail

(c) Presoaked (d) Presoaked, detail

**Figure 4.15:** SEM images of Torlon® hollow fibers coated with one coat of pure PDMS (RTV615, 0 wt% MFI) using the dip-coat with and without presoaking.

be a clear benefit to presoaking the fibers in water before applying a polymer layer.

For 20 wt% MFI coatings, though, the results are less clear. For both unfunctionalized and butanol-functionalized membranes, the separation factor was lower for presoaked samples than for untreated samples. The decrease was likely due to the decrease in membrane thickness that occurred when the membranes were presoaked. For thin flat-film membranes, aggregates of zeolite particles have been found to form pinhole defects resulting in decreased performance [45, 67]. Vane et al. found that membrane performance could be recovered by coating the defective membranes with a thin coat of pure PDMS [67]. A similar defect-filling procedure may be able to recover the performance for hollow fibers as well.

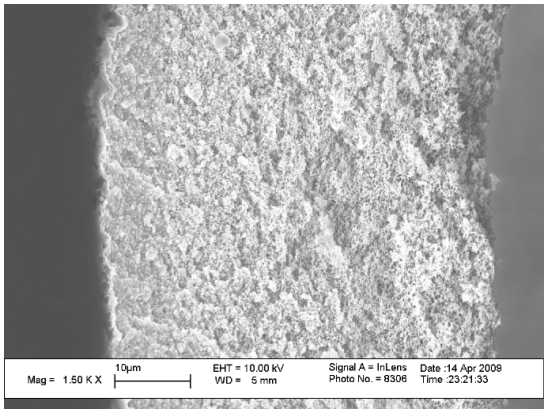


(a) 20 wt% MFI, unfunc., untreated

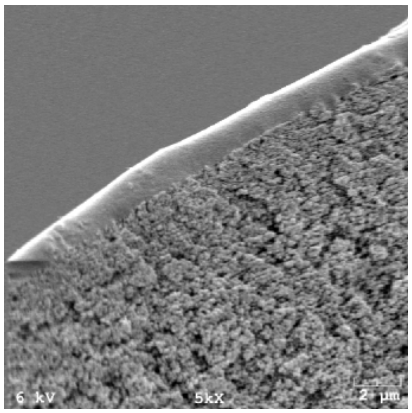


(b) 20 wt% MFI, unfunc., presoaked

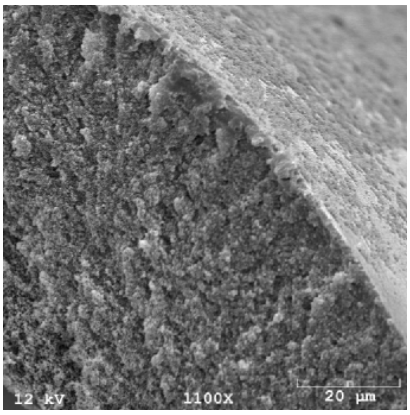


(c) 20 wt% MFI, BuOH-func., untreated

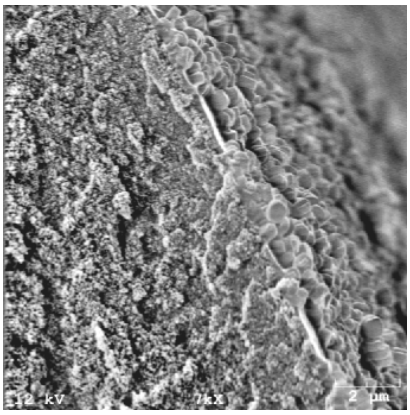


(d) 20 wt% MFI, BuOH-func., presoaked

**Figure 4.16:** SEM images of untreated and presoaked Torlon® hollow fibers coated with one coat 20 wt% unfunctionalized or butanol-functionalized MFI in PDMS using the U-tube method.

### 4.4.4 Effect of Zeolite Functionalization

In Figure 4.18, pervaporation results for unfunctionalized and butanol-functionalized hollow fibers are shown. Both with and without presoaking, the butanol-functionalized samples performed better than their unfunctionalized counterparts. For untreated samples, the average flux and separation factor for the functionalized MFI samples were almost double the unfunctionalized values. For presoaked samples, the flux and separation factor more than doubled. This improvement in performance may be due to better particle dispersion in the coatings formed with functionalized MFI. As

**Table 4.6:** Coating thicknesses and average pervaporation results for membranes prepared with and without presoaking.

| | Coating Thickness Avg. (Min-Max) ($\mu$m) | wt% EtOH in Permeate | $\beta_{E/W}$ | $J_E$ (kg/m$^2$hr) | $J_{Total}$ (kg/m$^2$hr) |
|---|---|---|---|---|---|
| **0 wt%** | | | | | |
| Untreated | 9.3 (4-23) | 27.1 | 7.47 | 0.077 | 0.284 |
| Presoaked | 2.6 (1-3) | 23.6 | 6.10 | 0.526 | 2.229 |
| **20 wt% Unfunc.** | | | | | |
| Untreated | 8.8 (5-10) | 17.6 | 3.93 | 0.105 | 0.596 |
| Presoaked | 3.2 (2-7) | 7.80 | 1.59 | 0.128 | 1.656 |
| **20 wt% BuOH-func.** | | | | | |
| Untreated | 2.3 (2-5) | 25.1 | 6.20 | 0.211 | 0.845 |
| Presoaked | 1.6 (1-4) | 17.4 | 4.02 | 0.294 | 1.846 |

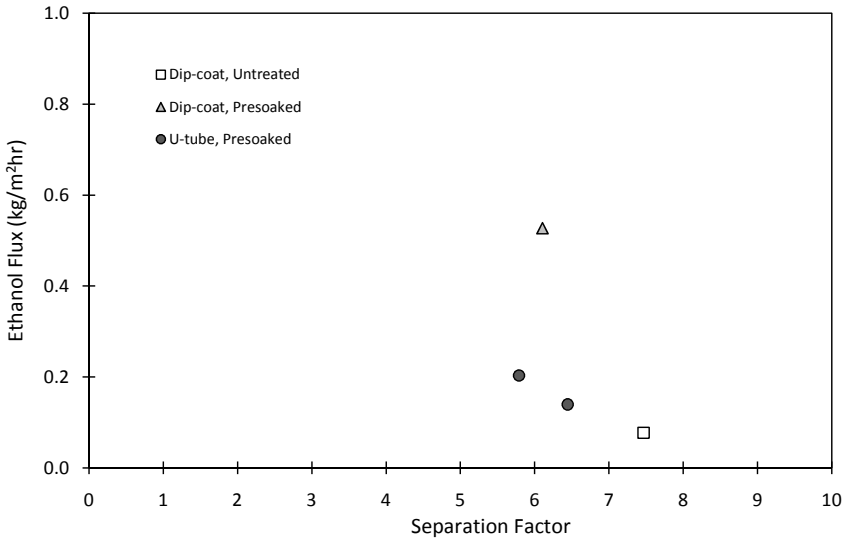


**Figure 4.17:** Ethanol flux versus separation factor for hollow fibers coated with one coat of pure PDMS (RTV615, 0 wt% MFI) using the dip-coat method with and without presoaking and the U-tube method with presoaking. Samples were tested with a 5 wt% ethanol feed at 65°C.

discussed above, the separation performance for both unfunctionalized and butanol-functionalized membranes was worse than for pure PDMS coatings. Improving the

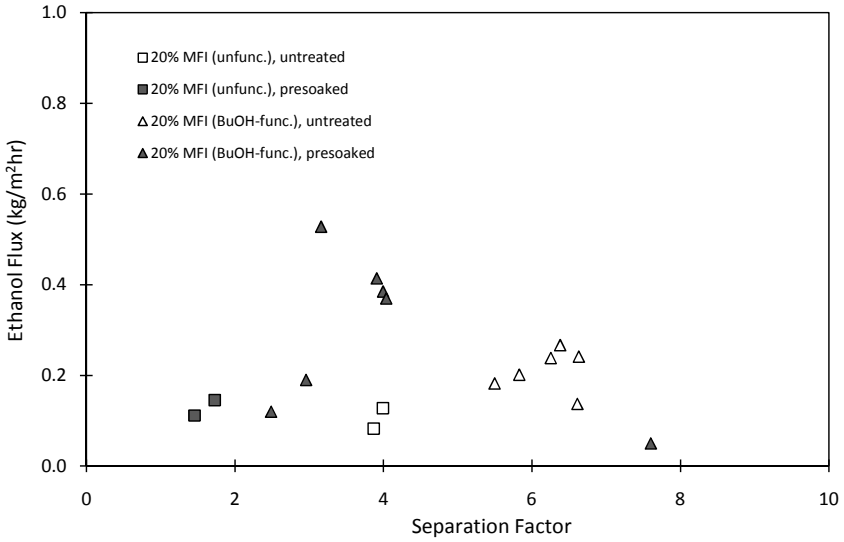


**Figure 4.18:** Ethanol flux versus separation factor for untreated or presoaked hollow fibers coated with one coat of 20 wt% MFI (unfunctionalized or butanol-functionalized) in PDMS using the U-tube method. Samples were tested with a 5 wt% ethanol feed at 65°C.

coating procedure or adding a defect-filling step may improve this performance.

### 4.4.5 Effect of Coating Method

The U-tube method was investigated to allow for sonication of the dope solution while coating fibers. SEM images of membranes prepared using the dip-coat method and the U-tube method are shown in Figure 4.19. The membranes were presoaked and then coated with one coat of pure PDMS (RTV615, 0 wt% MFI) using either the dip-coat or the U-tube method. Pervaporation tests were run and the results are given in Table 4.7 and are shown in Figure 4.17. Observed coating thickness are also listed in the table.

Although the observed thicknesses of both coatings are similar, the flux through the dip-coated sample is nearly three times larger than the flux through the sample prepared with the U-tube method. Such a large flux could occur if there were defects in the membrane, but the separation factor was near the expected value for pure

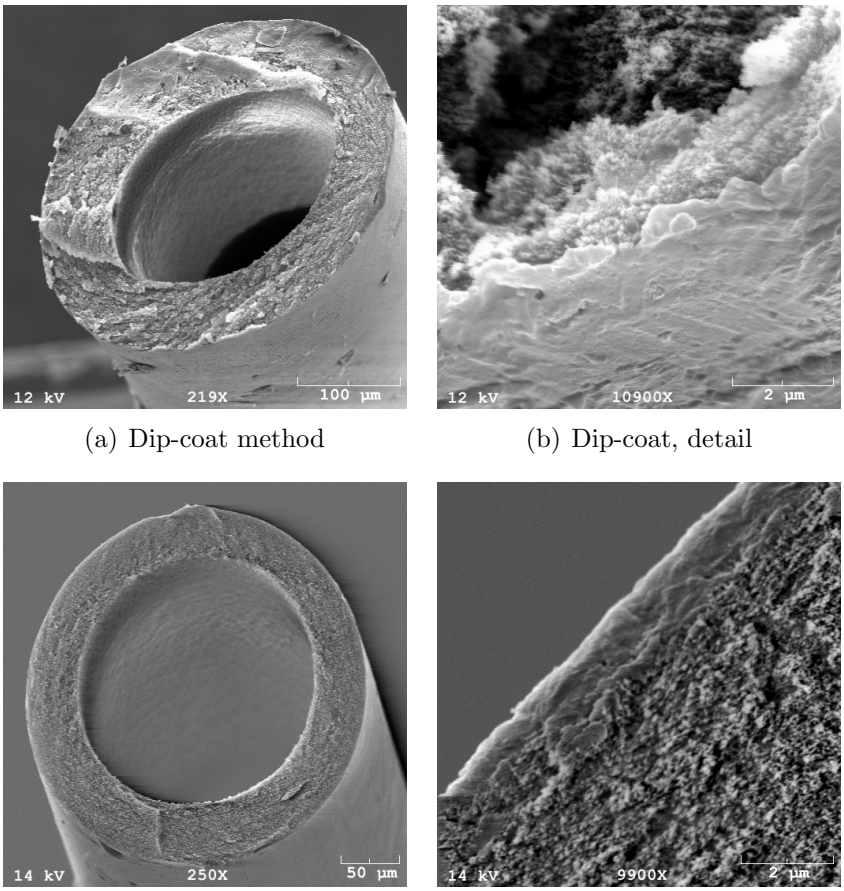


(a) Dip-coat method (b) Dip-coat, detail

(c) U-tube method (d) U-tube, detail

**Figure 4.19:** SEM images of presoaked Torlon® hollow fibers coated with one coat of pure PDMS (0 wt% MFI) using the dip-coat and U-tube methods.

PDMS, which suggests that defects were not an issue with this membrane. The increased flux could also occur if the actual coating thickness (as opposed to the observed coating thickness) were smaller for the membrane prepared using the dip-coat method. The actual coating thickness might be affected by the rate that the fiber is pulled through the dope solution. Faster rates may lead to a decreased actual thickness, as there is less time for the dope solution to interact with the water in the fiber pores. Although an attempt was made to estimate and maintain a constant coating rate for all samples, there was undoubtedly variation between the samples. It may be worthwhile to develop an automated coating procedure that could precisely control the coating rate to minimize variation from coating to coating.

**Table 4.7:** Coating thicknesses and pervaporation results for presoaked, 1-coat pure PDMS membranes prepared by different methods.

| | Coating Thickness Avg. (Min-Max) ($\mu$m) | wt% EtOH in Permeate | $\beta_{E/W}$ | $J_E$ (kg/m$^2$hr) | $J_{Total}$ (kg/m$^2$hr) |
|---|---|---|---|---|---|
| Dip-coat | 2.6 (1-3) | 23.6 | 6.10 | 0.526 | 2.229 |
| U-tube | 1.8 (1-2) | 26.2 | 6.45 | 0.160 | 0.609 |
| | | 23.6 | 5.79 | 0.233 | 0.986 |

When using the U-tube method, there was some difficulty preventing the fiber from touching the walls of the tube while removing from the dope solution. This caused several samples to be defective due to removal of the composite layer as the fiber was removed from the tube. This might be resolved by using a U-tube with a larger opening or by using a horn sonicator in the dope solution in the dip-coat method. Such improvements to to the sonicated coating method should be investigated further.

### 4.4.6 Effect of Increasing Zeolite Loading

Zeolite particles were added to the dope solution to see how the coating properties would be affected. SEM images of 0 and 20 wt% MFI-coated fibers are shown in Figure 4.20. The membranes were tested with a 5 wt% ethanol feed at 65°C. Pervaporation results are given in Table 4.6 and are shown in Figure 4.21.

When unfunctionalized zeolite was added, the separation factor decreased well below the pure PDMS value, very close to the value found for the bare hollow fiber. The ethanol flux was much lower than through the bare fiber, which indicated that some resistance was introduced by the coating. However, the high flux and low separation factor indicate that pinhole defects must be present, as discussed in Section 4.4.3. Further studies into the effect of defect-filling procedures and higher zeolite loadings should be performed to find an optimal coating composition for ethanol-water separations.

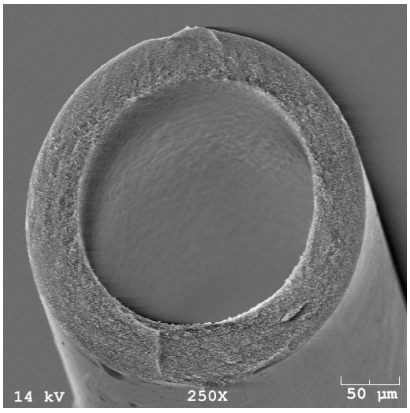


(a) 0 wt% MFI

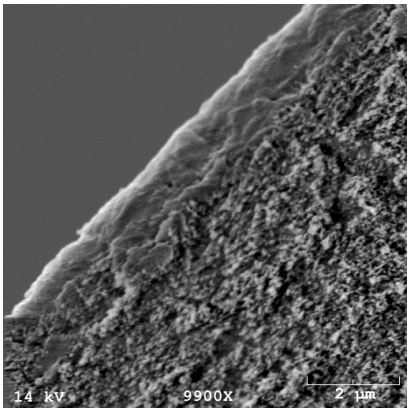


(b) 0 wt% MFI, detail

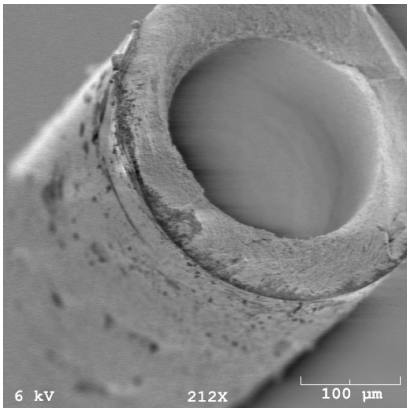


(c) 20 wt% MFI, unfunc.

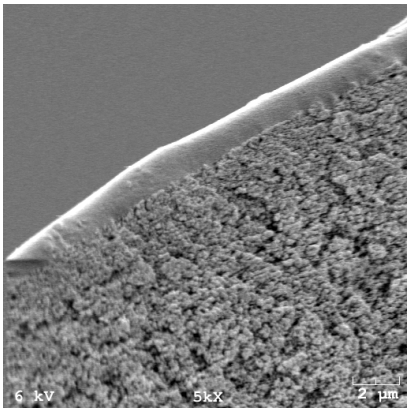


(d) 20 wt% MFI, unfunc., detail

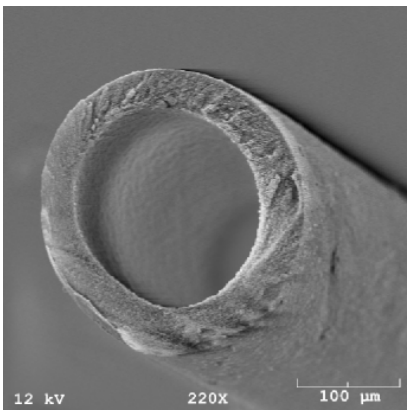


(e) 20 wt% MFI, butanol-func.

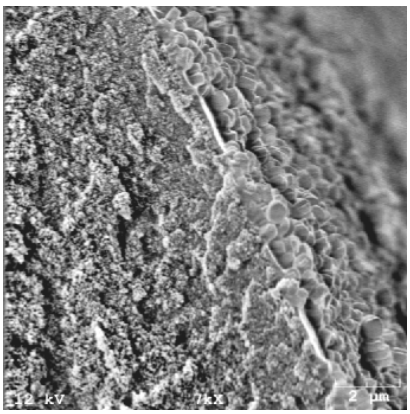


(f) 20 wt% MFI, butanol-func, detail

**Figure 4.20:** SEM images of presoaked Torlon® hollow fibers coated with one coat of 0 wt% and 20 wt% MFI using the U-tube method.

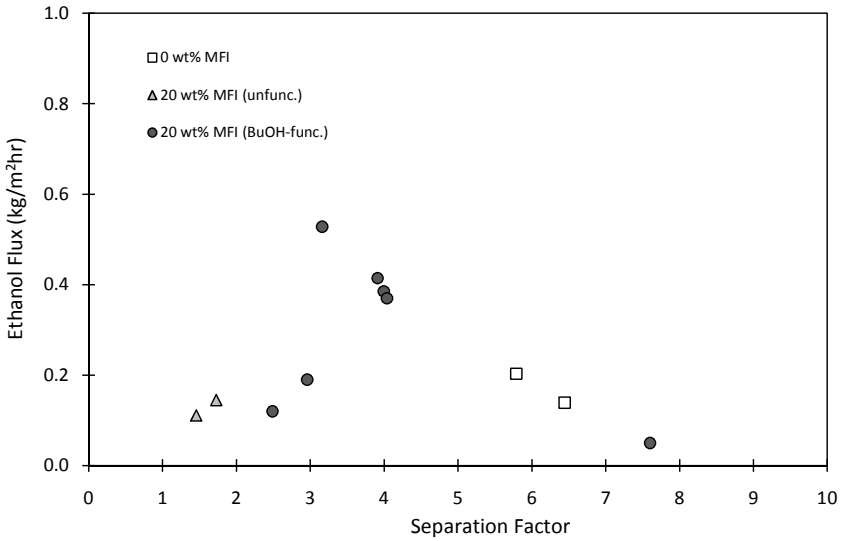


**Figure 4.21:** Ethanol flux versus separation factor for presoaked hollow fibers coated with one coat of 0 or 20 wt% MFI (unfunctionalized or butanol-functionalized) in PDMS using the U-tube method. Samples were tested with a 5 wt% ethanol feed at 65°C.

# CHAPTER V

# CONCLUSIONS

Flat-film MFI/PDMS nanocomposite membranes were prepared using different fabrication procedures. From the pervaporation results reported in the previous chapter, several conclusions can be drawn. Increasing the molecular weight of the prepolymer resulted in better pervaporation performance, however, the membranes were more difficult to fabricate due to the lower work-life of the polymer, which resulted in the formation of clumps of crosslinked polymer embedded within the membrane. Similarly, better pervaporation performance was seen with unfunctionalized MFI zeolite particles than with butanol-functionalized MFI, but the unfunctionalized particles formed a gel-like substance in the organic solvent, which made membrane fabrication more difficult and less reproducible than when functionalized particles were used. Neither low- nor high-temperature vacuum treatments affected the membrane performance.

Nanocomposite coatings on Torlon® hollow fibers were also created using various fabrication methods. The best flux through pure PDMS-coated fibers (0.526 kg/m$^2$hr) was very large compared to pure PDMS flat films in the literature (0.003-0.060 kg/m$^2$hr) while similar selectivities were achieved. This indicates that the very thin ($\sim$1-10 $\mu$m) coatings are defect-free. The thickness of the coatings was decreased by soaking the fibers in deionized water before coating with the dope solution. This presoaking step improved the membrane performance for pure PDMS samples. However, for 20 wt% MFI coatings, the presoaked coating thicknesses were extremely small and aggregates of MFI particles formed pinhole defects in the membranes, leading to a decrease in the pervaporation performance below the pure PDMS values.

## *5.1 Recommendations*

During the course of this work, several interesting challenges for membrane optimization were identified. These topics merit further investigation and are recommended for our continuing work on biofuel separation membranes.

- The optimal dope solution to maximize pervaporation performance of coated hollow fibers should be studied. The zeolite loading will need to be increased without the formation of pinhole defects. This might be accomplished by forming a thicker coating on the fiber by increasing the viscosity of the solution (by adding less solvent or by including a prepolymerization step). Alternatively, a defect-filling procedure may be able to recover membrane performance by filling pinhole defects with polymer.

- The relationship between the zeolite concentration in the dope solution and the final zeolite loading incorporated in the hollow fiber coating should be examined. For flat-film membranes, all zeolite particles in the dope solution will end up in the cured film. For hollow-fiber coatings though, there might be a different concentration of particles in the solution that adheres to the fiber than the concentration of particles in the bulk solution. This problem may be resolved by using a higher concentration of particles in the bulk solution. The relationship between the concentration of zeolite particles in the dope solution and the final zeolite loading in the hollow-fiber coating should be explored. Dope solutions with different zeolite concentrations could be used to coat hollow fibers. Then energy dispersive spectroscopy (EDS) could be used to determine the fraction of zeolite in the fiber coating. In this way, design graphs could be constructed for different zeolite particles (with or without surface treatment) and polymer sources to relate the bulk zeolite concentration to the final zeolite loading in the coating.

- The DMS-V41/HMS-064 polymer system should be further investigated with higher organic solvent fractions to increase the work-life of the dope solution. Using a larger total amount of dope solution may also be beneficial to lessen the variability of the amount of crosslinker added. This would extend the work-life by preventing too much crosslinker addition and would improve the repeatability of the coatings.

- A larger glass U-tube might be used or a horn sonicator might be immersed into the dope solution during the dip-coat procedure. These improvements would help to prevent damaging the coating while removing the fiber from the glass tube.

- Automatically controlling the rate at which the fibers are pulled through the dope solution should be explored to improve repeatability.

- Rotating the samples before or during curing should be investigated to improve the uniformity of the coating thickness.

- A defect-filling procedure should be tested to fill the pinhole defects formed by particle aggregates.

- Finally, long-term tests with simulated fermentation broths should be conducted to determine the lifespan of the coated hollow fibers and the degree of fouling from expected contaminants.

# REFERENCES


[1] L. R. Raymond, C. P. Deming, and M. W. Nichols, "Hard truths: Facing the hard truths about energy, a comprehensive view to 2030 of global oil and natural gas," National Petroleum Council, Tech. Rep., July 2007. [Online]. Available: http://downloadcenter.connectlive.com/events/npc071807/pdf-downloads/NPC_Facing_Hard_Truths.pdf [Feb. 2010].

[2] *Standard Specification for Denatured Fuel Ethanol for Blending with Gasolines for Use as Automotive Spark-Ignition Engine Fuel*, ser. D 4806 - 09. West Conshohocken, PA: ASTM International, 2009.

[3] L. M. Vane, "A review of pervaporation for product recovery from biomass fermentation processes," *Journal of Chemical Technology and Biotechnology*, vol. 80, pp. 603–629, 2005.

[4] P. R. D. Williams, D. Inman, A. Aden, and G. A. Heath, "Environmental and sustainability factors associated with next-generation biofuels in the US: What do we really know?" *Environmental Science & Technology*, vol. 43, pp. 4763–4775, 2009.

[5] A. E. Wheals, L. C. Basso, D. M. G. Alves, and H. V. Amorim, "Fuel ethanol after 25 years," *Trends in Biotechnology*, vol. 17, pp. 482–487, 1999.

[6] R. Wooley, M. Ruth, D. Glassner, and J. Sheehan, "Process design and costing of bioethanol technology: A tool for determining the status and direction of research and development," *Biotechnology Progress*, vol. 15, pp. 794–803, 1999.

[7] C. E. Wyman, "Biomass ethanol: Technical progress, opportunities, and commercial challenges," *Annual Review of Energy and the Environment*, vol. 24, pp. 189–226, 1999.

[8] S. A. Abbasi and N. Abbasi, "The likely adverse environmental impacts of renewable energy sources," *Applied Energy*, vol. 65, pp. 121–144, 2000.

[9] S. Kim and B. E. Dale, "Global potential bioethanol production from wasted crops and crop residues," *Biomass & Bioenergy*, vol. 26, pp. 361–375, 2004.

[10] R. S. Chambers, R. A. Herendeen, J. J. Joyce, and P. S. Penner, "Gasohol - Does it or doesn't it produce positive net energy," *Science*, vol. 206, no. 4420, pp. 789–795, 1979.

[11] H. Weinblatt, T. S. Reddy, and A. Turhollow, "Energy and precious fuels requirements of fuel alcohol production," U.S. Department of Energy, Tech. Rep., December 1982.

[12] S. P. Ho, "Ethanol process energy and cogeneration efficiency," Amoco Oil Company, Naperville, IL, Tech. Rep., 1989.

[13] D. Pimentel, "Ethanol fuels: Energy security, economics, and the environment," *Journal and Agriculture and Environmental Ethics*, vol. 4, pp. 1–13, 1991.

[14] D. R. Keeney and T. H. DeLuca, "Biomass as an energy source for the midwestern U.S." *American Journal of Alternative Agriculture*, vol. 7, pp. 137–143, 1992.

[15] D. Pimentel, "Ethanol fuels: Energy, economics and environmental impact," *International Sugar Journal*, vol. 103, p. 491, 2001.

[16] ——, "Ethanol fuels: Energy balance, economics, and environmental impacts are negative," *Natural Resources Research*, vol. 12, pp. 127–134, 2003.

[17] T. W. Patzek, S.-M. Anti, R. Campos, K. W. Ha, J. Lee, B. Li, J. Padnick, and S.-A. Ye, "Ethanol from corn: Clean renewable fuel for the future, or drain on our resources and pockets?" *Environment, Development and Sustainability*, vol. 7, pp. 319–336, 2005.

[18] D. Pimentel and T. W. Patzek, "Ethanol production using corn, switchgrass, and wood; Biodiesel production using soybean and sunflower," *Natural Resources Research*, vol. 14, pp. 65–76, 2005.

[19] G. Marland and A. F. Turhollow, "$CO_2$ emissions from the production and combustion of fuel ethanol from corn," *Energy*, vol. 16, pp. 1307–1316, 1991.

[20] D. Lorenz and D. Morris, "How much energy does it take to make a gallon of ethanol?" Institute for Local Self-Reliance, Tech. Rep., August 1995. [Online]. Available: http://www.ethanol.org/pdf/contentmgmt/ILSR_energy_balance.pdf [Feb. 2010].

[21] H. Shapouri, J. A. Duffield, and M. S. Graboski, "Estimating the net energy balance of corn ethanol," U.S. Department of Agriculture, Economic Research Service, Office of Energy, Agricultural Economic Report 721, July 1995. [Online]. Available: http://www.ers.usda.gov/publications/aer721/aer721.pdf [Feb. 2010].

[22] M. Wang, C. Saricks, and D. Santini, "Effects of fuel ethanol use on fuel-cycle energy and greenhouse gas emissions," Center for Transportation Research, Energy Systems Division, Argonne National Laboratory, Tech. Rep., January 1999. [Online]. Available: http://www.transportation.anl.gov/pdfs/TA/58.pdf [Feb. 2010].

[23] M. S. Graboski, "Fossil energy use in the manufacture of corn ethanol," National Corn Growers Association, Tech. Rep., August 2002. [Online]. Available: http://www.oregon.gov/energy/renew/biomass/docs/forum/FossilEnergyUse.pdf [Feb. 2010].

[24] S. Kim and B. E. Dale, "Allocation procedure in ethanol production system from corn grain - I. System expansion," *International Journal of Life Cycle Assessment*, vol. 7, pp. 237–243, 2002.

[25] H. Shapouri, J. A. Duffield, and M. Wang, "The energy balance of corn ethanol: An update," United States Department of Agriculture, Office of the Chief Economist, Office of Energy Policy and New Uses, Agricultural Economic Report 813, 2002. [Online]. Available: http://www.transportation.anl.gov/pdfs/AF/265.pdf [Feb. 2010].

[26] M. A. Delucchi, "A lifecycle emissions model (LEM): Lifecycle emissions from transportation fuels, motor vehicles, transportation modes, electricity use, heating and cooking fuels, and materials," Institute of Transportation Studies, University of California, Research Report UCD-ITS-RR-03-17-MAIN, December 2003. [Online]. Available: http://pubs.its.ucdavis.edu/publication_detail.php?id=273 [Feb. 2010].

[27] M. Wang, C. Saricks, and H. Lee, "Fuel-cycle energy and emission impacts of ethanol-diesel blends in urban buses and farming tractors," Illinois Department of Commerce and Economic Opportunities, Center for Transportation Research, Argonne National Laboratory, Argonne, IL, Tech. Rep., July 2003.

[28] H. Shapouri, J. Duffield, A. McAloon, and M. Wang, "The 2001 net energy balance of corn-ethanol," U.S. Department of Agriculture, Office of the Chief Economist, Tech. Rep., 2004. [Online]. Available: http://www.usda.gov/oce/reports/energy/net_energy_balance.pdf [Feb. 2010].

[29] S. Kim and B. E. Dale, "Environmental aspects of ethanol derived from no-tilled corn grain: Nonrenewable energy consumption and greenhouse gas emissions," *Biomass & Bioenergy*, vol. 28, pp. 475–489, 2005.

[30] A. E. Farrell, R. J. Plevin, B. T. Turner, A. D. Jones, M. O'Hare, and D. M. Kammen, "Ethanol can contribute to energy and environmental goals," *Science*, vol. 311, pp. 506–508, 2006.

[31] J. Hill, E. Nelson, D. Tilman, S. Polasky, and D. Tiffany, "Environmental, economic, and energetic costs and benefits of biodiesel and ethanol biofuels," *Proceedings of the National Academy of Sciences of the United States of America*, vol. 103, pp. 11 206–11 210, 2006.

[32] S. Kim, B. E. Dale, and R. Jenkins, "Life cycle assessment of corn grain and corn stover in the United States," *International Journal of Life Cycle Assessment*, vol. 14, pp. 160–174, 2009.

[33] T. E. Amidon, C. D. Wood, A. M. Shupe, Y. Wang, M. Graves, and S. Liu, "Biorefinery: Conversion of woody biomass to chemicals, energy and materials," *Journal of Biobased Materials and Bioenergy*, vol. 2, pp. 100–120, 2008.

[34] L. M. Vane, "Separation technologies for the recovery and dehydration of alcohols from fermentation broths," *Biofuels Bioproducts & Biorefining-BioFPR*, vol. 2, pp. 553–588, 2008.

[35] J. D. Seader and Z. M. Kurtyka, *Perry's Chemical Engineers' Handbook*, 6th ed. McGraw-Hill, 1984, ch. Distillation.

[36] J. Feldman, "Process for recovering ethanol from dilute aqueous solutions employing liquid extraction media," US Patent 4 409 406, 1993.

[37] M. T. Holtzapple and R. F. Brown, "Conceptual design for a process to recover volatile solutes from aqueous solutions using silicalite," *Separations Technology*, vol. 4, pp. 213–229, 1994.

[38] J. D. Seader and E. J. Henley, *Separation Process Principles*, 2nd ed. John Wiley & Sons, Inc., 2006.

[39] R. W. Baker, *Membrane Technology and Applications*. McGraw-Hill, 2000.

[40] M. Mulder, *Basic Principles of Membrane Technology*. Kluwer Academic Publishers, 1991.

[41] P. Shao and R. Y. M. Huang, "Polymeric membrane pervaporation," *Journal of Membrane Science*, vol. 287, pp. 162–179, 2007.

[42] S. L. Schmidt, M. D. Myers, S. S. Kelley, J. D. McMillan, and N. Padukone, "Evaluation of PTMSP membranes in achieving enhanced ethanol removal from fermentations by pervaporation," *Applied Biochemistry and Biotechnology*, vol. 63-5, pp. 469–482, 1997.

[43] T. Kashiwagi, K. Okabe, and K. Okita, "Separation of Ethanol from Ethanol Water Mixtures by Plasma-Polymerized Membranes from Silicone Compounds," *Journal of Membrane Science*, vol. 36, pp. 353–362, 1988.

[44] B. Moermans, W. De Beuckelaer, I. F. J. Vankelecom, R. Ravishankar, J. A. Martens, and P. A. Jacobs, "Incorporation of nano-sized zeolites in membranes," *Chemical Communications*, pp. 2467–2468, 2000.

[45] H. J. C. te Hennepe, D. Bargeman, M. H. V. Mulder, and C. A. Smolders, "Zeolite-filled silicone rubber membranes: Part 1. Membrane preparation and pervaporation results," *Journal of Membrane Science*, vol. 35, pp. 39–55, 1987.

[46] M.-D. Jia, K.-V. Peinemann, and R.-D. Behling, "Preparation and characterization of thin-film zeolite-PDMS composite membranes," *Journal of Membrane Science*, vol. 73, pp. 119–128, 1992.

[47] I. F. J. Vankelecom, D. Depré, S. Debeukelaer, and J. B. Uytterhoeven, "Influence of zeolites in PDMS membranes: Pervaporation of water/alcohol mixtures," *Journal of Physical Chemistry*, vol. 99, pp. 13 193–13 197, 1995.

[48] T. Ikegami, H. Yanagishita, D. Kitamoto, K. Haraya, T. Nakane, H. Matsuda, N. Koura, and T. Sano, "Production of highly concentrated ethanol in a coupled fermentation/pervaporation process using silicalite membranes," *Biotechnology Techniques*, vol. 11, pp. 921–924, 1997.

[49] ——, "Highly concentrated aqueous ethanol solutions by pervaporation using silicalite membrane - Improvement of ethanol selectivity by addition of sugars to ethanol solution," *Biotechnology Letters*, vol. 21, pp. 1037–1041, 1999.

[50] M. Nomura, T. Bin, and S. Nakao, "Selective ethanol extraction from fermentation broth using a silicalite membrane," *Separation and Purification Technology*, vol. 27, pp. 59–66, 2002.

[51] T. Ikegami, D. Kitamoto, H. Negishi, K. Haraya, H. Matsuda, Y. Nitanai, N. Koura, T. Sano, and H. Yanagishita, "Drastic improvement of bioethanol recovery using a pervaporation separation technique employing a silicone rubber-coated silicalite membrane," *Journal of Chemical Technology and Biotechnology*, vol. 78, pp. 1006–1010, 2003.

[52] H. Matsuda, H. Yanagishita, H. Negishi, D. Kitamoto, T. Ikegami, K. Haraya, T. Nakane, Y. Idemoto, N. Koura, and T. Sano, "Improvement of ethanol selectivity of silicalite membrane in pervaporation by silicone rubber coating," *Journal of Membrane Science*, vol. 210, pp. 433–437, 2002.

[53] X. Lin, X. S. Chen, H. Kita, and K. Okamoto, "Synthesis of silicalite tubular membranes by in situ crystallization," *AIChE Journal*, vol. 49, pp. 237–247, 2003.

[54] X. Lin, H. Kita, and K. Okamoto, "Silicalite membrane preparation, characterization, and separation performance," *Industrial & Engineering Chemistry Research*, vol. 40, pp. 4069–4078, 2001.

[55] T. Sano, H. Yanagishita, Y. Kiyozumi, F. Mizukami, and K. Haraya, "Separation of ethanol-water mixture by silicalite membrane on pervaporation," *Journal of Membrane Science*, vol. 95, pp. 221–228, 1994.

[56] T. Sano, M. Hasegawa, S. Ejiri, Y. Kawakami, and H. Yanagishita, "Improvement of the pervaporation performance of silicalite membranes by modification with a silane coupling reagent," *Microporous Materials*, vol. 5, pp. 179–184, 1995.

[57] X. Chen, Z. Ping, and Y. Long, "Separation properties of alcohol-water mixture through silicalite-I-filled silicone rubber membranes by pervaporation," *Journal of Applied Polymer Science*, vol. 67, pp. 629–636, 1998.

[58] T. Sano, S. Ejiri, K. Yamada, Y. Kawakami, and H. Yanagishita, "Separation of acetic acid-water mixtures by pervaporation through silicalite membrane," *Journal of Membrane Science*, vol. 123, pp. 225–233, 1997.

[59] N. Y. Chen, "Hydrophobic properties of zeolites," *Journal of Physical Chemistry*, vol. 80, no. 1, pp. 60–64, 1976.

[60] T. C. Bowen, R. D. Noble, and J. L. Falconer, "Fundamentals and applications of pervaporation through zeolite membranes," *Journal of Membrane Science*, vol. 245, pp. 1–33, 2004.

[61] C. Bartels-Caspers, E. Tusel-Langer, and R. N. Lichtenthaler, "Sorption isotherms of alcohols in zeolite-filled silicone-rubber and in PVA-composite membranes," *Journal of Membrane Science*, vol. 70, pp. 75–83, 1992.

[62] I. F. J. Vankelecom, E. Scheppers, R. Heus, and J. B. Uytterhoeven, "Parameters influencing zeolite incorporation in PDMS membranes," *Journal of Physical Chemistry*, vol. 98, pp. 12 390–12 396, 1994.

[63] B. Adnadjević, J. Jovanović, and S. Gajinov, "Effect of different physicochemical properties of hydrophobic zeolites on the pervaporation properties of PDMS-membranes," *Journal of Membrane Science*, vol. 136, pp. 173–179, 1997.

[64] I. F. J. Vankelecom, J. De Kinderen, B. M. Dewitte, and J. B. Uytterhoeven, "Incorporation of hydrophobic porous fillers in PDMS membranes for use in pervaporation," *Journal of Physical Chemistry B*, vol. 101, pp. 5182–5185, 1997.

[65] T. Ikegami, H. Yanagishita, D. Kitamoto, H. Negishi, K. Haraya, and T. Sano, "Concentration of fermented ethanol by pervaporation using silicalite membranes coated with silicone rubber," *Desalination*, vol. 149, pp. 49–54, 2002.

[66] T. Ikegami, H. Negishi, D. Kitamoto, K. Sakaki, T. Imura, M. Okamoto, Y. Idemoto, N. Koura, T. Sano, K. Haraya, and H. Yanagishita, "Stabilization of bioethanol recovery with silicone rubber-coated ethanol-permselective silicalite membranes by controlling the pH of acidic feed solution," *Journal of Chemical Technology and Biotechnology*, vol. 80, pp. 381–387, 2005.

[67] L. M. Vane, V. V. Namboodiri, and T. C. Bowen, "Hydrophobic zeolite-silicone rubber mixed matrix membranes for ethanol-water separation: Effect of zeolite and silicone component selection on pervaporation performance," *Journal of Membrane Science*, vol. 308, pp. 230–241, 2008.

[68] R. W. Baker, W. J. Koros, E. L. Cussler, R. L. Riley, W. Eykamp, and H. Strathmann, *Membrane Separation Systems: Recent Developments and Future Directions*. Noyes Data Corporation, 1991.

[69] J. G. Wijmans and R. W. Baker, "The solution-diffusion model - A review," *Journal of Membrane Science*, vol. 107, pp. 1–21, 1995.

[70] J. H. Petropoulos, "A comparative study of approaches applied to the permeability of binary composite polymeric materials," *Journal of Polymer Science Part B - Polymer Physics*, vol. 23, pp. 1309–1324, 1985.

[71] R. H. B. Bouma, A. Checchetti, G. Chidichimo, and E. Drioli, "Permeation through a heterogeneous membrane: The effect of the dispersed phase," *Journal of Membrane Science*, vol. 128, pp. 141–149, 1997.

[72] J. P. Boom, I. G. M. Pünt, H. Zwijnenberg, R. de Boer, D. Bargeman, C. A. Smolders, and H. Strathmann, "Transport through zeolite filled polymeric membranes," *Journal of Membrane Science*, vol. 138, pp. 237–258, 1998.

[73] A. Erdem-Şenatalar, M. Tatlier, and S. B. Tantekin-Ersolmaz, "Questioning the validity of present models for estimating the performances of zeolite-polymer mixed matrix membranes," *Chemical Engineering Communications*, vol. 190, pp. 677–692, 2003.

[74] E. E. Gonzo, M. L. Parentis, and J. C. Gottifredi, "Estimating models for predicting effective permeability of mixed matrix membranes," *Journal of Membrane Science*, vol. 277, pp. 46–54, 2006.

[75] S. A. Hashemifard, A. F. Ismail, and T. Matsuura, "Prediction of gas permeability in mixed matrix membranes using theoretical models," *Journal of Membrane Science*, vol. 347, pp. 53–61, 2010.

[76] R. Mahajan and W. J. Koros, "Mixed matrix membrane materials with glassy polymers. Part 1," *Polymer Engineering and Science*, vol. 42, pp. 1420–1431, 2002.

[77] Y.-C. Long, X. Chen, Z.-H. Ping, S.-K. Fu, and Y.-J. Sun, "MFI-Type Zeolite Filled Silicone-Rubber Membranes - Preparation, Composition, and Performance," in *Zeolites and Related Microporous Materials: State of the Art 1994*, ser. Studies in Surface Science and Catalysis, Weitkamp, J and Karge, HG and Pfeifer, H and Holderich, W, Ed., 1994, vol. 84, pp. 1083–1090.

[78] C. Baerlocher and L. McCusker, "Database of zeolite structures," Tech. Rep., 2010. [Online]. Available: http://www.iza-structure.org/databases/ [Feb. 2010].

[79] N. Peng and T. S. Chung, "The effects of spinneret dimension and hollow fiber dimension on gas separation performance of ultra-thin defect-free Torlon® hollow fiber membranes," *Journal of Membrane Science*, vol. 310, pp. 455–465, 2008.

[80] M. R. Kosuri and W. J. Koros, "Defect-free asymmetric hollow fiber membranes from Torlon®, a polyamide-imide polymer, for high-pressure $CO_2$ separations," *Journal of Membrane Science*, vol. 320, pp. 65–72, 2008.

[81] N. Peng, T.-S. Chung, and J.-Y. Lai, "The rheology of Torlon® solutions and its role in the formation of ultra-thin defect-free Torlon® hollow fiber membranes for gas separation," *Journal of Membrane Science*, vol. 326, pp. 608–617, 2009.

[82] N. Peng, T.-S. Chung, and K. Y. Li, "The role of additives on dope rheology and membrane formation of defect-free Torlon® hollow fibers for gas separation," *Journal of Membrane Science*, vol. 343, pp. 62–72, 2009.

[83] M. R. Kosuri and W. J. Koros, "Asymmetric hollow fiber membranes for separation of $CO_2$ from hydrocarbons and fluorocarbons at high-pressure conditions relevant to $C_2F_4$ polymerization," *Industrial & Engineering Chemistry Research*, vol. 48, pp. 10 577–10 583, 2009.

[84] S. Takegami, S. Tujii, and H. Yamada, "Dehydration of ethanol-water mixture by pervaporation using poly(amide-imide) hollow fiber membrane," *Nippon Kagaku Kaishi*, pp. 194–198, 1993.

[85] W. Qiu, M. Kosuri, F. Zhou, and W. J. Koros, "Dehydration of ethanol-water mixtures using asymmetric hollow fiber membranes from commercial polyimides," *Journal of Membrane Science*, vol. 327, pp. 96–103, 2009.

[86] X. Li and S. Wang, "Some characteristics of pervaporation for dilute ethanol-water mixtures by alcohol-permselective composite membrane," *Separation Science and Technology*, vol. 31, pp. 2867–2873, 1996.

[87] R. K. Iler, *The Chemistry of Silica*. John Wiley & Sons: Toronto,Canada, 1979.

[88] T. Ishikawa, M. Matsuda, A. Yasukawa, K. Kandori, S. Inagaki, T. Fukushima, and S. Kondo, "Surface silanol groups of mesoporous silica FSM-16," *Journal of the Chemical Society - Faraday Transactions*, vol. 92, pp. 1985–1989, 1996.

[89] G. C. Ossenkamp, T. Kemmitt, and J. H. Johnston, "New approaches to surface-alkoxylated silica with increased hydrolytic stability," *Chemistry of Materials*, vol. 13, pp. 3975–3980, 2001.

[90] ——, "Toward functionalized surfaces through surface esterification of silica," *Langmuir*, vol. 18, pp. 5749–5754, 2002.

[91] C.-H. Cheng, T.-H. Bae, B. A. McCool, R. R. Chance, S. Nair, and C. W. Jones, "Functionalization of the internal surface of pure-silica MFI zeolite with aliphatic alcohols," *Journal of Physical Chemistry C*, vol. 112, pp. 3543–3551, 2008.

[92] Y. Mitamura, Y. Komori, S. Hayashi, Y. Sugahara, and K. Kuroda, "Interlamellar esterification of H-magadiite with aliphatic alcohols," *Chemistry of Materials*, vol. 13, pp. 3747–3753, 2001.

[93] N. Qureshi and H. P. Blaschek, "Butanol recovery from model solution/fermentation broth by pervaporation: Evaluation of membrane performance," *Biomass & Bioenergy*, vol. 17, pp. 175–184, 1999.

[94] N. Qureshi, M. M. Meagher, J. Huang, and R. W. Hutkins, "Acetone butanol ethanol (ABE) recovery by pervaporation using silicalite-silicone composite membrane from fed-batch reactor of Clostridium acetobutylicum," *Journal of Membrane Science*, vol. 187, pp. 93–102, 2001.

[95] F. Lipnizki, S. Hausmanns, and R. W. Field, "Influence of impermeable components on the permeation of aqueous 1-propanol mixtures in hydrophobic pervaporation," *Journal of Membrane Science*, vol. 228, pp. 129–138, 2004.

[96] F. Zhou, "Novel pervaporation for separating acetic acid and water mixtures using hollow fiber membranes," Ph.D. dissertation, Georgia Institute of Technology, August 2005.

[97] R. W. Chafin II, "Torlon and silicalite mixed matrix membranes for xylene isomer purification," Ph.D. dissertation, Georgia Institute of Technology, May 2007.

[98] L. C. Boudreau, "Preparation and characterization of highly oriented films and membranes of zeolite a," Ph.D. dissertation, University of Massachusetts Amherst, May 1999.

[99] H. Van Koningsveld, J. C. Jansen, and H. Van Bekkum, "The monoclinic framework structure of zeolite H-ZSM-5 - Comparison with the orthorhombic framework of as-synthesized ZSM-5," *Zeolites*, vol. 10, pp. 235–242, 1990.